DEVELOPMENT OF CURCUMIN-LOADED NANOCOMPOSITE HYDROGELS FOR WOUND HEALING

By
Miss Khin Cho AYE

A Thesis Submitted in Partial Fulfillment of the Requirements
for Doctor of Philosophy PHARMACEUTICAL TECHNOLOGY
(INTERNATIONAL PROGRAM)
Department of PHARMACEUTICAL TECHNOLOGY
Silpakorn University
Academic Year 2024

-

โดย
MissKhin Cho AYE

วิทยานิพนธ์นี้เป็นส่วนหนึ่งของการศึกษาตามหลักสูตรปรัชญาดุษฎีบัณฑิต
เทคโนโลยีเภสัชกรรม (หลักสูตรนานาชาติ) แบบ 1.2 ปรัชญาดุษฎีบัณฑิต
ภาควิชาเทคโนโลยีเภสัชกรรม
มหาวิทยาลัยศิลปากร
ปีการศึกษา 2567

DEVELOPMENT OF CURCUMIN-LOADED NANOCOMPOSITE HYDROGELS FOR WOUND HEALING

By
Miss Khin Cho AYE

A Thesis Submitted in Partial Fulfillment of the Requirements
for Doctor of Philosophy PHARMACEUTICAL TECHNOLOGY
(INTERNATIONAL PROGRAM)
Department of PHARMACEUTICAL TECHNOLOGY
Academic Year 2024

Title	Development of Curcumin-loaded Nanocomposite Hydrogels for Wound Healing
By	Miss Khin Cho AYE
Field of Study	PHARMACEUTICAL TECHNOLOGY (INTERNATIONAL PROGRAM)
Advisor	Associate Professor Prasopchai Patrojanasophon, Ph.D.
Co advisor	Professor Praneet Opanasopit, Ph.D. Assistant Professor Chaiyakarn Pornpitchanarong, Ph.D.

Faculty of Pharmacy, Silpakorn University in Partial Fulfillment of the Requirements for the Doctor of Philosophy

.....Dean of Faculty of Pharmacy
(Professor Pornsak Sriamornsak, Ph.D.)

Approved by

.....Chair person
(Associate Professor Wipada Samprasit, Ph.D.)

.....Advisor
(Associate Professor Prasopchai Patrojanasophon, Ph.D.)

.....Co advisor
(Professor Praneet Opanasopit, Ph.D.)

.....Co advisor
(Assistant Professor Chaiyakarn Pornpitchanarong, Ph.D.)

.....Committee
(Assistant Professor Boonnada Pamornpathomkul, Ph.D.)

630830002 : Major PHARMACEUTICAL TECHNOLOGY (INTERNATIONAL PROGRAM)
Keyword : Curcumin, Nanosuspensions, Liposomes, Chitosan, Hyaluronic acid, Poly (vinyl alcohol), Polyvinylpyrrolidone, Optimization, Hydrogels, Nanocomposite hydrogels, Antioxidant activity, Wound healing

Miss Khin Cho AYE : Development of Curcumin-loaded Nanocomposite Hydrogels for Wound Healing Thesis advisor : Associate Professor Prasopchai Patrojanasophon, Ph.D.

Efforts to improve wound healing outcomes have led to research on novel dressings. This study focuses on developing curcumin-embedded nanocomposite hydrogels for the efficient delivery of curcumin (Cur) in wound healing. Although Cur has potent healing properties, its poor aqueous solubility hinders its effectiveness. To address this, curcumin nanosuspension (Cur-NS) and curcumin liposome (Cur-L) formulations were optimized using the Box-Behnken design to enhance particle size, size distribution, zeta potential, and Cur content. The optimized nano-Curs were then evaluated for morphology, drug release profile, cytotoxicity, and healing efficacy based on antioxidant and cell migration effects. The amorphization of Cur-NS was assessed through its thermal properties, crystallinity, and stability. The hydrogel formulations were optimized using a simplex centroid mixture design and a central composite design. Cur-NS was incorporated into genipin-crosslinked chitosan-polyvinylpyrrolidone (CS-PVP) hydrogel, while a polyvinylpyrrolidone-co-itaconic acid (PNVP-ITA) copolymer was synthesized to enhance the properties of the hydrogel containing hyaluronic acid (HA), polyvinyl alcohol (PVA), and Cur-L embedded into the HA/PVA/PNVP-ITA hydrogel. Interactions between hydrogels and nano-Curs were assessed using Fourier-transform infrared spectroscopy (FTIR). Their drug release kinetics were studied, and *in vivo,* skin recovery was investigated on incisional wounds of the Wistar rat model. The optimized Cur-NS, containing 2% Tween® 20, 4.97% Pluronic® F127, and 1 mg/mL Cur, yielded stable nano-sized particles with a slight negative charge and a Cur content of 1.16 ± 0.03 mg/mL. Cur-NS (5% w/w of polymers) was incorporated into the optimized hydrogels containing 70% CS and 30% PVP, achieving 97.54 ± 4.54% loading efficiency. Meanwhile, the optimized liposomes were constructed from 2.7% Tween® 20, 0.04% oleic acid, and 8.1% Cur, yielding negatively charged particles with a narrow size distribution and a Cur content of 19.92 ± 0.54 µg/mg. The optimized hydrogel contained 5% HA and 10% PVA, with properties improved by adding synthesized PNVP-ITA. Cur-L (0.5% w/w of polymers) was successfully integrated into the HA/PVA/PNVP-ITA hydrogel via absorption with an efficiency of 95.22 ± 4.24%. Nano-Curs enhanced its antioxidant effect in an aqueous medium by improving its solubility. Both Cur-NSs and Cur-Ls were released from the hydrogel matrix via diffusion-erosion and diffusion-controlled mechanisms, following the Korsmeyer-Peppas model. These hydrogels were safe for normal human fibroblast (NHF) cells and induced skin recovery faster than a commercial patch within 5 days. Overall, this study offers a promising solution for wound care.

ACKNOWLEDGEMENTS

I would like to express my deepest gratitude to everyone who supported me in completing my thesis and earning my Ph.D. First and foremost, I am profoundly grateful to my thesis advisor, Associate Professor Dr. Prasopchai Patrojanasophon, and co-advisor, Professor Dr. Praneet Opanasopit, for their unwavering mentorship, valuable guidance, and consistent encouragement. Their expertise and insightful critiques have greatly shaped my research.

I also extend special thanks to my co-advisor, Assistant Professor Dr. Chaiyakarn Pornpitchanarong, for his extensive support, technical guidance, and invaluable contributions in shaping my research. I am very appreciative of Dr. Nitjawan Sahatsapan for her invaluable guidance and supervision, which were crucial in helping me acquire essential laboratory skills and advance my research journey.

I am immensely thankful to the thesis exam committee members, Associate Professor Dr. Wipada Samprasit and Assistant Professor Dr. Boonnada Pamornpathomkul, for their engagement, astute critiques, and constructive recommendations that have significantly enhanced my work.

I am deeply honored and grateful to be the recipient of the International Postgraduate Scholarship (Ph.D. in Pharmaceutical Technology) provided by the Faculty of Pharmacy, Silpakorn University. I would like to express my sincere gratitude to the scholarship committee for recognizing my potential and supporting my academic journey.

My gratitude also goes to the National Research Council of Thailand (Grant no. N41A640127 and N42A650551) and the Research and Creative Fund of the Faculty of Pharmacy at Silpakorn University for their crucial financial support. I am honored by their confidence in the significance of this study. Additionally, I thank the Faculty of Pharmacy at Silpakorn University for providing facilities, instrumental support, and dedicated staff.

Special appreciation goes to my seniors, juniors, and colleagues from the Pharmaceutical Development of Green Innovation Group (PDGIG), especially Mrs. Areerut Sripattanaporn, for their camaraderie, inspiration, and practical assistance. Their

collective knowledge and collaboration have greatly aided my personal and academic growth.

Lastly, I express my heartfelt thanks to my beloved family and friends. Their constant support, endless encouragement, and unwavering belief in me have been the cornerstones of my journey, providing the strength and perseverance needed to complete this academic endeavor.

Khin Cho AYE

TABLE OF CONTENTS

Page

LIST OF TABLES

Page

LIST OF FIGURES

Page

LIST OF ABBREVIATIONS

%	Percent
%EE	Percent entrapment efficiency
%SW	Percent swelling
®	Registered trademark
°C/min	Degree Celsius per minute
µg	Microgram
µg/mg	Microgram per milligram
µg/mL	Microgram per milliliter
µL	Microliter
µm	Micrometer
µm/h	Micrometer per hour
ºC	Degree Celsius
^{1}H-NMR	Proton nuclear magnetic resonance spectroscopy
3D	Three dimensional
Abs	Absorbance
ANOVA	Analysis of variance
ATR-FTIR	Attenuated total reflection Fourier-transformed infrared
BCS	Biopharmaceutical Classification System
CFU/mL	Colony forming unit per milliliter
CHO	Cholesterol
cm^2	Square centimeter
CO_2	Carbon dioxide

Conc	Concentration
CS	Chitosan
Cur	Curcumin
Cur-L	Curcumin liposome
Cur-NS	Curcumin nanosuspension
DC	Degree of crosslinking
DMEM	Dulbecco's Modified Eagle Medium
DMSO	Dimethyl sulfoxide
DoE	Design of experiments
DPPH	2,2-Diphenyl-1-picrylhydrazyl
DSC	Differential scanning calorimetry
e.g.	Example
ECM	Extracellular matrix
EGF	Epidermal growth factor
Eq.	Equation
ES	Erosion
FGF	Fibroblast growth factor
Fig	Figure
g	Gram
g/cm^2	Gram per square centimeter
g/m^2/24 h	Gram per square centimeter per 24 h
h	Hour
H_2O	Water

HA	Hyaluronic acid
HPLC	High-performance liquid chromatography
IC50	The half-maximal inhibitory concentration
IL-1	Interleukin-1
ITA	Itaconic acid
kDa	Kilodalton
Kg	Kilogram
LC	Loading capacity
Log P	Partition coefficient
LPS	Lipopolysaccharide
MBA	N, N'-methylene bis-acrylamide
mg	Milligram
mg/g	Milligram per gram
mg/kg	Milligram per kilogram
mg/mL	Milligram per milliliter
min	Minute(s)
mL	Milliliter
mm	Millimeter
mM	Millimolar
mm/s	Millimeter per second
mm^2	Square millimeter
MMP	Matrix metalloproteinase
MS	Mechanical strength

MTT	3-[4,5-dimethylthiazol-2-yl]-2,5 diphenyl tetrazolium bromide
mV	Millivolts
MW	Molecular weight
MWCO	Molecular weight cut-off
n	Numbers
NHF	Normal human foreskin fibroblasts
nm	Nanometer
NPs	Nanoparticles
NS	Nanosuspension
NVP	N-vinyl pyrrolidone
O_2	Oxygen
PBS	Phosphate buffer saline
PC	Phosphatidylcholine
PDGF	Platelet-derived growth factor
PDI	Polydispersity Index
PNVP-ITA	Poly(vinylpyrrolidone-co-itaconic acid)
ppm	Parts per million
PVA	Polyvinyl alcohol
PVP	Polyvinylpyrrolidone
PXRD	Powder X-ray diffraction
R^2	Regression coefficient
RH	Relative humidity
ROS	Reactive oxygen species

RPM	Round per minute
S.aureus	Staphylococcus aureus
SD	Standard deviation
SEM	Scanning electron microscopy
TEM	Transmission Electron Microscopy
TGF-β	Transforming growth factor-β
TNF-α	Tumor necrosis factor- α
TSA	Trypticase soy agar
TSB	Tryptic soy broth
UV	Ultraviolet
UV-vis	Ultraviolet-visible
v/v	Volume by volume
V50	2,2'-Azobis(2-methylpropionamidine) dihydrochloride
w/v	Weight by volume
w/w	Weight by weight
WVTR	Water vapor transmission rate

CHAPTER 1
INTRODUCTION

1.1. Statement of the problem and its significance

The skin, the outermost layer of the body, is susceptible to injuries due to its protective functions against the environment. Skin injuries, such as bruises, ulcers, and cuts, generally heal efficiently through a well-regulated healing process. Approximately, 300 million people suffer from severe acute wounds including burns, traumatic, and surgical wounds, and face challenges in healing completely. The healing processes are often interrupted by various factors such as infections, foreign bodies, hypoxia, or metabolic issues of the wound microenvironment, leading to chronic or non-healing wounds (1). The rising prevalence of chronic wounds globally is a concerning trend. This increase is primarily due to the intricate healing challenges in patients with conditions such as aging, diabetes, obesity, and persistent infections. The global advanced wound care market is estimated to reach $18.7 billion by 2027 (2). The growing number of severely acute and chronic wounds and associated costs impact the health care system and quality of life.

Wound dressings play a vital role in achieving rapid and complete wound healing, there is a massive rising demand for new and effective wound dressing materials ensuring effective wound management and optimal recovery. Traditional dressings have been used to stop bleeding, absorb fluids, and protect wounds from harm. However, they provide limited benefits for wound closure and infection prevention. Moreover, their strong adherence to the wound surface may lead to further lesions to new tissue during the removal of the dressing. As they rely on a passive healing approach, the extensive use of these materials is unreliable in managing chronic or hard-to-heal wounds (3). Advanced dressings such as hydrogel, film, foam, and hydrocolloid have been developed to accelerate the wound healing process, avoid wound complications, and enhance patient compliance. Fundamentally, these dressings provide a moist environment around the wound to reduce scar formation and aid cell migration, facilitating the healing process (4). Among advanced dressings, hydrogels have gained great interest in the development of innovative wound dressings to address the challenges in wound care.

Hydrogels possess a porous and hydrated three-dimensional (3D) polymeric network that mimics natural soft tissues, providing an environment beneficial to wound healing. Hydrogels create a moist environment around the wound, which is important for rapid healing. Hydrogel dressings offer soothing and cooling effects, providing pain relief for the patient. Hydrogels can absorb significant wound exudate, maintain a clean wound bed, and prevent infections. Hydrogels exchange gases like CO_2, O_2, and H_2O, enabling the wound tissues to breathe (5). Their network structures enable the incorporation of various biomolecules and active compounds, facilitating controlled or efficient drug delivery. Their versatility makes them a promising dressing material for developing wound care solutions. Hydrogel networks can be formed by the chemical or physical crosslinking between a wide range of natural or synthetic polymeric chains. The choice of polymers and crosslinking strategies is crucial in designing a hydrogel. Natural polymers are the preferred choice for hydrogel synthesis due to their intrinsic biocompatibility and immunomodulatory properties, which aid in wound repair. Chitosan (CS), a natural cationic polysaccharide obtained from partial deacetylation of chitin, is attractive as a promising dressing material. This is due to its abundant natural source and its biocompatibility, cellular binding capacity, wound healing, and antimicrobial activity (6). Hyaluronic acid (HA) is a biopolymer composed of repeated disaccharide units of glucuronic acid and N-acetylglucosamine. Its hydrophilic properties allow it to form a 3D network, enabling the gradual release of encapsulated active compounds. HA has excellent biocompatibility and biological functions, such as promoting keratinocyte migration and angiogenesis, contributing to wound healing without scarring (7). Biopolymer hydrogels often lack the mechanical strength and stability required for specific wound types, particularly deep or heavily exudating wounds. Adding synthetic polymers to the network is often necessary to address this limitation. This approach combines the desirable biological and chemical properties of polysaccharides and synthetic polymers, resulting in wound dressings that exhibit superior mechanical strength and biological functionality. The selected synthetic polymers for this study are polyvinylpyrrolidone (PVP) and polyvinyl alcohol (PVA). PVP is a nonionic, synthetic polymer known to confer high polarity, cross-linkable due to its structure. PVP hydrogels have been attracted for controlled drug release systems, wound dressings, as they are biological inert, biocompatible (8). PVA is a synthetic

biocompatible polymer that has been employed as the main component of several hydrogel dressings, owing to its relatively high mechanical strength, water retention, and gel-forming characteristics (9). Regarding crosslinking techniques, genipin-crosslinked chitosan hydrogels have gained attention due to the growing demand for biocompatible hydrogels. Genipin, a biological extract, obtained from gardenia fruit has low toxicity compared to other chemical crosslinkers such as glutaraldehyde (10). It is also known as an effective crosslinker for polymers containing amino groups like chitosan. The freeze-thaw process is indeed a popular physical cross-linking method for creating hydrogels. It is known for its simplicity as it does not require special techniques, instruments, or reagents. This method can result in hydrogels with high biocompatibility, excellent mechanical properties, a good swelling ratio, and non-toxic characteristics. It's a cost-effective and straightforward way to create hydrogels with desirable properties (11). In contrast, chemical crosslinking creates stronger bonds within the hydrogel network, resulting in improved mechanical strength and stability of physical hydrogels. Thus, the metal coordination complex is a safe chemical cross-link procedure suitable for biomedical applications (12). Polymers rich in hydroxyl, carbonyl, and carboxyl groups facilitate the formation of metal-coordinate covalent bonds, resulting in a compact hydrogel with enhanced toughness and durability, making it suitable for wound healing (13).

Treatment of chronic and severely acute wounds requires active interventions, including either drugs or bioactive molecules integrated into the dressing or the dressing material. There is increasing interest in plant-derived bioactive compounds because of their lower side effects and diverse biological properties for wound healing. One potent natural compound is curcumin (Cur), derived from *Curcuma longa Linn*. Due to their importance in wound healing, Cur has been extensively studied for its bio-functional properties, containing antioxidant, radical scavenging, antimicrobial, and anti-inflammatory activities, all crucial for wound healing (14-16). Moreover, it has been reported that topically administered Cur stimulates the production of growth factors essential in the wound healing process. It accelerates angiogenesis and facilitates rapid wound restoration (15, 16), which results from various types of wounds, such as trauma (17), burns (18), and diabetes wounds (19). Despite its promising attributes, Cur has

limitations related to poor solubility and instability when exposed to light, hindering its bioavailability and efficacy in wound care. Nanoformulation emerges to overcome these obstacles, offering a stable Cur form while enhancing its photostability and water solubility as well as the pharmacological response to achieve its action on wound healing. Incorporated nanoformulation of Cur in hydrogel could provide dual functions of the dressing material from the effect of hydrogel and the bioactivities of Cur. Moreover, nanomaterial-based wound dressings are essential in treating wounds and are used across various medical settings, from minor to life-threatening injuries.

Recently, many studies have been reported on the wound healing efficiency of Cur-loaded nanocomposite hydrogels utilizing a range of nanoparticle carriers and hydrogel designs. M. Alibolandi et al. developed a dextran hydrogel incorporating curcumin-nano micelles composed of PEG-PLA copolymers for full-thickness dermal wound healing (20). They reported the sustained release of curcumin-nano micelles from the hydrogel resulted in decreased inflammatory responses, induced fibroblast proliferation, and promoted collagen synthesis and angiogenesis in the healing process (20). Cardoso-Daodu and co-workers synthesized Cur-loaded liposomes infused in lysine-collagen hydrogel to enhance surgical wound healing. The *in vivo* wound healing evaluation exhibited superior healing performance, with 79.2% wound contraction at day 3 and complete wound closure by day 7 with no scarring (21).

The stability of nanoformulation and the physicochemical properties of hydrogels are broadly affected by various formulation parameters, such as surfactant types, their concentrations, and polymer composition (22). Thus, the optimum conditions which provide stable nanocurcumin and proper hydrogel properties are observed using experimental design techniques before the incorporation of nanocurcumin into the hydrogels. The Design of experiments (DoE) aims to determine the main interaction effects of parameters and reduce development time and the number of experiments.

In this study, two nanocomposite hydrogel patches were developed including Cur-NS-loaded CS/PVP and Cur-L-loaded HA/PVA/PNVP-ITA hydrogels, aiming for innovative wound repair solutions. Using a Box-Behnken design approach, we optimized the formulations of Cur-NS and Cur-L, to ensure their stability and efficacy. On the other hand, the genipin-crosslinked CS/PVP and bifunctional crosslinked

HA/PVA hydrogel formulations were optimized through a simplex centroid mixture design and central composite design. A synthesized PNVP-ITA polymer was added to the post-optimized HA/PVA hydrogel to enhance its properties for better functionality. Subsequently, optimal hydrogel patches were used to incorporate various concentrations of nanocurcumin, selecting those with the maximal loading capacity for further investigations. These nanocomposite hydrogels were thoroughly analyzed to assess their physiological and morphological attributes and release profiles. Additionally, the therapeutic efficacy and safety of these hydrogel patches were evaluated on incisional wounds in Wistar rats were evaluated, exploring their potential to enhance the wound healing process.

1.2. Objectives

1. To prepare and optimize nanocurcumin and polymeric hydrogel patches with desired characteristics and properties for wound healing applications using Design Expert® software.
2. To characterize nanocurcumin-incorporated hydrogel patches for their hydrogel properties, morphology, and release kinetics of Cur from the hydrogels.
3. To evaluate their *in vitro* biocompatibility and *in vivo* wound healing efficiency of Cur-loaded nanocomposite hydrogels treated to an incisional wound of Wistar rats.

1.3. Hypothesis

1. Optimized nanocurcumin can be loaded into the optimized hydrogel patches with enhanced loading efficiency and release performance.
2. The developed Cur-loaded nanocomposite hydrogels have desirable properties, morphology, and biocompatibility.
3. The greater progression of wound healing can be found in Wistar rats treated with nanocomposite hydrogels compared to controls (sterile gauze and commercial wound healing patch).

1.4. Scope of research work

1. Preparation and optimization of nanocurcumin using Box-Behnken design.

- Curcumin nanosuspension (Cur-NS) was prepared using a bottom-up approach, and curcumin liposome (Cur-L) was prepared using a thin-layer hydration method.
- The optimized Cur-NS and Cur-L were further characterized for their physio-chemical stability, morphology, and chemical interactions using Nano-sizer, content assay, DSC, PXRD, and FTIR. After that, their antioxidant and wound healing activity were evaluated using DPPH and Scratch assays.

2. Preparation and optimization of hydrogel patches using Mixture and Central Composite design.
   - CS/PVP hydrogel was prepared by crosslinking using genipin, a natural crosslinker, and its properties were analyzed to obtain the optimal formulation.
   - HA/PVA hydrogel was prepared using dual crosslinking methods: freeze-thaw cycling and metal coordination complexation with a small amount of the crosslinker aluminum glycinate and malic acid. The newly synthesized copolymer PNVP-ITA (polyvinylpyrrolidone-co-itaconic acid) was added to the optimized hydrogel formulation to enhance its properties.
3. Fabrication, characterization, and evaluation of nanocomposite hydrogels.
   - Cur-NS was incorporated into the genipin-crosslinked CS/PVP hydrogels by direct incorporation of Cur-NS into the polymeric solution during the mixing stage.
   - Cur-L was loaded into the HA/PVA/PNVP-ITA hydrogels by absorption method.
   - The developed nanocomposite hydrogels were characterized by their swelling, mechanical toughness, WVTR, morphology, loading efficiency, and release kinetics.
   - *In vivo* wound healing activities of both nanocomposite hydrogels were evaluated using an incisional wound model in Wistar rats.

CHAPTER 2
LITERATURE REVIEWS

2.1. Wound

2.1.1. Definition and etiology

A wound is an injury to the body that typically involves breaking the skin and often damages the underlying tissues, disrupting its anatomical structure and functions. The wound can be superficial to the dermis or sometimes full thickness into the dermis, subcutaneous, and even muscle or bone, which may be caused by violence, accidents, or surgery. Immediately after injury, the human body responds with a complex cellular process consisting of four overlapping cascades: hemostasis, inflammation, proliferation, and maturation, aiming to restore the functions of injured tissue (23).

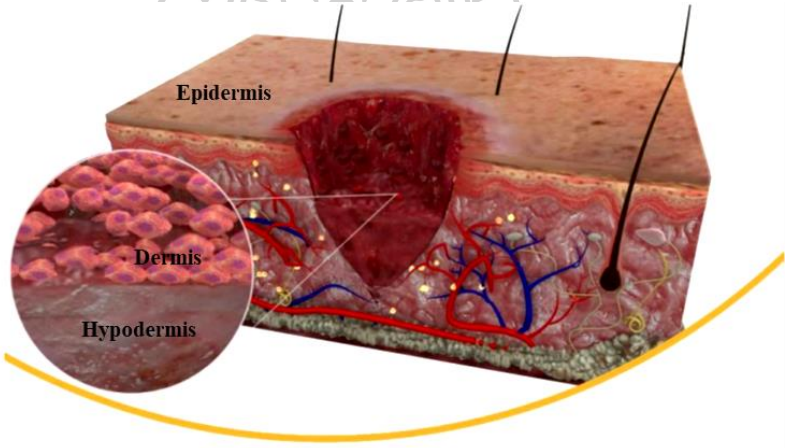

Figure 1. The image of a skin wound *(24)*

2.1.2. Wound healing processes

2.1.2.1. Hemostasis

The initial phase of wound repair is hemostasis, where damaged blood vessels constrict rapidly. Platelet aggregation and fibrin clot formation stop bleeding. Following initial vasoconstriction, vasodilation occurs, allowing the influx of pro-inflammatory cytokines and growth factors like transforming growth factor (TGF-β), platelet-derived growth factor (PDGF), fibroblast growth factor (FGF) and epidermal growth factor (EGF). Platelets are crucial for recruiting immune cells to the injury site and initiating inflammation (23, 25, 26).

2.1.2.2. Inflammatory

The second stage, inflammation, begins shortly after injury. Neutrophils, attracted by chemo-attractants such as interleukin-1 (IL-1), tumor necrosis factor-alpha (TNF-α), and bacterial endotoxins like lipopolysaccharide (LPS), are recruited into the wound from damaged vessels. They release reactive oxygen species (ROS), antimicrobial peptides, and proteolytic enzymes, clearing bacteria and necrotic tissue via phagocytosis. Macrophages follow, releasing inflammatory cytokines and growth factors that stimulate neo-angiogenesis and activate keratinocytes, fibroblasts, and endothelial cells. Excessive inflammation delays healing, while insufficient immune cell recruitment hinders repair (23, 25, 26).

2.1.2.3. Proliferation

The proliferative healing phase is characterized by extensive activation of keratinocytes, fibroblasts, macrophages, and endothelial cells to orchestrate wound closure, matrix deposition, and angiogenesis. Keratinocytes migrate laterally across the wound to reform the epidermal layer, releasing matrix metalloproteinase (MMP) to aid their migration path. Fibroblasts are the main cell type responsible for granulation tissue formation. The TGF-β and PDGF guide fibroblasts to either become pro-fibrotic, producing extracellular matrix (ECM) proteins, or differentiate into myofibroblasts, which facilitate wound contraction. Macrophages play a significant role in angiogenesis by aiding microvascular endothelial cell proliferation, migration into the wound bed, and collagen deposition (23, 25, 26).

2.1.2.4. Maturation

In the maturation phage, epidermal tissue reorganization occurs through collagen replacement. MMPs help in the degradation of collagen type III and synthesis of collagen type I. These sequential changes in the ECM require a fine balance between collagen degradation and synthesis, achieved through temporal regulation of key MMPs. Once collagens type I are highly organized, increasing the integrity and tensile strength of the wound (23, 25, 26).

2.1.3. Acute and Chronic wounds

Wounds are generally classified as acute or chronic based on the nature and duration of the healing process. Acute wounds result from unexpected accidents or surgical procedures, and their healing process follows a predictable time based on factors such as size, depth, and the extent of damage to various layers of the skin. Chronic wounds may develop when the healing process fails to heal within a fixed time, and the inflammatory phases persist for a long time. Prolonged and increased levels of inflammatory cells can damage tissues due to an imbalance between MMPs and their corresponding tissue inhibitor metalloproteinases, especially during the tissue formation. Excessive protease activity in the wound results in the breakdown of essential proteins required for ECM formation, ultimately hindering the healing process. Chronic wounds are mostly caused by repeated tissue insults or underlying physiological conditions like diabetes, impaired angiogenesis, and patient-related factors (1, 27).

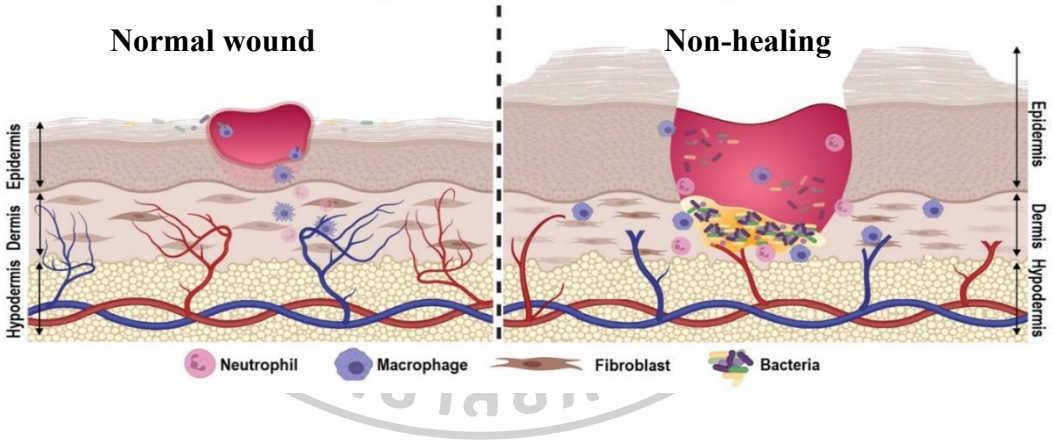

Figure 2. Pathophysiology of normal and chronic or non-healing wounds (28)

2.2. Wound dressings

2.2.1. What are wound dressings?

A wound dressing is a clean and sterile pad applied over a wound. It is designed to be in direct contact with the wound surface. The purpose of the dressing is not only to cover or protect the wound from further harm but also to promote natural healing.

2.2.2. Wound dressings treatment

The management of wounds dates back to ancient Egyptian times when grease-soaked gauze bandages were used. Traditionally, gauze has been a widely used dressing

for mechanical wound protection. It aids in rapidly drying the wound surface but is permeable to bacteria and can be adherent, potentially causing trauma upon removal (29). Due to these challenges, Professor George D. introduced the moist wound healing theory concept in 1962 (30). He demonstrated that a moist environment significantly accelerates tissue regeneration by promoting wound epithelialization. Later, researchers emphasized the importance of developing dressings that do not adhere to damaged tissues. They also highlighted the significance of dressings with absorbent capabilities to remove excess exudate (31). Generally, ideal wound dressings should meet various requirements to manage different types of wounds effectively.

Table 1. Characteristics required for an ideal wound dressing

Feature	Description
Moisture	Regulating the moisture level around the wound to promote cell migration and proliferation.
Absorption of excess exudate	Eliminating excess exudate present in the wound to avoid the potential of infections.
Gases permeability	Allowing the transmission of gases like O_2, enabling the wound tissues to breathe for cell activity.
Adhesiveness	Providing appropriate adhesiveness to the wound site (excessive adhesive sustains an injury)
Prevention of wound infections	Protecting bacterial infections could impair wound healing and prolong its duration.
Minimum pain	Minimizing patient pain during application and removal.
Mechanical and physical properties	Offering mechanical protection and resembling the nature of native skin.
Non-toxic, Biocompatible	Free from toxic materials that can damage and lead to dire consequences
Costly acceptable	Providing an affordable wound dressing

2.2.3. Types of wound dressings

2.2.3.1. Passive dressings

Passive dressings are wound coverings that primarily serve as a protective barrier over the wound. They are designed to provide a physical barrier against external contaminants, absorb wound exudate, and maintain a moist environment conducive to the natural healing process. Passive dressings do not actively interact with the wound

bed or influence the wound healing process beyond providing a sterile and moist environment (32). Examples of passive dressings include gauze, non-adherent dressings, and some types of film and foam dressings.

2.2.3.2. Interactive dressings

Interactive dressings, also known as advanced or interactive wound dressings, are designed to actively interact with the wound environment to promote healing (32). These dressings often contain additional substances such as hydrogels, alginates, antimicrobial agents, growth factors, or enzymes that facilitate wound healing. Interactive dressings can help maintain a balanced moisture level, absorb excess exudate, provide a conducive environment for cell migration and tissue regeneration, and may have antimicrobial properties to prevent infections. These dressings actively participate in wound-healing and can be particularly useful for chronic or complex wounds (33). Examples of interactive dressings include hydrogels, hydrocolloids, foam dressings, and semi-permeable film dressings.

2.2.3.2.1. Film dressings

Transparent film dressings can be considered the evolution of gauzes into more sophisticated bandages, being able to provide a moist wound environment simultaneously, ensure gas exchange and prevent contamination from external bacteria. Moreover, film dressings are easy to adapt and remove without causing the patient pain. However, they do not possess swelling capability, and thus, their application is not recommended for the treatment of wounds that produce large amounts of exudate (29, 33, 34).

2.2.3.2.2. Foam dressings

Conversely to transparent film dressings, foam dressings can absorb large amounts of fluids while ensuring thermal insulation and gas exchange. Hence, foams are indicated for the treatment of exudate-rich wounds. Due to their remarkably high absorbance capability, this type of dressing could be left in place for up to 7 days in not-infected wounds, while daily changes are recommended in the presence of infections. Many research studies have reported the design of foams for wound healing applications, mainly focusing on identifying the highest-performance material in absorption capability (29, 33, 34).

2.2.3.2.3. Hydrocolloid dressings

Hydrocolloids are occlusive dressings with two layers: the inner one contains a suspension of hydrophilic colloidal particles designed to balance moisture, and the outer polyurethane layer is impermeable to bacteria. They combine gel-forming agents (carboxymethylcellulose, gelatin, and pectin) with other materials, such as elastomers and adhesive coatings, which may potentially cause dermatitis. Due to their nature, hydrocolloids are best used on dry wounds, and they can be applied for several days without changing due to the inner layer being able to hold and maintain fluid. However, this type of wound dressing is not recommended for infected wounds due to their occlusive properties and strong adhesive properties, which are possible for reinjury of the wound tissues during removal (29, 33, 34).

2.2.3.2.4. Hydrogel dressings

Hydrogel-based wound dressings are widely used in wound care treatments because they absorb fluids, facilitate gas exchange (O_2, CO_2, and H_2O), and painlessly adhere to the wound. Being composed of 80-90% water, hydrogels maintain a moist wound environment, aiding autolytic debridement and accelerating cellular healing. Their similarity to ECM ensures biocompatibility and their unique structure allows for incorporating phytochemicals and biomolecules, providing additional therapeutic benefits. These features support cells and enhance healing, leading to faster and more effective wound resolution. Consequently, a significant surge in research interest has focused on developing innovative hydrogel dressings for wound healing applications (31, 33, 34).

2.3. Nanocomposite hydrogel wound dressings

2.3.1. Hydrogels

2.3.1.1. What are hydrogels?

Hydrogels are 3D hydrophilic polymeric networks with a porous and water-insoluble matrix. The presence of hydrophilic functional groups such as amine ($–NH_2$), carboxylic (–COOH), sulfate ($–SO_3H$), and hydroxyl (–OH) groups in their structure enables them to absorb water or biological fluids ten to thousands of times of their dry weight. Their crosslinked polymeric structure can retain their structural integrity from dissolving in water (35).

2.3.1.2. Hydrogel properties for wound healing

2.3.1.2.1. Biocompatibility

Since hydrogel dressings are designed to be directly applied on the wound surface, it is important to be non-toxic and free from foreign body response. Thus, biocompatibility is the primary property of hydrogel dressing for wound healing applications. To achieve biocompatible hydrogel, a hydrogel can be prepared using biocompatible components such as high-purity polymer solutions and biocompatible techniques of harmless conditions to avoid unexpected toxicity (36, 37).

2.3.1.2.2. Adhesiveness and removability

Hydrogels in wound dressings need firm adhesion to create a protective environment, preventing fluid leakage and bacterial infections. Like those formed through Schiff base reactions, adhesive hydrogels provide substantial strength by binding aldehyde and tissue amino groups, ensuring effective wound coverage and healing. Hydrogel wound dressings, requiring periodic changes for optimal efficacy and infection prevention, must be easily removable without causing damage to newly formed wound tissue (36, 37).

2.3.1.2.3. Mechanical property

Different types of wounds need appropriate mechanical properties: stiffness, toughness, stretchability, and compressibility, not only to ensure comfort and convenience of wearing dressings but also to regulate the healing process. The mechanical properties of hydrogels can be controlled by adjusting the polymer type, concentration of polymer used, the presence of network structure, and formulation techniques. The mechanical properties of hydrogel dressings are assessed through compression strength and modulus (Young's modulus), tensile strength, and percent elongation at break (36, 37).

2.3.1.2.4. Swelling ability

The ability of hydrogel dressings to swell in water or biological fluids without dissolving or compromising their structural integrity is a crucial property. Swelling enables absorption of wound exudate, maintains moisture, aids in debridement, facilitates nutrient diffusion, and allows drug release. The swelling rate is influenced

by utilized biomaterial properties, hydrophilic groups, crosslinking agents, and density. The gravimetric method often determines a swelling index (36, 37).

2.3.1.2.5. Gases permeability

The highly porous hydrogel structure facilitates the perfusion of gases like CO_2, O_2, and H_2O, which is crucial in accelerating cell activity in wound tissue. This property is vital for regulating the moist environment around the wound, allowing moisture to pass through the dressing material, and controlling water loss during wound healing (36, 37).

2.3.1.3. Preparation of hydrogels

Hydrogels can be prepared from a variety of natural and synthetic polymers using a range of different compositions. The polymer chains are interconnected via physical and chemical cross-linking techniques, forming covalent bonds and non-covalent bonds such as ionic interactions, hydrogen bonds, or hydrophobic interactions.

2.3.1.4. Common polymers used for hydrogel preparation

Synthetic and natural polymers have been utilized widely to develop hydrogel dressings. As wound dressings require low toxicity, excellent biocompatibility, and enhanced cell migration, natural polymers become a research focus point. Commonly studied natural polymers for hydrogel preparation include chitosan, collagen, starch, cellulose, sodium alginate, and hyaluronic acid (5). However, the mechanical limitations of natural polymers have led to their combination with synthetic polymers and other materials to improve their mechanical properties. Synthetic materials such as polyethylene glycol (PEG), PVA, polyacrylamide (PAA), PVP, and poly (ε-caprolactone) (PCL) offer specific functionalities, robust mechanical properties, affordability, and a wide range of options (38). Using pre-functionalized polymers and/or cross-linkers is another strategy. Cross-linkers are small and multi-functional molecules that can react with the functional groups of natural polysaccharides (hydroxyl, carboxylic acid, or amino groups).

2.3.1.4.1. Chitosan

CS is a cationic polysaccharide consisting of β-(1-4)-D-glucosamine and *N*-acetyl-D-glucosamine groups, obtained from partially deacetylated chitin found in

crustacean shells. Owing to its intrinsic properties: antifungal, antibacterial, hemostatic, and promoting cell growth, it has been widely studied as a polymeric backbone in hydrogel development for wound treatments. chitosan promotes platelet aggregation and fibrin clot formation through electrostatic interactions. It also disrupts bacterial cell walls, inhibiting their proliferation. Additionally, chitosan stimulates cytokine production, including TGF-β and IL-1, enhancing fibroblast growth and collagen production (39). However, the primary limitation hindering the use of CS in wound repair is its insufficient mechanical strength. Thus, CS needs to be crosslinked, either physically or chemically, to form a stable hydrogel. While physical hydrogels offer certain advantages, their networks are reversible and unstable. There is a growing interest in using biologically safe crosslinkers like genipin in chemically crosslinked hydrogels. An important feature of genipin is its high selectivity, specifically reacting to the primary amino groups (NH_2) present in CS (40).

2.3.1.4.2. PVP

PVP is a nonionic synthetic polymer usually obtained through free radical polymerization of *N*-vinylpyrrolidone (NVP) in water with hydrogen peroxide as an initiator. PVP is widely used in hydrogel dressing materials due to its biological inertness and biocompatibility. Its high polarity and ability to accept protons make it cross-linkable, forming chemical complexes (41). PVP hydrogels are transparent and exhibit good adhesive and cohesive properties, although they might have limited swelling. This can be improved by blending it with other polymers like polysaccharides.

2.3.1.4.3. Hyaluronic acid

HA is an attractive biopolymer composed of repeating di-saccharide units of D-glucuronic acid and *N*-acetyl-D-glucosamine, linked by β-1,4-glycosidic linkages. It is produced through microbial fermentation. HA is a primary component of mammalian connective tissue, making it a valuable biomaterial for wound dressings (42). It possesses inherent bacteriostatic properties and contributes to wound healing by reducing inflammation, stimulating endothelial cell proliferation, angiogenesis, keratinocyte migration, and supporting scar-free wound healing. Additionally, HA is non-irritating, non-reactive with biological tissue, and permeable to metabolites (39). However, HA-based hydrogels exhibit limitations, such as low mechanical strength and

rapid degradation. Thus, researchers have been exploring various strategies to enhance HA-hydrogels' features. Wu et. al., (2017) used ethylene dichloride (EDC) to facilitate the crosslinking of HA with gelatin, aiming to promote hydrogel properties and enhance wound healing efficiency (43). Fahmy et. al., (2015) developed an ampicillin-loaded PVA-HA hydrogel membrane using the freeze-thawing method. Their observation revealed that the low content of HA (up to <20%) in the PVA network improved the physiochemical properties and biological activity of the membrane (44). Therefore, this study specifically focuses on the freeze-thawing technique due to its non-toxic nature and widespread use. During the freeze-thaw cycle, the polymer solution undergoes freezing, inducing crystal growth that acts as cross-linking points between polymer chains and/or crosslinkers. Thawing then relaxes the polymer chains, allowing them to move freely and form a 3D structure with increasing cross-link points. Moreover, small quantities of aluminum glycinate and maleic acid could be incorporated as crosslinkers, forming HA and PVA networks to attain favorable hydrogel properties for wound applications.

2.3.1.4.4. PVA

PVA is a synthetic biocompatible polymer employed as the main component of several hydrogel dressings owing to its relatively high mechanical strength, water retention, and good transparency. Also, the hydroxyl group of the alcohol moiety can be crosslinked to form PVA hydrogel by different crosslinking techniques including the freeze-thawing cycle, electron beam irradiation and using cross-linkers like glutaraldehyde (45).

2.3.2. Nanocurcumin

2.3.2.1. Curcumin

Turmeric is a popular spice derived from the rhizomes of *Curcuma longa Linn*, belonging to the ginger family. The main constituent of turmeric is Cur, also known as diferuloylmethane, with a chemical structure of 1,7-bis(4-hydroxy-3-methoxyphenyl)-1,6-heptadien-3,5-dione. Cur is a yellowish polyphenol compound with a long history of use as an antimicrobial, anti-inflammatory, and wound-healing agent. Its popularity is attributed to its safety, cost-effectiveness, and multifunctional biological activities, including anti-inflammatory, antioxidant, anticarcinogenic, and anti-infectious

properties. Furthermore, the wound-healing properties of curcumin have received tremendous attention. It accelerates wound healing by exerting its action on various stages of wound repair (46).

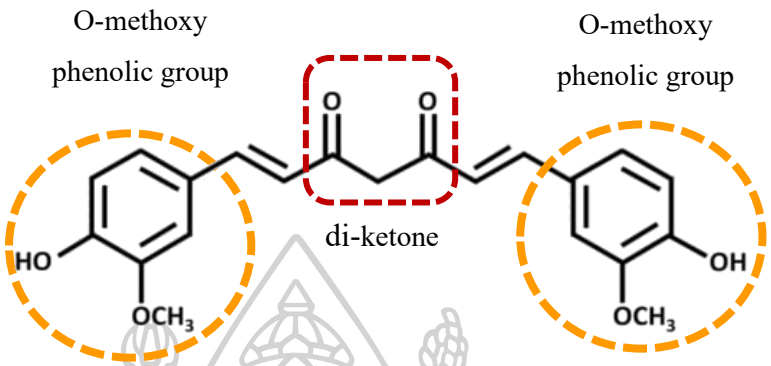

Figure 3. Chemical structure of curcumin (47)

2.3.2.2. Mechanism of wound healing activities of curcumin

Inflammation is a critical phase in the wound-healing process. Effectively controlling inflammation is highly desirable during healing; thus, curcumin's free radical scavenging and anti-inflammatory properties are particularly advantageous in accelerating wound healing. Cur has been reported to regulate various cellular signaling pathways and modulate gene expression (48). The presence of β-diketone and phenol functional groups in the structure of Cur confers excellent antioxidant properties. These properties are attributed to the stimulation of cytoprotective signaling pathways, including the nuclear factor erythroid 2-related factor 2 (Nrf2) pathway. These pathways have been identified as linked molecular mechanisms in wound healing that cause oxidative stress and increased ROS. Moreover, Cur inhibits the production of key inflammatory mediators such as IL-1, TNF α, and nuclear factor NFκB, essential in regulating genes causing inflammation. It also suppresses angiotensin II-induced inflammation by reducing cyclooxygenase-2 (COX-2) expression, prostaglandin, and thromboxane synthesis (49). Cur hinders the growth of microorganisms by disrupting the cell membrane and causing apoptosis, making it beneficial in treating infected wounds (50). Cur significantly enhances the proliferation phase of wound repair, including fibroblast proliferation, re-epithelialization, neovascularization, collagen deposition, granulation tissue formation, and the apoptosis of unwanted cells.

2.3.2.3. Challenges and improvements of curcumin activities

Chemically, Cur is a lipophilic, low MW compound (368.4 g/mL), soluble in organic solvents like ethanol, acetonitrile, and chloroform. It belongs to the Biopharmaceutical Classification System (BCS) class 2. The partition coefficient (Log P) is estimated to be 3.29, and its water solubility is about 0.6 μg/mL. It is a light-sensitive molecule. It is stable in acidic or neutral environments, while under alkaline conditions, it is easily degraded, leading to a change in color from yellow-orange to red (51).

Its physicochemical properties hinder its applications in wound healing despite its significant potential for repairing wounds. The poor water solubility, bioavailability, and instability upon exposure to light are the main obstacles to the effective delivery of Cur to wounds. Several new formulations like sponges (52), polymeric bandages (53), alginate foams (54), and collagen films (55) have been developed to achieve the application of Cur at the wound site. The Cur in these formulations was shown with increased bioavailability compared to raw curcumin. However, no significant differences in their wound healing effects were found, which may be due to Cur's burden of cell infiltration potential at the wound site. Therefore, the nano-formulation of Cur is an attractive option to maximize the wound-healing efficacy of such a beneficial compound. Encapsulation of Cur inside nanoparticles (NPs) like polymeric NPs (56), polymeric micelles (57), and liposomes (58), can provide a more stable form of Cur, protecting it from degradation against light, as well as improving water solubility, skin penetration, controlled delivery by chance of reduced dose, and low toxicity.

Nanosuspensions (NSs) are nanotechnology that form a nanosized drug particle and apply to most water-insoluble compounds. The NSs entirely consisted of poorly water-soluble drugs without any matrix material or carrier. The advantages of NSs are enhanced solubility and bioavailability, the possibility of dose reduction, and improved physical and chemical stability of the drugs (59). Moreover, the preparation methods include the “top-down” and “bottom-up” approaches which are simple, convenient, and yield a desirable NS formulation. Stabilizers, polymers, or surfactants are usually required for the preparation of NS for the compound would present steric with or

without electrostatic stabilization preventing the particle growth via Ostwald ripening or agglomeration (60). Several Cur-NS formulations have been reported for different purposes and using various stabilizers and preparation techniques. Bi et. al., (2017) reported the preparation of Cur-NSs with PVP as a stabilizer and investigated the cytotoxicity and cellular internalization for anticancer effect (61). An emulsion-templated freeze-drying technique was used to prepare Cur-NSs by Elbaz et. al., (2021) as a plausible oral delivery system (62). Yet, a proper design of the Cur-NS formulation has not been reported and the studies on Cur-NSs toward the wound healing effect are still limited.

Another nanocarrier approach is liposomes, which are lipid-based nanocarriers renowned for their ability to encapsulate hydrophobic compounds like Cur efficiently and their cutaneous delivery in wound therapy. Liposomes are spherical phospholipid bilayer nanoparticles that can entrap lipophilic molecules in their phospholipid bilayer, thus improving their solubility and protecting them from chemical instability (63). The liposomal membrane's fluidity can be altered by incorporating surfactants and unsaturated fatty acids, imparting elasticity. Elastic or deformable liposomes are new liposomes that can easily squeeze through the skin cells for better permeation (64). Moreover, modifying composition can tailor physicochemical properties like particle size and entrapment efficiency, thus directly affecting better efficacy in wound treatment. Taking advantage of all these merits, Xu et al. prepared a novel liposome with a hydrogel core of silk fibroin which effectively encapsulated bFGF. The vehicles remarkably improved the stability of bFGF in wound fluids and maintained cell proliferation activity compared to traditional liposomes. Moreover, the liposomes with hydrogel core expedited wound healing, particularly by promoting angiogenesis (65). Ternullo et. al., developed Cur-in deformable liposomes using polysorbate 20, stearyl amine, and sodium deoxycholate to attain elastic liposomes with different surface charges. All deformable liposomes exhibited relatively high Cur entrapment and optimal skin penetration, as well as superior anti-inflammatory and anti-bacterial qualities compared to conventional liposomes. Moreover, all liposomes were non-toxic to the human fibroblast cells and even promoted cell proliferation. Among the liposomes with different surface charges, cationic liposomes showed enhanced multi-

targeting properties (66). To the best of our knowledge, limited literature is available exploring incorporating Cur-Ls into hydrogel formulations, offering a tailored solution for effective and accelerated wound repair.

2.3.3. Nanocomposite hydrogels

2.3.3.1. What are nanocomposite hydrogels?

Nanocomposite hydrogel dressings are designed by incorporating nanomaterials into a polymeric hydrogel network. This combination results in a hybrid material that takes advantage of the synergistic properties of both the hydrogel and the incorporated nanomaterials (67). This can enhance properties such as mechanical strength, drug delivery capabilities, and wound healing activities, making them an area of active research and development in wound care.

2.3.3.2. Preparation of nanocomposite hydrogels

The uniform distribution of NPs or drug-loaded NPs in the hydrogel structure can be achieved by applying different approaches. NPs can be added to (a) pre-formed hydrogels, (b) polymer solutions before gel formation, and (c) monomer polymerization in the presence of NPs. It is also possible to incorporate NPs in the polymer network using strategies (a) and (b) (67).

The method choice depends on the application requirements and desired properties of the nanocomposite hydrogel, emphasizing the importance of stability and homogeneity in achieving optimal performance in various fields, including drug delivery, tissue engineering, and sensing technologies.

2.3.3.2.1. Incorporation of NPs into a pre-formed hydrogel matrix

The incorporation of liposomes into a hydrogel matrix after gelation, utilizing the absorption method, represents an innovative approach in drug delivery systems. After the hydrogel has solidified, pre-formed liposomes are gently introduced into the gel structure, allowing it to absorb the liposomes through its porous network (68). This method provides a stable environment for the liposomes, protecting their cargo and ensuring controlled release kinetics. The porous structure of the hydrogel offers an ideal substrate for liposome absorption, allowing for efficient encapsulation and enhancing the stability of the incorporated liposomes.

2.3.3.2.2. NPs addition to the polymer solutions and subsequently gelation

Incorporating nanosuspensions into polymer solutions, followed by gelation, is a promising approach in nanomedicine and drug delivery. In this method, nanosuspensions, which consist of nano-size particles dispersed in a liquid medium, are blended with polymer solutions. Subsequent gelation or cross-linking of the polymer solution entraps the nanosuspension within the resulting polymeric network (68). This strategy offers numerous advantages, including improved stability and controlled release of nanoparticles, making it valuable for targeted drug delivery systems.

CHAPTER 3
METHODOLOGY

3.1. Materials and Equipments

3.1.1. Materials

- 2,2′-azobis(2-methylpropionamidine) dihydrochloride (V50) (Sigma Aldrich St.)
- 2,2-diphenyl-1-picrylhydrazyl (DPPH) (Sigma Aldrich St.)
- Acetonitrile (Honeywell, USA)
- Cholesterol (Nanjing Xinbai Pharmaceutical Co., Ltd., Nanjing, China)
- Curcumin (Sigma-Aldrich St. Louis, MO, USA)
- Deuterium oxide (D_2O) (Cambridge Isotope Laboratories Tewksbury, MA, USA)
- Dimethyl sulfoxide (DMSO) (Fisher Chemical, Fisher Scientific, UK)
- Dulbecco's modified Eagle's medium (DMEM) (Gibco BRL, Rockville, MD, USA)
- Ethanol (Merck & Co. Darmstadt, Germany)
- Fetal bovine serum (FBS) (Gibco BRL, Rockville, MD, USA)
- Genipin (Sigma Aldrich, St. Louis, MO, USA)
- Human normal foreskin fibroblast (NHF) cells (ATCC, Rockville, MD, USA)
- Hyaluronic acid (HA, MW = 1,550 kDa) P.C. Chemicals (Bangkok, Thailand)
- Itaconic acid (ITA) (Sigma Aldrich, St. Louis, MO, USA)
- Methanol (Honeywell, USA)
- Methyl-thiazolyl diphenyl tetrazolium bromide (MTT), (Sigma Aldrich St. Louis, MO, USA)
- *N*-vinylpyrrolidone (NVP) (Sigma Aldrich, St. Louis, MO, USA)
- Oleic acid (Sigma Aldrich, St. Louis, MO, USA)
- Penicillin-streptomycin (Gibco BRL, Rockville, MD, USA)
- Phosphatidylcholine (Lucas Meyer GmbH, Düsseldorf, Germany)
- Pluronic® F-127 (Sigma Aldrich, St. Louis, MO, USA)
- Polyethylene glycol (PEG) 400 (Sigma Aldrich, St. Louis, MO, USA)
- Polyvinyl alcohol (PVA) (MW 60 kDa) (Merck & Co. Darmstadt, Germany)

- Polyvinylpyrrolidone (PVP) (MW 1,300 kDa) (Sigma Aldrich, St. Louis, MO, USA)
- Tryptic Soy Agar (TSA) (Himedia™)
- Tryptic Soy Broth (TSB) (Himedia™)
- Tween® 20 (P.C. Chemicals, Bangkok, Thailand)

3.1.2. Equipments

- Attenuated Total Reflectance Fourier transformed infrared spectrophotometer (ATR-FTIR) (Nicolet iS5, Thermo Scientific, USA)
- 15-mL, 50-mL centrifuge tube (Megazyme, Bray, Co. Wicklow, Ireland)
- 24-wells Cell Culture plate ((Costar®, Corning Incorporated, ME, USA)
- 6-wells Cell Culture plate ((Costar®, Corning Incorporated, ME, USA)
- 96-wells Cell Culture plate ((Costar®, Corning Incorporated, ME, USA)
- Aluminum foil
- Analytical balance (Model BSA3202S-CW, Sartorius)
- Autoclave (LS-2D, Scientific promotion. Co., Ltd.)
- Bath sonicator
- C18 column (Agilent Technologies, Senta Clara, CA, USA)
- CO_2 incubator
- Dialysis membrane (MW cut-off 3.5, 6-8 kDa) ((Fisher Chemical, Fisher Scientific, UK)
- Differential scanning calorimeter (DSC) (Sapphire, Perkin Elmer, USA)
- Freeze dryer (FreeZone2.5, LABCONCO, USA)
- Gloves and masks
- High-performance liquid chromatography (HPLC; Agilent Technologies, 2200 series, Santa Clara, CA, USA)
- Incubator shaker (Model: GFL 3031, ProfiLab24 GmbH, Berlin, Germany)
- Inverted fluorescence microscope (Nikon® T-DH, Japan)
- Magnetic stirrer and magnetic bars
- Micropipette tip (200 µL, 1000 µL)
- Microplate reader (VICTOR Nivo TM, Perkin Elmer, MA, USA)

- Microcentrifuge tube (1.5 mL, 2 mL)
- Nuclear magnetic resonance spectroscopy (^{1}H-NMR) (Bruker AVANCE III HD, Billerica, MA, USA).
- Nylon syringe filter (0.22 µm, 0.45 µm) (SNP Scientific Co., Ltd, Bangkok)
- ONILAB Vortex Mixer (Bio Laboratories Pte Ltd, USA)
- pH meter (HORIBA compact pH meter B-212)
- Probe Sonicator (Sonic VibraCell™, CT, USA)
- Rotary evaporator (R-100, Buchi, Japan)
- Scanning electron microscope (SEM) (Tescan Mira 3, Czech Republic series, Santa Clara, CA, USA)
- Texture analyzer (TA. XT Plus, Stable Micro Systems, Godalming, UK)
- Thermometer
- Transmission electron microscope (TEM) (Philips® Model TECNAI 20)
- Universal Oven (Model: XU032, France-Etuves Asia Co.,Ltd)
- X-ray diffractometer (XRD) (Mini Flex 150 II, Rigaku, Tokyo, Japan)
- Zeta sizer (Nano ZS series, Malvern Instruments, Malvern, UK)

3.2. Preparation and optimization of nanocurcumin using Box-Behnken design

3.2.1. Curcumin Nanosuspension

3.2.1.1. Experimental design

A Box-Behnken factorial design was utilized to statistically assess the main, interaction, and quadratic effects of independent variables on dependent variables for optimizing the Cur-NS formulation. The independent variables include the stabilizers measured responses were particle size (Y_1), polydispersity index (PDI) (Y_2), zeta potential (Y_3), and Cur content yielded (Y_4). The experimental design used DesignExpert® software version 11.0.0 (Stat-Ease® Inc, USA). This design features three levels (low, medium, and high) with uncoded values, and their respective levels are detailed in Table 2. Response values were analyzed using analysis of variance (ANOVA) provided by the software, and the optimal conditions for each factor were investigated. Additionally, the obtained model was validated.

Table 2. The uncoded values of different variables and their respective levels of Box-Behnken design for optimization of Cur-NSs

Variables	Uncoded variable level		
	Low (-1)	**Center (0)**	**High (+1)**
Independent variables			
Tween® 20 (%)	0.5	1.25	2
Pluronic® F-127 (%)	0	2.5	5
Curcumin (mg/mL)	1	3	5
Dependent variables			
Particle size (nm)	Minimize		
PDI	In range		
Zeta potential (mV)	In range		
Cur content (mg/mL)	Maximize		

3.2.1.2. Preparation of Cur-NS

Cur-NSs were prepared using a solvent-antisolvent precipitation method and a bottom-up approach. Ethanol acts as the solvent, while purified Milli-Q water is the antisolvent. In a typical procedure, Cur was dissolved in 5 mL of ethanol, then gradually

added to 10 mL of water containing predetermined amounts of Tween® 20 and Pluronic® F-127, as specified by the experimental design in Table 3, under vigorous magnetic stirring. The resulting mixture was left to stir overnight in a fume hood to ensure complete removal of the organic solvent. Subsequently, the suspensions were ultrasonicated in two 15-min sessions at 30% amplitude, with the temperature maintained at 5±3°C using an ice bath. The resulting Cur-NSs were then centrifuged at 8,000 rpm for 20 min. The supernatant was collected, freeze-dried, and stored for further analysis.

Table 3. The experiment was designed using Box-Behnken and the observed responses from each run

Run	Factors			Responses			
	Tween® 20(%)	Pluronic® F-127 (%)	Curcumin (mg/mL)	Size (nm)	PDI	Zeta (mV)	Conc (mg/mL)
1	2	2.5	1	61.12	0.359	-8.07	0.785
2	1.25	5	5	24.00	0.267	-7.08	0.831
3	1.25	2.5	3	33.45	0.388	-1.57	0.628
4	1.25	2.5	3	45.85	0.165	-14.68	0.582
5	1.25	2.5	3	86.19	0.366	-1.60	0.616
6	1.25	2.5	3	28.44	0.393	-14.42	0.654
7	2	2.5	5	63.49	0.299	-2.92	0.749
8	1.25	5	1	57.79	0.336	-3.25	0.810
9	0.5	2.5	5	45.51	0.408	-10.86	0.420
10	2	5	3	35.36	0.338	-7.25	1.140
11	0.5	5	3	37.70	0.361	-12.29	0.678
12	1.25	0	5	168.77	0.163	-3.39	0.226
13	0.5	0	3	169.33	0.359	-2.42	0.083
14	0.5	2.5	1	68.88	0.152	-10.33	0.360
15	1.25	0	1	153.00	0.256	-3.15	0.401
16	1.25	2.5	3	42.72	0.152	-3.07	0.629
17	2	0	3	198.83	0.322	-8.02	0.461

3.2.2. Curcumin liposomes

3.2.2.1. Experimental design

A three-level Box-Behnken design was used to optimize the Cur-loaded deformable liposome, which helps in understanding the effects of variables and their interactions on the responses. The concentration of Tween® 20 (X_1), oleic acid (X_2), and Cur (X_3) were chosen as independent variables. The desired critical parameters of Cur-Ls, such as particle size (Y_1), PDI (Y_2), zeta potential (Y_3), and LC (loading

capacity) (Y_4), were selected as response variables. The variables and their levels are depicted in Table 4. The results of the applied experimental design were analyzed using the ANOVA test by the DesignExpert® software. In addition, the conditions of each factor for optimizing the Cur-L formulation were confirmed and validated.

Table 4. Independent and dependent variables and respective levels of Box-Behnken design for optimization of Cur-L

Variables	Uncoded variable level		
	Low (-1)	Center (0)	High (+1)
Independent variables			
Tween® 20 (%)	0	1.5	3
Oleic acid (%)	0	0.75	1.5
Curcumin (%)	1	5.5	10
Dependent variables			
Particle size (nm)	Minimize		
PDI	In range		
Zeta potential (mV)	In range		
LC of Cur (µg/mg)	Maximize		

3.2.2.2. Preparation of Cur-L

Cur-Ls were prepared using the thin-film hydration method. The liposomes were formed using 50 mM phosphatidylcholine (PC) and 50 mM cholesterol (CHO) at a 10:2 molar ratio, with different concentrations of Tween® 20, oleic acid, and Cur (Table 5). The concentration of Tween® 20, oleic acid, and Cur were expressed as a percentage of the total lipid content. Briefly, accurately weighted Cur and lipids were dissolved in a mixture of chloroform and methanol (in a 2:1 v/v ratio). Next, the solvents were evaporated by a nitrogen gas flow to make a thin film at the bottom of a test tube. These thin films were further dried by storing them in a desiccator for 10 h to eliminate any residual solvent. Subsequently, the thin films were hydrated with the phosphate-buffered saline (PBS) pH 7.4 containing Tween® 20 and oleic acid by vortex mixing for 10 min. This liposomal suspension was then sonicated using a probe sonicator (Vibra cell™, Sonics, and Materials, CT, USA) for 15 min, two times, to reduce the size of the liposomes. To remove any excess Cur, the liposomal suspension was then subjected to centrifugation at 12,000 rpm for 30 min at 4ºC. Finally, the Cur-

L present in the supernatants was carefully collected and stored at 4ºC for subsequent investigations. As a control, Cur was dissolved in the solvents without lipids, and followed the same thin film hydration process as above to assess the presence of free Cur in the supernatant after centrifugation.

Table 5. Experimental designed using Box-Behnken and the observed responses from each run

Run	Factors			Responses			
	Tween® 20(%)	Oleic acid (%)	Curcumin (%)	Size (nm)	PDI	Zeta (mV)	LC (µg/mg)
1	1.5	0.75	5.5	86.61	0.2	-35.7	6.6
2	0	0.75	10	114.1	0.39	-17.9	1.9
3	1.5	0.75	5.5	87.2	0.18	-37.3	11.2
4	3	1.5	5.5	80.2	0.14	-34.7	10.8
5	0	0	5.5	78.1	0.15	7.3	10.4
6	0	0.75	1	96.9	0.2	-25.3	2.1
7	1.5	1.5	1	99.5	0.16	-45	3.5
8	1.5	1.5	10	110	0.17	-39.7	7.2
9	3	0	5.5	58.2	0.01	-12.4	17.6
10	3	0.75	1	63	0.25	-30.5	3.4
11	1.5	0.75	5.5	75.1	0.2	-35.7	14
12	1.5	0.75	5.5	88.6	0.2	-38.6	11.7
13	1.5	0.75	5.5	76.7	0.22	-34	10.1
14	3	0.75	10	61.2	0.22	-32.4	17
15	1.5	0	1	64.4	0.17	-9.2	5.9
16	1.5	0	10	73.2	0.21	-7.57	21.8
17	0	1.5	5.5	112.6	0.21	-40.3	2

3.3. Characterization and evaluation of optimized nanocurcumin

3.3.1. Particle size, PDI, and zeta potential measurement

After the preparation of Cur-NSs and Cur-Ls, the particle size, polydispersity index (PDI), and zeta potential were analyzed with a dynamic light scattering system using a Zetasizer Nano ZS (Malvern Instruments Ltd., Worcestershire, UK). The samples were diluted 100-fold with ultrapure Milli-Q water to reach the appropriate concentration for the analysis. Each sample was measured in triplicate at a scattering angle of 90° and a temperature of 25°C.

3.3.2. Drug content analysis

The analysis of Cur content in the freshly prepared Cur-NS and Cur-L formulations using a reversed-phase HPLC (Agilent 1220 Infinity II, Agilent Technologies, Santa Clara, USA). Each sample was centrifuged at 10,000 rpm for 10 min at 25ºC, and the resulting supernatant was then diluted in methanol, filtered through a 0.45-µm nylon filter, and subsequently subjected to HPLC analysis (69). In the case of Cur-Ls, the drug content within the liposomes was determined by extracting Cur from the liposomes using methanol (250 µL of Cur-L is stirred in 250 µL of methanol) before dilution for HPLC analysis. A C18 analytical column with dimensions of 4.6×250 mm and particle size of 5 µm was used as the stationary phase, and an injection volume of 20 µL was employed. The mobile phase was a 50:50 mixture of acetonitrile and 2 %v/v acetic acid in water, with a 1.2 mL/min flow rate. The column temperature was kept at 33 ± 0.5°C, and the detection was performed at 425 nm using a UV–vis spectrophotometric detector. To create a standard curve for Cur, standard solutions were prepared in methanol, covering a concentration range from 0.78 to 50 µg/mL. The loading capacity of Cur in the liposomes was calculated using the following equation.

$$LC(\%) = \frac{Measured\ amount\ of\ Cur\ in\ the\ liposomes}{Total\ weight\ of\ lipids}\ x\ 100 \qquad Eq.1$$

3.3.3. Transmission electron microscopy (TEM)

The shape, size, and arrangement of the optimized Cur-NS and Cur-L were examined using a Transmission Electron Microscope (TEM) (Philips TECNAI 20, UK). Freshly prepared samples were carefully dropped onto carbon-coated copper grids, and the grid surfaces were allowed to dry under ambient conditions before observation.

3.3.4. Powder X-ray diffraction (PXRD)

A high-resolution X-ray diffractometer (Mini Flex 150 II, Rigaku, Tokyo, Japan) was used to assess the crystalline state and any potential microstructural changes in the NS during preparation and storage. The X-ray diffractometer scanned at a rate of 4°C/min, and samples were analyzed at a 2θ angle range of 5–40°. The PXRD patterns of pure Cur, stabilizers (Pluronic® F-127, Tween® 20), their physical mixture, and Cur-NS powder were recorded and compared.

3.3.5. Differential scanning calorimetry (DSC)

A differential scanning calorimeter (Sapphire, Perkin Elmer, USA) was used to examine the thermal properties of Cur-NS powder. About 5 mg of each sample was placed in a hermetically sealed aluminum pan and heated at a rate of 10°C/min under a constant flow of nitrogen, with DSC thermograms being recorded. Aluminum oxide served as the standard reference material for temperature calibration.

3.3.6. Fourier-transformed infrared spectroscopy (FTIR)

An attenuated total reflection Fourier-transform infrared (ATR-FTIR) spectrometer (Nicolet iS5, Thermo Fisher Scientific, MA, USA) was employed to investigate potential interactions between the Cur and the stabilizers. The analyses were conducted with a resolution of 4 cm^{-1} and a scanning range of 4000 to 500 cm^{-1}.

3.3.7. *In vitro* drug release study

The *in vitro* release profile of Cur-NS was examined using the dynamic dialysis method, modified from previous studies (70). A pure Cur suspension was prepared with a Cur concentration of 1 mg/mL in the release medium to compare Cur-NS. A total of 2 mL of each sample was placed in a dialysis bag (MWCO, 6-8 kDa). The bags were immersed in a glass bottle containing 40 mL of a medium of PBS (pH 7.4) and ethanol in a 50:50 volume ratio to achieve sink conditions for Cur and Cur-NS. The glass bottles were then placed in a shaker incubator, shaken at 120 rpm, and maintained at 37 ± 0.5°C. At specified time points (15, 30 min, 1, 2, 4, 8, 12, and 24 h), a 1 mL aliquot was withdrawn, and fresh medium was added to maintain a constant volume. The cumulative release of Cur at each time point was analyzed using HPLC.

3.3.8. Stability study

The stability of the optimized Cur-NSs was assessed to understand the impact of stabilizers on the physical stability of the formulation. Following lyophilization, the Cur-NSs were stored in sealed high-quality polypropylene tubes, shielded from direct sunlight, under various storage conditions: 25 ± 2°C with 60 ± 5%RH, and 5 ± 3°C with 60 ± 5%RH. These conditions correspond to accelerated and long-term stability study conditions as recommended by the ICH Q1 (R2) guideline and the ASEAN guideline on the stability study of drug products intended for refrigerator storage (71). Samples were collected at designated time points (days 0, 7, 15, and 30), redispersed in high-

purity water to achieve a Cur concentration of 0.5 mg/mL, and analyzed. The Cur-NSs are quantitatively assessed for particle size, PDI, and zeta potential using a Zetasizer. Additionally, the concentration of Cur in the Cur-NSs is quantified using HPLC to determine chemical stability. The Cur content is calculated as a recovery percentage relative to the initial amount using Eq. 2.

$$\%\ Recovery = \frac{Amount\ of\ Cur\ analyzed}{Initial\ amount\ of\ Cur}\ x\ 100 \qquad Eq.2$$

3.3.9. DPPH Assay

The antioxidant activity of Cur was assessed by the DPPH (2,2-Diphenyl-1-picrylhydrazyl) assay, adapted from the previously published method (72). To determine the ability of Cur to scavenge DPPH free radicals in aqueous medium, Cur-NS, Cur-L, and Cur suspension were prepared in PBS at concentrations ranging from 1 to 256 µg/mL. The Cur suspension was subjected to 6 h of bath sonication for maximum dissolution. In a 96-well plate, each sample was mixed with a freshly prepared 0.2 mM DPPH methanolic solution at a 1:1 volume ratio. The scavenging reaction occurred in the dark at room temperature for 30 min. Absorbance was measured at 515 nm using a VICTOR Nivo Multimode Plate Reader (PerkinElmer, Germany). A blank sample containing PBS and DPPH solution served as a control. The percent inhibition of DPPH radicals was calculated following Eq. 3, and IC50 values were determined by a logarithmic fit plot.

$$\%\ Inhibition = \frac{(Abs.of\ control - Abs.of\ sample)}{Abs.of\ control}\ x\ 100 \qquad Eq.3$$

3.3.10. Cytotoxicity

The potential cytotoxic effects of Cur, Cur-NS, and Cur-L on normal human foreskin fibroblast (NHF) cells were evaluated using an MTT assay. NHF cells were cultured in serum-supplemented DMEM and seeded into a 96-well plate at a density of 10,000 cells per well. The cells were incubated at 37°C with 95% air and 5% CO_2 until they reached 80% confluence. Subsequently, the cells were exposed to Cur, Cur-NSs, or Cur-Ls in serum-free DMEM at concentrations ranging from 0.1 to 100 µg/mL for 24 h. After exposure, the cells were rinsed with sterile PBS (pH 7.4) and treated with 25 µL of 1 mg/mL MTT solution in FBS-supplemented DMEM. Following a 3 h

incubation period, the formazan precipitate formed was dissolved using 100 µL of DMSO, and absorbance was measured at 550 nm using a VICTOR Nivo Multimode Plate Reader (Perkin Elmer, MA, USA). Finally, the percentage of relative cell viability was calculated with Eq. 4.

$$\%\ relative\ cell\ viability = \frac{Abs.sample - Abs.blank}{Abs.control - Abs.blank}\ x\ 100 \qquad Eq.4$$

3.3.11. *In vitro* wound healing assay (scratch assay)

The wound healing potential of the optimized Cur-NS was evaluated using the scratch assay, following established protocols (73). In brief, the 2×10^5 NHF cells per well were seeded into a 6-well plate. Once the cell monolayer reached confluency, a scratch was created using a sterile micropipette tip. The cell debris was then washed away with sterile PBS, and the cells in each well were treated with either Cur or Cur-NS at a concentration of 1 µg/mL. Untreated wells served as controls. The cells were incubated in an atmosphere-controlled incubator. At 0, 24, and 48 h, images of cell migration across the scratch were captured using an inverted microscope. ImageJ software was used to measure the wound healing area, and the percentage of wound closure over time was calculated using Eq. 5.

$$\%\ Wound\ closure = ((A_o - A_t)/A_o))\ x\ 100 \qquad \text{Eq. 5}$$

Where, A_0 is the area of the wound measured immediately after scratching, and A_t is the area measured at 24 h or 48 h after the scratch.

3.4. Preparation and optimization of hydrogel patches using experimental designs

3.4.1. Genipin-crosslinked CS/PVP hydrogel patches

3.4.1.1. Experimental design

A simplex centroid mixture design was used to optimize the composition of hydrogel formulations with maximized swelling rate Y_1, gel fraction Y_2, and mechanical strength Y_3. This mixture design approach is an efficient way to the effect of composition change on the properties of the obtained hydrogels, in which all ingredients of the mixture sum up to 100%. To determine the experimental parameters, preliminary tests were conducted to explore the range of mixtures where a hydrogel

could be successfully formed using genipin as the crosslinker. Considering that genipin was a well-recognized cross-linking agent for polymers containing amines, a concentration of genipin was explored between 0.5 and 2% w/w of the CS polymer to set a constant concentration for all experiments. The proportion of 3% w/w CS, 5% w/w PVP, and 5% PVA in the hydrogel formulation were investigated. In this study, the lower and upper limit for the mixture's components was illustrated in Table 6. The ANOVA analysis was performed, which was provided in the software to obtain the composition of hydrogel patch formation with the optimal hydrogel properties (Y_1, Y_2, and Y_3).

Table 6. Variables and levels of each component selected for the mixture design for the hydrogels

Mixture components	Levels (%)	
	Lower	Upper
A: 3% CS	70	100
B: 5% PVP	0	30
C: 5% PVA	0	30

3.4.1.2. Preparation of genipin-crosslinked CS/PVP hydrogel patches

The hydrogel patches were prepared according to the composition defined by each experimental point Table 7. Initially, individual polymer solutions were prepared at their specific concentrations. CS was dissolved in a 1% v/v acetic acid solution and stirred overnight at room temperature to get a 3% w/w viscous solution with a pale-yellow color. A transparent 5% PVP solution was obtained by dissolving PVP in pure water with constant stirring for 2 h at room temperature. To obtain a 5% PVA solution, PVA was dispersed in hot water (heated at 80ºC) and continuously stirred for 2 h. Regarding a 2% w/v genipin solution, genipin was dissolved in water in an ultrasonic water bath for 20 min. First, the polymer solutions were mixed by magnetic stirring at ambient temperature for 20 min to ensure a homogeneous polymer mixture. The genipin solution was then added to the mixture in two separate portions, with 5-minute intervals between each addition. Next, the hydrogel solutions were poured into a plastic mold after degassing. The mold was incubated at 40ºC overnight to facilitate crosslinking.

Before analysis, the mold sample was hermetically sealed with paraffin and stored in a refrigerator.

Table 7. Experimental points of independent factors and response variables used in DoE

Experimental points	Factors (%)			Responses		
	A:3%CS	B:5%PVP	C:5%PVA	Y_1: %SW	Y_2: DC	Y_3: MS
1	85	15	0	558.10	80.11	229.10
2	85	0	15	412.09	81.38	245.27
3	70	0	30	342.89	80.92	230.00
4	85	0	15	413.61	82.86	244.63
5	85	15	0	587.40	78.74	228.50
6	70	15	15	264.63	85.22	224.00
7	100	0	0	375.67	81.58	231.83
8	70	30	0	439.19	87.90	238.00
9	70	30	0	414.65	88.26	239.00
10	90	5	5	288.19	79.41	232.77
11	80	10	10	242.36	81.65	239.80
12	70	0	30	407.07	79.38	231.00
13	100	0	0	321.83	81.17	231.57
14	75	20	5	306.31	82.46	235.17
15	75	5	20	263.11	84.08	241.27

3.4.2. HA/PVA/PNVP-ITA hydrogel patches

3.4.2.1. Synthesis and characterization of PNVP-ITA copolymer

PNVP-ITA was synthesized by a surfactant-free emulsion polymerization reaction. The aim was to create a polymer containing carboxyl and carbonyl groups to enhance the cross-linking density in optimized hydrogels. In this process, V50 (2% w/w) was used as a radical polymerization initiator and added to 100 mL of deionized water, which was heated to 75°C while flushed with nitrogen to maintain an inert atmosphere. Concurrently, NVP (10 mmol) and ITA (30 mmol) were dissolved in 10 mL of chloroform. This monomer solution was gradually introduced into the heated initiator solution under inert conditions and allowed polymerize for at least 18 h. The reaction mixture was then cooled down and purified by dialysis (using a MWCO 3.5 kDa membrane) against deionized water for 3 days, with the water being replaced every 6 h. Finally, the purified polymer was collected after lyophilization. To confirm the

polymerization between the NVP and ITA, the synthesized polymer was characterized using FTIR and ^{1}HNMR. FTIR was performed as described in section 3.3.6. ^{1}H-NMR analysis was applied using a 300 MHz nuclear magnetic resonance spectroscopy (Bruker AVANCE III HD, Billerica, MA, USA). The NMR spectra were recorded by chemical shifts in parts per million (ppm) over 0-14.

3.4.2.2. Experimental design

A central composite design was used to optimize HA and PVA hydrogel formulation. In this study, two components of hydrogel were chosen as independent variable factors: HA (A_1) and 20% PVA (A_2) , whereas water (85%) was considered a constant. By changing the amount of two factors concurrently and keeping their total concentration constant, the produced swelling rate (Y_1), mechanical strength (Y_2), and gel fraction (Y_3) were observed as responses. The design was applied to analyze the resulting data using the DesignExpert® software version 11.0.0. In addition, the compositions for the formulation of hydrogel patch with the desired swelling rate, mechanical strength, and gel fraction were determined and validated. The lower and upper limits for the components of the mixture are shown in Table 8.

Table 8. Factors and their examined levels in Mixture Design

Mixture component	**Levels (%)**	
	Lower	**Upper**
A_1: HA	0	5
A_2: 20%PVA	10	15

3.4.2.3. Preparation of HA/PVA/PNVP-ITA hydrogel patches

The PVA solution (20 %w/v) was prepared by dispersing PVA powder in hot deionized water (80°C) and stirred until homogeneous. The PVA solution was mixed with HA in specific percentages (Table 9). Further, aluminum glycinate (0.2%) and malic acid (0.1%) were obtained as cross-linker and cross-linking regulators. Malic acid was added to the polymer mixture, whereas aluminum glycinate was dispersed in 30% glycerin. Then, the glycerin dispersion was added to the polymer mixture and gently mixed until homogeneous. The mixtures (10 g) were slowly poured into an acrylic mold

to avoid air bubbles in the patch. These polymer mixtures were subjected to 4 freeze-thaw cycles. A cycle of freezing at −20°C for 18 h and thawing at room temperature for 6 h was conducted (74). The optimized hydrogel patch was added with 2 wt% PNVP-ITA to improve the properties of the hydrogel patch.

Table 9. Experimental runs generated by central composite design with Input Factors and Output Responses

Formulation	Input factors		Output responses		
	A_1: HA (%)	**A_2: PVA (%)**	**Y_1: Swelling (%)**	**Y_2: Young's modulus (Pa/%)**	**Y_3: Erosion (%)**
H1	2.5	12.5	168.45	97.43	38.02
H2	2.5	12.5	191.72	100.28	37.16
H3	5	10	208.37	146.03	38.55
H4	0	15	123.93	100.06	20.03
H5	0	15	120.39	98.02	16.31
H6	5	10	172.02	143.87	37.16
H7	1.25	13.75	213.11	103.63	35.64
H8	3.75	11.25	161.23	106.19	37.71
H9	5	10	187.00	142.91	37.90
H10	0	15	121.55	99.35	18.51

3.5. Incorporation of nanocurcumin into the optimized hydrogel patches

3.5.1. Loading of Cur-NS into the genipin-crosslinked CS/PVP hydrogel patches

The hydrogel polymeric solution was prepared first using the same method as previously described in section 3.4.1.2. During the mixing stage, lyophilized Cur-NSs were integrated at various concentrations (1, 3, and 5% w/w, referred to as Cur-1, Cur-3, and Cur-5) based on the weight of the polymers. To achieve a uniform distribution of Cur in the hydrogel, the mixture of Cur-NSs and the polymers was stirred mechanically for an additional 30 min. Following this, 0.5 mL of a 2% Genipin solution was introduced into the resulting mixture, and the subsequent steps of degassing, molding, and crosslinking were performed, as previously explained. The Cur-NS-

loaded hydrogels were gently washed with water to eliminate virtually all unreacted (free) molecules.

3.5.2. Loading of Cur-L into the HA/PVA/PNVP-ITA hydrogel patches

The optimized Cur-L was incorporated into the pre-formed HA/PVA/PNVP-ITA hydrogel through absorption. In brief, the hydrogel was cut into 1.5 x 1.5 cm^2 and accurately weighed. These hydrogel samples were then immersed in a solution of Cur-L equivalent to 0.5% w/w of the polymer (Cur-0.5%) for 24 h at room temperature while protecting them from light. Subsequently, the Cur-L loaded hydrogels were gently wiped with tissue to remove any unloaded Cur-L from their surface and then stored at 2-8°C, protected from light, for further investigations.

3.6. Characterization and evaluation of Cur-loaded nanocomposite hydrogels

3.6.1. Swelling (%)

Determining the percent swelling of hydrogels is an essential step in the characterization of hydrogel patches to confirm the hydrogel formation and their absorbency capacity. The measurement was performed using a gravimetrical method. PBS (pH 7.4) was used as the swelling medium to mimic the properties of wound fluid. The pre-weight of each experimental sample (1.5 × 1.5 cm^2) was dried in a hot air oven at 60°C. Then, the dried samples were introduced into a glass bottle filled with 10 mL of PBS and maintained at 37°C. If their swelling equilibrium was reached, the weight of swollen samples was recorded. The percentage of swelling was calculated following Eq. 6.

$$Swelling\ (\%) = ((W_s - W_{d1})/W_{d1})\ x\ 100 \qquad Eq.6$$

Where, W_s and W_{d1} represent the weight of hydrogel in a swollen state and a dry state.

3.6.2. Crosslinking (%)

The crosslinking percentage was examined to verify the crosslinking density within the polymeric chains of the hydrogel matrix. Hydrogel samples size of 1.5 × 1.5 cm^2, were cut and dried to attain a constant weight. Subsequently, these dried samples were immersed in PBS (pH 7.4) at room temperature until they reached equilibrium swelling. The swollen samples were then dried at 60°C until a constant weight (W_{d2})

was achieved. The percentage of crosslinking, also referred to as the insoluble gel fraction, was determined using Eq. 7.

$$Crosslinking\ (\%) = (W_{d2}/W_{d1})\ x\ 100 \qquad Eq.7$$

Where, W_{d1} and W_{d2} represent the dried weight of hydrogel before and after swelling.

3.6.3. Erosion (%)

The hydrogel erosion was studied to determine the cross-linking density of the patch. Each hydrogel was dried in an oven at 60°C until a constant weight was achieved (W_0). Then, the patch was swollen in 25 mL of deionized water for 24 h and dried under the same condition. The final dried hydrogel was re-weighed (W_i). The percentage of erosion was computed using equation 8:

$$\%Erosion = ((W_o - W_i)/W_o)\ x\ 100 \qquad Eq.\ 8$$

Where, W_0 and W_i represent the initial and final dried weight of hydrogel.

3.6.4. Mechanical properties

The appropriate mechanical properties of hydrogel dressings are pivotal for ensuring essential physical integrity that support the promotion of wound healing, particularly in terms of their ability to withstand applied forces as wearable patches. To assess these properties, both compression test and tensile test were conducted using a texture analyzer (TA.XT Plus, Stable Micro Systems, Godalming, UK). The compression test was carried out using a 5-mm stainless steel ball probe attached to a texture analyzer, with the compressive mode at a constant speed of 2 mm/s. The probe was lowered and pressed onto the hydrogel samples (which are cut into square shapes with an area of 15 x 15 mm) until it broke. To perform a tensile test, the prepared samples were cut into a dumbbell shape with a length of 35 mm and a width of 2 mm. Both ends of the dumbbell-shaped samples were clamped and stretched at a constant velocity of 1 mm/s until the breaking point. The values of compressive strength, and Young's modulus were calculated with the following equations.

$$Compressive\ strength = \frac{Maximum\ force\ at\ breaking\ point}{Cross\ section\ area} \qquad Eq.9$$

$$Young's\ modulus = \frac{Stress}{Strain} \qquad Eq.10$$

3.6.5. Water vapor transmission rate (WVTR)

The water vapor transmission rate of the optimized hydrogel patches was investigated to ensure efficient gases exchange through the patch as well as moisture transfer efficiency. The circular-shaped samples were prepared and then placed on the open end of the glass bottles filled with 10 mL of distilled water. The bottles, with the hydrogel samples, were weighed and incubated at 37°C and 75%RH for 24 h. Following the incubation time, the bottle weights were measured again to determine WVTR using Eq. 11.

$$WVTR = (W_0/W_t)/A \qquad Eq.11$$

Where, W_0 and W_t represent the weight of the bottles with the samples before and after incubation, whereas A is the area of the bottle mouth.

3.6.6. Morphology analysis (Scanning Electron Microscope)

The microstructure of the optimized hydrogels, particularly their pore topology, was observed using an SEM (Mira3, Tescan, Czech Republic). Obtaining accurate information about the morphology of hydrogels in their natural swollen state is crucial to obtaining hydrogels with optimal properties for their applications. Therefore, the hydrogel samples were first swelled in water for 1 h and then lyophilized. Before SEM observation, the lyophilized samples were cut into transverse sections and consequently coated with a thin layer of gold to make conductive specimens in a vacuum. Then the images of each sample were captured using an accelerating voltage of 10 kV at 100x, 200x and 1000x magnification.

3.6.7. Infrared spectroscopic analysis (FTIR)

The structural characterization of hydrogel samples was conducted using an ATR-FTIR spectrometer (Nicolet iS5, Thermo Fisher Scientific, MA, USA). The FTIR spectra were recorded across the wavelength range of 4000 to 500 cm^{-1} with a resolution of 4 cm^{-1}.

3.6.8. Loading capacity (LC) and entrapment efficiency (EE)

The HPLC analysis was used to determine the total amount of Cur in the hydrogel patch. To do this, accurately weighted samples were first crushed and then placed in methanol-containing bottles (30 mL). The hydrogel fragments are

continuously shaken at 50 rpm for 4 h using a shaking incubator. The drug extracted from the hydrogel was then diluted in methanol and filtered through a 0.45-μm nylon filter before being quantified using an HPLC (Agilent 1220 Infinity II, Agilent Technologies, Santa Clara, USA). The LC and EE (%) were calculated using equations 12 and 13, respectively.

$$LC = \frac{Measured\ amount\ of\ Cur\ in\ the\ hydrogel\ patch}{Total\ weight\ of\ the\ hydrogel\ patch} \qquad Eq.12$$

$$LE(\%) = \frac{Measured\ amount\ of\ Cur\ in\ the\ hydrogel\ patch}{Theoratical\ loaded\ amount\ of\ Cur}\ x\ 100 \qquad Eq.13$$

3.6.9. *In vitro* drug release studies

The release capacity of Cur-NSs from the CS/PVP hydrogels was assessed by the swelling method. The hydrogels, weighing approximately 1 to 1.5 g, were immersed in glass bottles containing 40 mL of releasing medium PBS (pH 7.4) with 0.5% Tween® 80) to maintain sink condition. Subsequently, the glass bottles were introduced into a shaker incubator, subjected to continuous shaking at 100 rpm, and maintained at a constant temperature of 37 ± 0.5°C. An aliquot of the release medium was withdrawn at specific time intervals (5, 15, 30, 45 min, 1, 2, 4, 8, 12, and 24 h). The removed volume was then replenished with the same medium volume, ensuring a constant volume of 40 mL. The cumulative release of Cur at each time point was then analyzed using the HPLC method described earlier. Moreover, the release behavior of Cur-Ls from HA/PVA/PNVP-ITA hydrogel was also examined. The hydrogel (1×1 cm^2) was taken from a randomly selected area, which was expected to contain 175 μg of Cur. The Cur solution and Cur-Ls samples could be prepared at an equivalent initial Cur content to quantify their release via dialysis. First, 1 mL of the sample solution was enclosed within a dialysis bag (CelluSep® T2, TX, USA; MWCO, 6–8 kDa). The bag was placed in a glass bottle containing 10 mL of 20% PEG 400 in PBS (pH 7.4) to establish appropriate sink condition (75). The experiment was conducted at 32 ± 2°C inside a shaking incubator agitated at 100 rpm. At 0, 0.25, 0.5, 1, 2, 6, 8, and 12 h intervals, 1 mL aliquot of the release medium was withdrawn and replaced with an equal volume of fresh medium. Cur content was quantified using HPLC to calculate the cumulative drug release. To study the release mechanism of Cur from the hydrogel, the obtained

data were fitted to kinetics release models, such as zero-order, first-order, Higuchi, Korsmeyer-Peppas, etc.

3.6.10. *In vitro* biocompatibility studies

The biocompatibility of the prepared hydrogel patches was examined by conducting cell viability assessments using an MTT assay on NHF cells. Briefly, 50,000 cells were seeded per well in a 48-well plate and then incubated at 37°C in a 5% CO_2 atmosphere for 24 h. The hydrogel samples were sterilized by UV light exposure for 30 min on each side and subsequently immersed in DMEM for 2 h. The fully swollen hydrogels were placed on top of monolayer cells and further incubated for 24 h after adding 0.5 mL of DMEM. After that, the cells were rinsed with PBS (pH 7.4), and then incubated for 3 h with an MTT solution. The resulting formazan precipitate was dissolved by adding DMSO. The cell viability was evaluated by measuring the absorbance at 550 nm. The assay was performed in triplicate, and the % cell viability was determined using Eq. 14.

$$Cell\ viability(\%) = \frac{Abs.sample - Abs.blank}{Abs.control - Abs.blank}\ x\ 100 \qquad Eq.14$$

3.6.11. *In vitro* antibacterial studies

The antibacterial efficacy of hydrogels, with and without nanocurcumin, was evaluated using a disc diffusion method specifically against *Staphylococcus aureus* (S. *aureus*). Initially, a well-isolated colony of S. *aureus* was suspended in a tryptic soy broth (TSB) medium and allowed to incubate overnight. The bacterial concentration was then adjusted to 10^8 CFU/mL (0.5 McFarland turbidity). After sterilizing the hydrogel samples through a 30-min UV exposure on both sides, they were placed on a top of bacterial suspension-spread tryptic soy agar (TSA) plates and incubated at 37°C for 24 h. The antibacterial activity was determined by measuring the inhibition zone formed by each sample.

3.6.12. *In vivo* wound healing studies

The animal protocol (ID project no. 2/2566; March 23, 2023) was approved by the institutional animal ethics committee of Silpakorn University, Nakhon Pathom, Thailand. Male Wistar rats, aged 7 weeks and weighing 310-360 g, were obtained from the National Laboratory Animal Center at Mahidol University in Nakhon Pathom,

Thailand. The rats assigned to this study were individually housed in polypropylene cages and divided into three groups, each containing three rats.

Group I was provided with a gauze bandage (negative control).

Group II received a commercial wound healing patch (positive control).

Group III was given a CurL-embedded HA/PVA/PNVP-ITA hydrogel patch or a CurNS-loaded CS/PVP hydrogel patch.

The rats were kept under controlled room conditions at a temperature of 25 ± 2°C, with a relative humidity of 60 ± 10% and a 12/12-hour light-dark cycle. They were fed a typical laboratory diet and given unrestricted access to water (082G/15, National Laboratory Animal Center, Mahidol University, Nakhon Pathom, Thailand). An 8-mm-diameter circular wound was created with sterile scissors on the dorsal thoracic region of each rat (one incision on the left and one on the right) under proper anesthesia induced by intraperitoneal administration of pentobarbital (50 mg/kg). All sample patches, sized 1.5 × 1.5 cm, were terminally sterilized using UV light for 15 min per side before testing. For Group III, the patches were applied to the wounds and covered with Tegaderm™ occlusive film to prevent displacement during the experiment. Progressive changes in wound size were photographed and measured using a ruler to calculate the percentage of wound recovery (Eq. 15) on days 0, 3, 5, 7, and 10.

$$Wound\ recovery\ (\%) = ((A_o - A_t)/A_o))\ x\ 100 \qquad Eq.15$$

Here, A_0 is the initial wound area, while A_t represents the wound area observed at different time intervals.

3.7. Statistical analysis

All measurements were performed in triplicate, and the results were presented as mean values ± standard deviation (SD). Statistical analysis was conducted using SPSS® software version 19 (SPSS Inc., Chicago, IL). An independent two-sided t-test was used for comparing two groups, while an ANOVA followed by a post-hoc or Tukey test was applied for comparisons among multiple groups. A p-value of less than 0.05 was considered statistically significant.

CHAPTER 4
RESULTS AND DISCUSSION

4.1. Nanocurcumin

4.1.1. Curcumin Nanosuspensions

4.1.1.1. Optimization of Cur-NSs formulation using Box-Behnken design

The design of experiments was employed to determine the optimal conditions and composition for preparing Cur-NSs. The Box-Behnken design was chosen for optimization because it can create higher-order response surfaces with fewer runs compared to a standard factorial approach. The independent variables included Tween® 20 (X_1: 0.5–2%), Pluronic® F-127 (X_2: 0–5%) as system stabilizers, and the amount of Cur (X_3: 1–5 mg/mL). These variables were input into the design program, which generated 17 experimental runs. The concentration ranges were determined based on preliminary studies to ensure the formation of Cur-NSs. The responses, including particle size, PDI, zeta potential, and Cur concentration, were measured after characterizing each experimental run, and the results are presented in Table 3. The Cur-NSs produced from the designed experiments had particle sizes ranging from 24 to 198 nm, with a PDI ranging from 0.152 to 0.408. The PDIs below 0.5 indicate that the Cur-NSs were relatively homogeneous, and the dispersion of the NSs after the preparation procedure was satisfactory (76). The zeta potential of all Cur-NSs was slightly negative (ranging from -14.68 to -1.57 mV), which can be attributed to the combined effects of the curcumin's chemical properties, the interaction with the nonionic surfactants, and the adsorption of ions from the surrounding medium (77). Finally, the concentration of Cur analyzed from its supernatant after centrifugation ranged between 0.083 and 1.140 mg/mL. Several factors influenced the resulting particle size and zeta potential, including the molecular structure and initial particle size. Regarding the zeta potential, both Pluronic® F-127 and Tween® 20 are nonionic components. The carbonyl groups on their structures may lead to more negative zeta potential values under certain conditions (78-80). The center points were repeated to validate these influences and to provide a more accurate prediction of the parameter impacts. Tween® 20 and Pluronic® F-127 were chosen as stabilizers in this study due to their desirable safety profiles as polymeric surfactants, and their combination was expected to yield a more stable nanosuspension (NS) formulation.

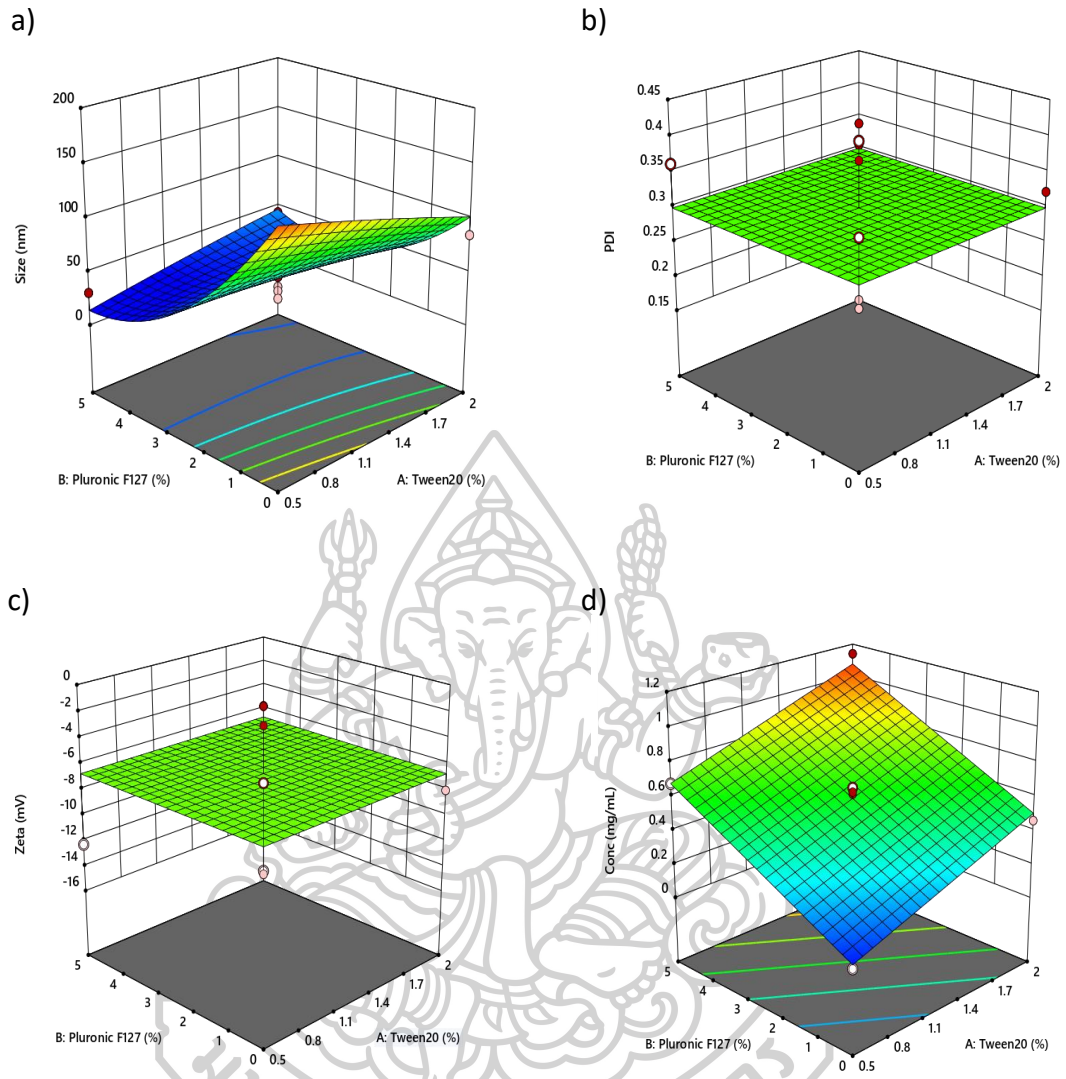

Figure 4. The 3D surface response plots show the effect of independent factors (A: Tween® 20 and B: Pluronic® F-127with C: Cur content fixed at the center point) on various responses: **a)** particle size, **b)** PDI, **c)** zeta potential, and **d)** Cur concentration.

After the responses were analyzed by the software, the relationships between the input factors (amount of Tween® 20 and Pluronic® F-127, with Cur content fixed at the center point) and each response were illustrated in the 3D surface plot (Fig. 4). As shown in Fig. 4(a), the variation in the amount of Tween® 20 had no impact on particle size, whereas the addition of Pluronic® F-127 resulted in smaller particle sizes (indicated by the blue areas). The concentrations of the stabilizers did not significantly influence the PDI and zeta potential of the Cur-NSs, as demonstrated in Fig. 4(b) and (c), respectively. Meanwhile, increased percentages of Tween® 20 and Pluronic® F- 127

led to a higher concentration of Cur (shown by the red areas) after the preparation of Cur-NSs Fig. 4(d).

$$Y_1 \text{ (Size)} = 47.33 + 4.67X_1 - 66.89X_2 - 4.88X_3 - 7.16\,X_1X_2 + 6.44X_1X_3 - 12.39X_2X_3 + 10.92X_1^2 + 52.06X_2^2 + 1.50X_3^2 \quad \text{Eq. 16}$$

$$Y_4 \text{ (Conc)} = 0.5914 + 0.1992X_1 + 0.2861X_2 - 0.0162X_3 \quad \text{Eq. 17}$$

For predicting the significant dependent variables, the coded equations to estimate particle size and Cur concentration are presented in Eq. (16) and Eq. (17), respectively. It is possible to predict the response for specific levels of each component using the equation expressed in terms of coded factors. By comparing the factor coefficients, the coded equation can determine the relative importance of the components. The equations suggest that Pluronic® F-127 (X_2) has the greatest impact on particle size and Cur content compared to the other independent variables. Increasing the amount of Pluronic® F-127 in the formulation increases both the particle size of the Cur-NS and the Cur content, as indicated by the equations. This parameter also interacts with other parameters (X_1 and X_3), which further emphasizes its influence on particle size. However, the influence of X_2 on Cur content alone is insufficient to cause significant changes.

Based on the results of each experiment conducted, the data were analyzed and optimized for the formulation of Cur-NS using DesignExpert® software. The criteria presented in Table 10 were used to analyze the optimal Cur-NS formulation. All input parameters were kept within the range studied. The particle size range obtained from the 17 experiments was within the nanoscale, making the entire range acceptable and used as the criterion for selecting the optimized Cur-NS. Although the independent variables did not significantly influence the PDI or zeta potential, the optimization criteria required the PDI to be maintained below 0.3, indicating a more homogeneous particle size distribution. Lastly, the concentration of Cur acquired was requested to be maximized which would provide greater yield of Cur. The optimized Cur-NS formulation was found to contain 2% Tween® 20, 4.97% Pluronic® F-127, and 1 mg/mL of Cur. The optimized formula demonstrated a high desirability value of 0.952. The multi-response optimization was evaluated using desirability, with acceptable and

excellent desirability values ranging between 0.8 and 1, indicating the high quality of the formulation (81). Confirmation experiments (n = 3) were conducted to verify the optimized Cur-NS formulation, comparing predicted responses with actual values obtained from the experiments (Table 11). It was found that all responses were comparable to the predicted values ($p > 0.05$). This indicates that the optimized formulation was achieved, providing nanosized homogeneous particles with a slightly negative surface charge and maximized Cur concentration. The optimized Cur-NSs were then prepared for further experiments.

Table 10. The criteria for the optimization of Cur-NS and the optimized formulation

Factors	Goal	Lower limit	Upper limit	Solution	Desirability
X_1: Tween® 20 (%)	is in range	0.5	2	2	0.952
X_2: Pluronic® F-127 (%)	is in range	0	5	4.97	
X_3: Curcumin (mg)	is in range	1	5	1	
Size (nm)	minimize	50	190		
PDI	is in range	0.1	0.3		
Zeta (mV)	none	-14.68	-1.57		
Conc (mg/mL)	maximize	0.0833793	1.14049		

Table 11. The comparison of the software-predicted values and experimentally observed values of the optimized Cur-NSs formulation

Responses	Predicted mean	Actual mean	P-value
Size (nm)	51.98 ± 18.90	47.51 ± 10.67	0.7395
PDI	0.30 ± 0.09	0.27 ± 0.13	0.8024
Zeta (mV)	-6.73 ± 4.49	-8.98 ± 4.00	0.5520
Conc: (mg/mL)	1.09 ± 0.05	1.16 ± 0.03	0.1211

4.1.1.2. Characterization and evaluation of the optimized Cur-NS

4.1.1.2.1. Transmission electron microscopy (TEM)

TEM confirmed the morphology and size of the Cur-NS. As shown in Fig. 5, the Cur-NS appeared mostly spherical with some irregular-shaped particles. The particle size was approximately 50 nm, consistent with the findings from the dynamic light scattering method used by the Zetasizer. The examination confirmed that the Cur-NS was successfully prepared under the optimized conditions developed.

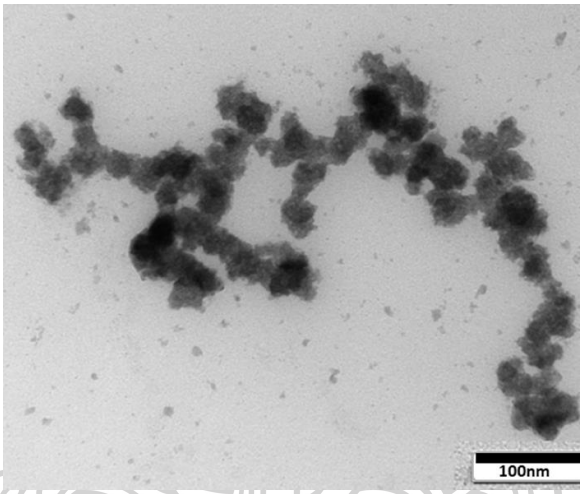

Figure 5. TEM image of Cur-NSs showing somewhat spherical and some irregular-shape particles with the size correlated to the optimization

4.1.1.2.2. Thermal property and crystallinity

The thermal properties of the Cur-NS were examined using DSC, and their crystallinity was investigated using PXRD. Fig. 6(a) and (b) show the DSC thermogram and PXRD pattern of Cur-NSs, Cur, and the stabilizers. The properties of Cur-NS were found to be altered compared to Cur, especially after stabilization with Tween® 20 and Pluronic® F-127. The thermal characteristics of Cur-NS were influenced by Pluronic® F-127, and the changes observed in the drug relative to Cur powder were no longer present. Similarly, the crystallinity of Cur-NS appeared to have shifted from the crystalline form of Cur to an amorphous state, as evidenced by the absence of the crystalline pattern observed in Cur. The amorphous pattern of Cur-NS was not observable due to interference from the pattern of the stabilizer, Pluronic® F-127. Several studies have reported that the formulation of nanosuspensions can result in the formation of the amorphous form of the active ingredient, or in some cases, a mixed

form of crystalline and amorphous states (82-85). Crystalline nanosuspension, often referred to as nanocrystals, consists of pure active ingredients in nano-scaled particles. The amorphous state is desirable for hydrophobic drugs like Cur, as it enhances drug dissolution and efficacy in aqueous environments (86, 87).

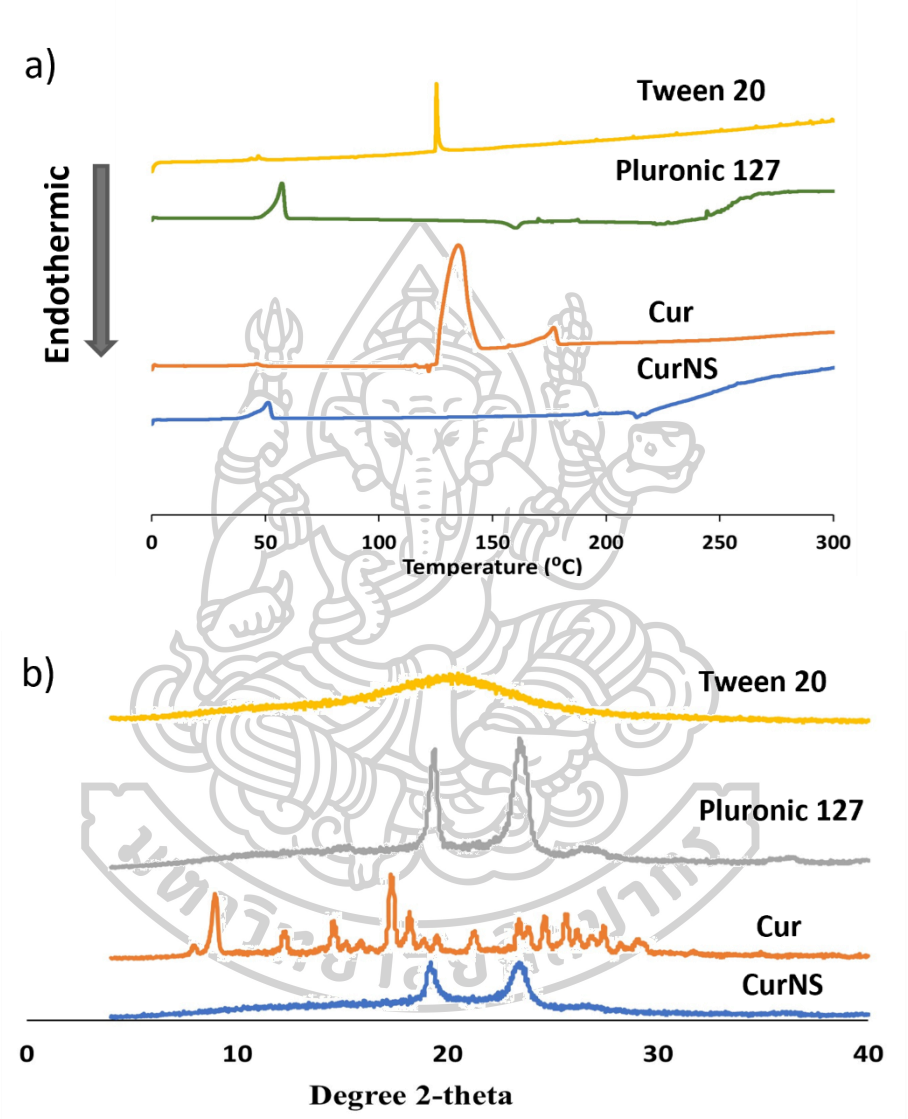

Figure 6. a) The DSC thermogram and **b)** PXRD pattern of Cur, Cur-NS, Tween® 20, and Pluronic® F-127

4.1.1.2.3. Fourier-transformed infrared spectroscopy (FTIR)

The interaction between the nanosized Cur and the stabilizers was examined using ATR-FTIR. The spectrum of Cur showed a broad O-H stretching peak at 3324 cm^{-1}, and C=O and C=C peaks of substituted aromatic rings at 1627 cm^{-1} and 1595 cm^{-1}, respectively. Additionally, the spectrum of Cur showed peaks for C=C of

aliphatic alkene at 1510 cm^{-1} and ether C-O at 1264 cm^{-1} (Fig. 7). Pluronic® F-127 influenced the presentation of Cur-NS as observed in the DSC thermogram and PXRD pattern. The spectra of Cur-NS and Pluronic® F-127 showed peaks for C-H stretching at 2853 cm^{-1}, O-H bending at 1453 cm^{-1}, and polymeric C-O stretching at 1336 cm^{-1} (88). However, the spectrum of Cur-NS showed consistency with the Cur spectrum at the C=O stretching and C=C of the substituted aromatic ring, indicating a mixture of Cur with the stabilizers. Thus, no clear interaction between the stabilizers and Cur was observed. A more sensitive instrument, such as atomic force microscopy, may be required to determine interactions in the dry state (89).

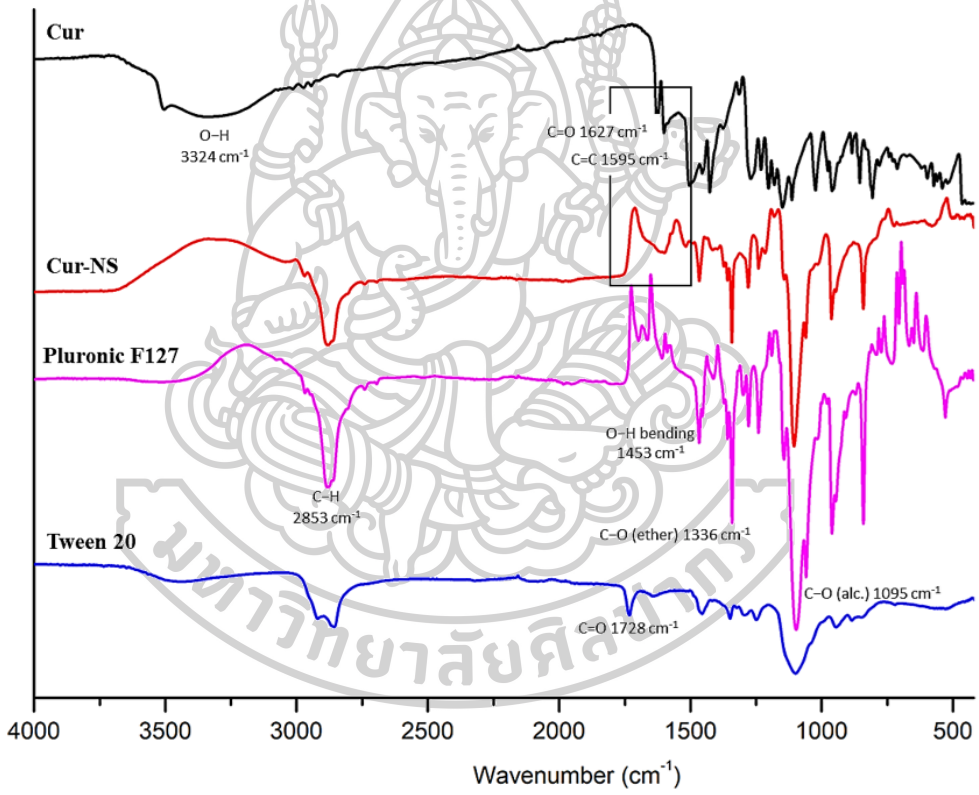

Figure 7. The ATR-FTIR spectra of Cur, Cur-NS, Pluronic® F-127, and Tween® 20

4.1.1.2.4. Stability study

The stability of Cur-NSs was monitored by storing them at different temperatures (5°C and 25°C) and re-assessing particle size, PDI, zeta potential, and %EE at different time intervals. Results indicated that Cur remained fully stable at both temperatures for up to 7 days. However, the stability was slightly enhanced at 5°C, permitting storage for up to 15 days, as demonstrated in Table 12. Particle growth and

a decrease in % recovery was observed by day 15 when stored at 25°C. These trends persisted through day 30 for both storage conditions. However, after one month, the redispersed Cur-NSs appeared yellowish and clear, with no precipitation or undissolved particles observed (Fig. 8). The stability of the Cur-NSs remained considerable after 30 days of storage under both conditions. Therefore, the Cur content should be re-evaluated before use, as its concentration may decrease following extended storage periods.

Table 12. The stability of Cur-NSs after being stored at 4 and 25°C for 30 days

Cur-NSs stored at 5°C				
Time	**Size (nm)**	**PDI**	**Zeta potential (mV)**	**%Recovery**
Day 0	33.43±0.25	0.28±0.04	-7.56±7.36	97.56±7.36
Day 7	42.89±14.66	0.20±0.20	-8.20±0.15	95.97±5.91
Day 15	51.01±13.87	0.27±0.08	-7.98±2.43	95.97±5.91
Day 30	74.96±51.96	0.45±0.19	-11.67±0.18	79.82±6.13
Cur-NSs stored at 25°C				
Time	**Size (nm)**	**PDI**	**Zeta potential (mV)**	**%Recovery**
Day 0	35.95±0.76	0.32±0.01	-8.76±1.39	97.96±11.72
Day 7	49.94±5.44	0.18±0.02	-6.16±0.23	92.52±3.37
Day 15	70.19±15.54	0.23±0.12	-9.60±8.40	80.15±4.46
Day 30	101.97±23.84	0.20±0.02	-12.69±0.74	79.29±3.43

Figure 8. The freshly prepared Cur-NS (Day 0) and re-dispersed Cur-NS (Day 30)

4.1.1.2.5. *In vitro* drug release study

The release from the dialysis bag was conducted to demonstrate and compare the dissolution of Cur-NS with Cur solution. With an equivalent amount of Cur and under identical experimental conditions, Cur-NS exhibited a significantly more rapid release than Cur solution. At 12 hours, the release of Cur was about 23%, whereas the release of Cur-NS was nearly complete (89%) at this time point (Fig. 9). This accelerated release was attributed to the dissolution of the nanosized Cur-NS, which underwent polymorphic changes and were aided by surfactant dispersion, resulting in a faster dissolution rate compared to Cur. This finding aligns with literature reports indicating that NS formulations of poorly soluble drugs show improved dissolution compared to their amorphous counterparts (87, 90, 91). For a drug to be effective, it needs first dissolve to facilitate absorption into the systemic circulation. A higher dissolution rate enhances the efficiency of Cur's biological action under physiological conditions (92).

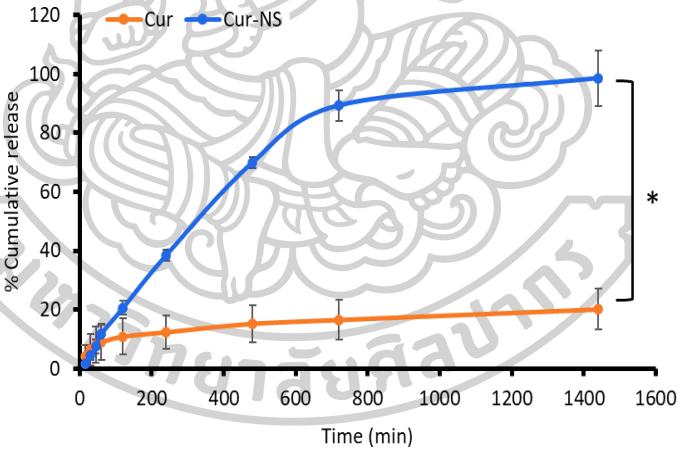

Figure 9. The release profiles of Cur and Cur-NS at pH 7.4 under sink condition (n=3). (*Significant difference, $p < 0.05$)

4.1.1.2.6. DPPH assay

The antioxidant properties of Cur-NSs were compared to those of a Cur suspension using the DPPH radical scavenging assay. This assay relies on the reduction of the stable, purple DPPH radical to a yellow non-radical form, with the color change indicating antioxidant activity. As illustrated in Figure 10, the Cur suspension exhibited limited DPPH scavenging activity across all tested concentrations, reaching a

maximum inhibition of only 25% at the highest concentration. This low activity is attributed to the poor solubility and dispersion of Cur in aqueous medium, hindering its interaction with DPPH radicals. In contrast, Cur-NSs demonstrated significantly higher DPPH scavenging activity at all concentrations, highlighting their enhanced antioxidant potential. The IC50 value, which indicates the concentration needed to scavenge 50% of the DPPH radicals, was determined to be 25.14 ± 3.46 µg/mL for Cur-NSs, based on a logarithmic fit of the dose-response curve. The improved solubility and bioavailability of Cur in nanosuspension form, which allows for better dispersion in the aqueous medium and more effective radical scavenging. This enhanced antioxidant activity can be beneficial in the wound healing process, primarily by reducing inflammation (17). The anti-inflammatory effect of Cur is attributed to its ability to modulate and scavenge free radicals produced by lipoxygenases. Additionally, the molecular structure of Cur, featuring phenolic groups in the ortho and/or para positions of the aromatic rings, provides high electron-shifting properties, enhancing its ROS scavenging capabilities. (49, 93, 94). Therefore, Cur-NSs, with their potent antioxidant effects, may serve as valuable assets in promoting wound healing.

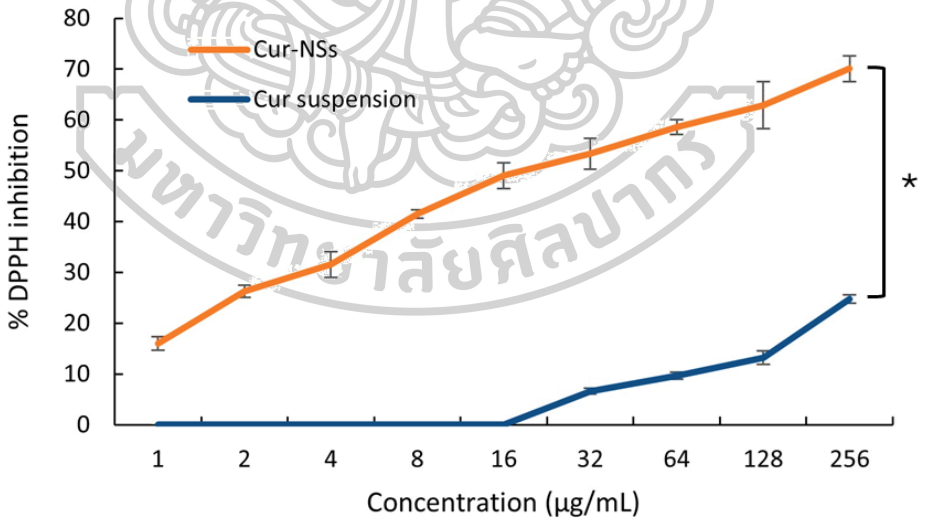

Figure 10. The antioxidant activity of Cur-NSs and Cur suspension was examined through DPPH radical inhibition (*Significant difference, $p<0.05$)

4.1.1.2.7. Cytotoxicity

To optimize Cur-NS for wound healing, its potential toxicity towards NHF cells was evaluated. The results showed that both Cur-NS and Cur were non-toxic,

maintaining cell viability over 80% across all tested concentrations (as shown in Fig. 11). Given that Cur is a naturally occurring compound widely used in cuisine and traditional medicine, its physical modification into NS did not compromise its safety profile, indicating its suitability for topical skin applications (95).

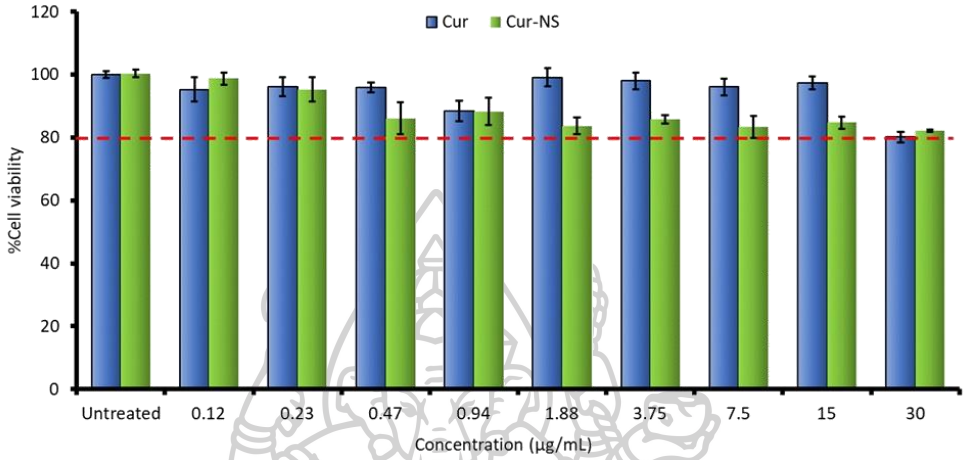

Figure 11. The cytotoxic effect of Cur and Cur-NS toward NHF cells

4.1.1.2.8. *In vitro* scratch assay

To evaluate the effectiveness of Cur-NS in the wound healing process, an *in vitro* scratch assay was conducted. This simple and cost-effective method was used to demonstrate and compare the rate of gap closure, simulating the wound healing process. (73, 96). Based on the data presented in Table 13 and Figure 12, it is clear that the percentage of wound closure increases over time for both Cur and Cur-NS treatments. The observed data indicates that wound closure is more significant in cells treated with Cur-NS compared to those treated with Cur and the untreated control cells at both 24 and 48 hours. The calculated cell migration rates further support this observation. The highest migration rate was recorded for the Cur-NS treatment at 2.23 ± 0.24 µm/h ($p < 0.05$), while Cur treatment resulted in a migration rate of 1.57 ± 0.10 µm/h, and the control group had the lowest rate at 1.13 ± 0.28 µm/h. This enhanced cell migration rate with Cur-NS can be attributed to the preparation method of the samples in DMEM, an aqueous medium. This medium may limit the solubility of Cur, but in the Cur-NS formulation, the active ingredient dissolves more effectively when the cells encounter the aqueous solution, thereby enhancing cell migration. Overall, the data suggests that Cur-NS is more effective in promoting wound closure and cell migration compared to

Cur alone, likely due to improved solubility and availability of the active ingredient in the Cur-NS formulation. The enhanced rates of cell movement indicate that the Cur-NS formulation is promising for further development as a wound-healing treatment. Previous research has shown that Cur can speed up the wound healing process when dissolved in suitable solvents, such as dimethyl sulfoxide or oleic acid.(17, 53). In this study, the solubility of Cur was enhanced by transforming it into an optimized NS formulation. This modification increased the efficacy of Cur in promoting wound closure by accelerating the rate of cell migration.

Table 13. Wound closure rate illustrated by the image-based monitoring of NHF migration at 0, 24, and 48 h under an inverted microscope (4× magnification)

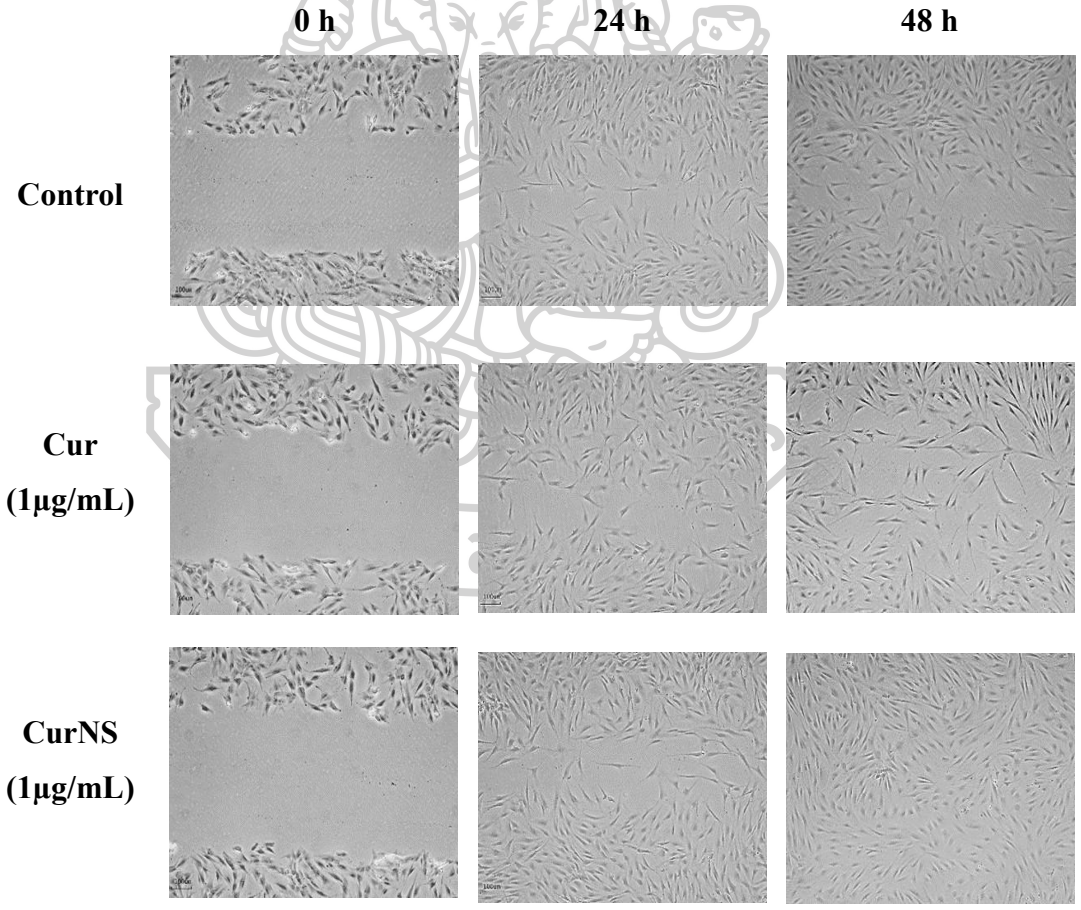

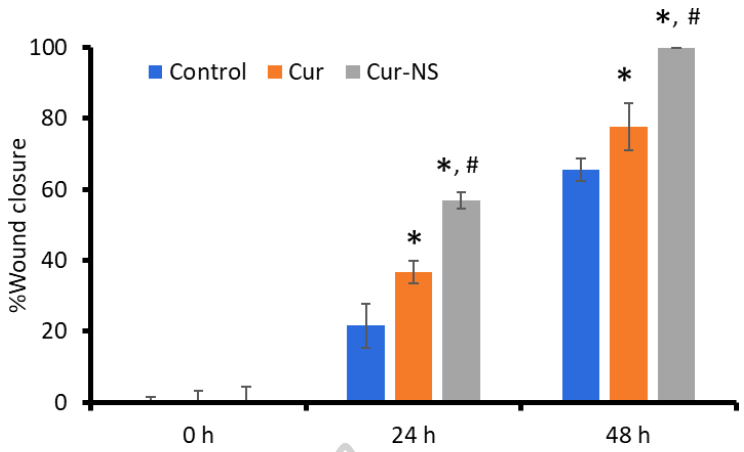

Figure 12. The percentage of wound closure when treated with Cur or Cur-NS at different times (n=3) (*Significant difference compared to control, #compared to Cur, $p < 0.05$)

4.1.2. Curcumin Liposomes

4.1.2.1. Optimization of Cur-Ls formulation using Box-Behnken design

PC and CHO were selected for the development of a liposomal formulation, forming a lipid bilayer via the film hydration method. The lipid composition plays a crucial role in determining various characteristics of liposomes, including particle size, rigidity, fluidity, stability, and electric charge (97). An optimized molar ratio of 5:1 for PC and CHO was identified based on vesicle size and uniformity. To enhance liposomes properties like flexibility, stability, and penetrability, and improve entrapment efficiency of the drug, ultra-deformed liposomes were developed. Specifically, non-toxic and biocompatible edge activators like Tween® 20, along with oleic acid, were used as penetrating enhancers (98). The experimental design was used to determine the optimal variables necessary to achieve a specific response goal while minimizing the number of experiments required. The Cur in deformable liposomes were optimized by investigating the effects of the independent variables such as Tween® 20 (%) (X_1), Oleic acid (%) (X_2), and the concentration of Cur (X_3) and their interaction using a Box-Behnken Design (BBD) implemented with Design-Expert software. The software produced 17 experimental runs, including five center points after applying the data. Table 5 displays the responses on size (nm) (Y_1), PDI (Y_2), Zeta (mV) (Y_3), and LC (µg/mg) (Y_4) observed after the characterizations of each run. The particle size of Cur-Ls from all formulations varied from 58 to 114 nm, which was an appropriate size range

to enhance dermal delivery by facilitating penetration while maintaining sufficient drug encapsulation and retention. As per the reported studies, the observed particle size of Cur-Ls is within the acceptable range for skin penetration (99, 100). The PDI values were from 0.01 to 0.39 as shown in Table 5, which indicates all the experimental runs had a dispersion of particle size within an acceptable range (100). The zeta potential of all the Cur-Ls ranged from 7.3 to -45 mV. The majority of liposomes exhibited a negative charge, attributed to the presence of amphiphilic molecules such as Tween® 20 and oleic acid. Both of these molecules contain polar groups (ether oxygen in Tween® 20 and carboxyl groups in oleic acid) that become exposed on the outer surface of the liposome when integrated into its lipid bilayer. In an aqueous environment, these polar groups ionize, leading to the generation of negative charges (101, 102). The loading capacity of Cur in the liposomes was between 1.9 and 21.8 µg/mg. Tween® 20 in liposomal formulations enhances drug loading by improving solubility, stabilizing liposomes, altering membrane properties, and facilitating drug-liposome interactions. The five central points were carried out to validate and refine the assessment of the influences of the parameters, aiming for a more accurate prediction of their impacts. Figure 13 shows the 3D diagrams for each of the four responses, which are used to analyze the interactions between two variables (Tween® 20 and oleic acid), with Cur concentration fixed at the center point and to examine the combined effects of these factors on the responses. The plot in Fig. 13 (A) illustrates that the amount of Tween® 20 (X_1) had a negative impact on particle size (Y_1), with liposome diameter increasing as the amount of Tween® 20 decreased. The reduction in particle size with higher levels of Tween® 20 is likely due to steric repulsion between the particles (103). Additionally, the addition of the surfactant caused a destabilizing effect within the bilayer. The amphiphilic structure of Tween® 20 enhanced the interaction between the phospholipid bilayer and the aqueous environment, leading to the formation of smaller liposomes and preventing or minimizing aggregation (104). Conversely, increasing the amounts of oleic acid (X_2) and Cur (X_3) led to an increase in particle size due to the incorporation of Cur into the liposome bilayers. The following linear model equation (Eq. 18) was generated to define the correlation between the particle size and the different levels of independent variables:

$$Y_1 \text{ (Size)} = 83.86 - 17.39X_1 + 16.05X_2 + 4.34X_3 \quad \text{Eq. 18}$$

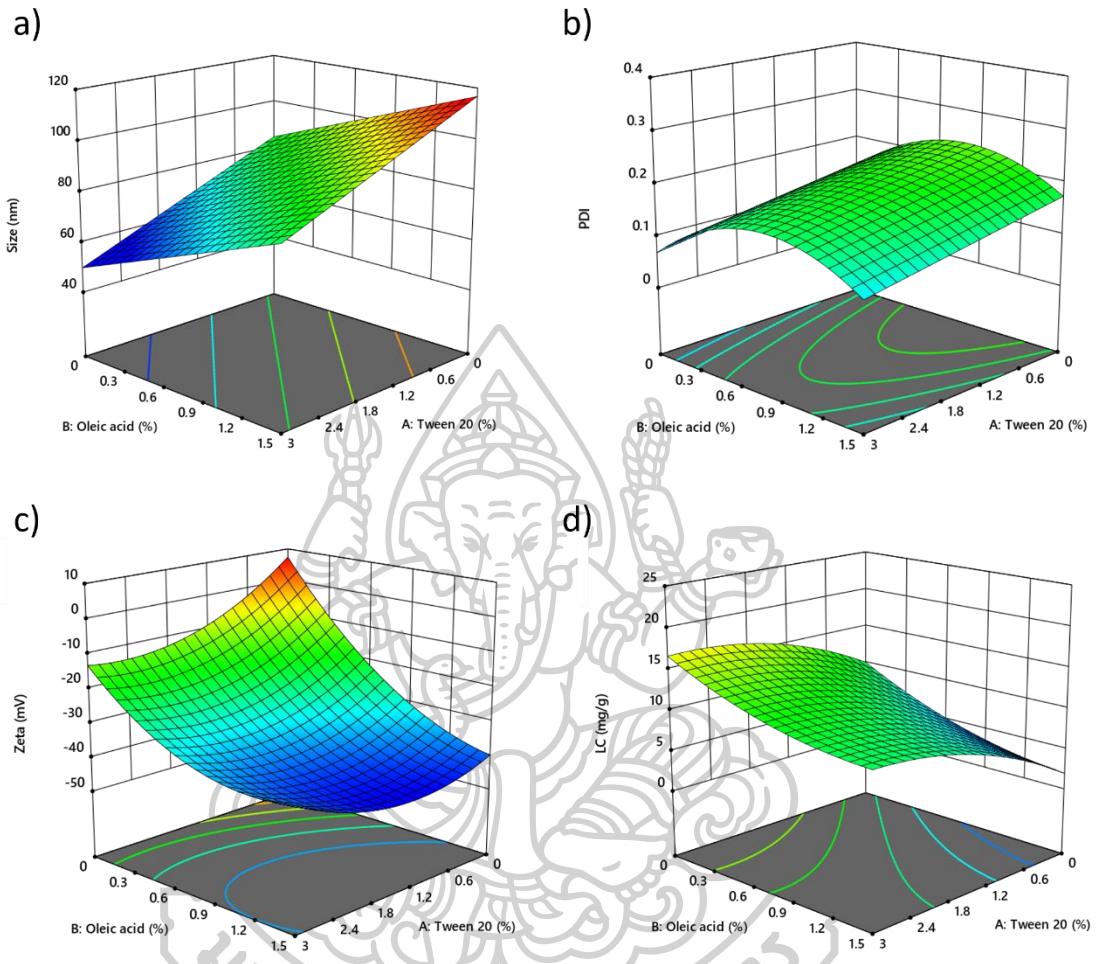

Figure 13. The 3D surface response plots illustrate the influence of independent factors chosen for the formulations on **a)** particle size, **b)** PDI, **c)** zeta potential, and **d)** LC of Cur

Figure 13 (B) illustrates that the PDI (Y_2) for all liposomes ranged from 0.01 to 0.39, reflecting the size homogeneity of the liposome formulations. Varying the amounts of Tween® 20 (X_1) and oleic acid (X_2) had no significant impact on the PDI value. The regression equation (Eq. 19) suggests that all components positively influenced the PDI value. However, according to the multiple regression equation model, the interaction between the two factors (X_1X_3) resulted in negative consequences.

Y_2 (PDI) $=0.2032 - 0.0413X_1 + 0.0175X_2 + 0.0262X_3 - 0.0550X_1X_3 - 0.0796X_2^2 + 0.0579X_3^2$ Eq. 19

The regression equation (Eq. 20) for Zeta Potential (Y_3) showed that the amount of Cur and the interaction between two factors (X_1X_2 and X_2X_3) had a positive effect. The ionization of polar groups of edge activators in an aqueous environment results in an increased negative charge on the particle surface and lead to decreased zeta potential (105). The positive zeta potential was observed only in the liposome formulation without Tween® and oleic acid. As the phospholipid is cationic, it can contribute positive zeta potential of the liposome, especially in the absence of edge activators Fig. 13 (C).

Y_3 (Zeta) $= -36.26 - 4.23X_1 - 17.23X_2 + 1.55X_3 + 6.32X_1X_2 - 2.32X_1X_3 + 0.9175X_2X_3 + 7.54X_1^2 - 8.70X_2^2 + 2.20X_3^2$ Eq. 20

The increased Cur loading (Y_4) was correlated with higher quantities of Tween® 20 and Cur itself, while a reduced Cur content was associated with increased oleic acid, as shown in the 3D plot Fig. 13 (D). This is probably because of the repulsive force between the carboxylates of oleic acid and the partial negative charge of Cur, also explained in the following Eq. 21.

Y_4 (LC) $=10.72 + 4.05X_1 + 4.03X_2 + 4.12X_3 + 0.04X_1X_2 + 3.45X_1X_3 + 3.05X_2X_3 + 2.01X_1^2 + 1.49X_2^2 - 2.61X_3^2$ Eq. 21

Considering the outcomes of each experiment, the data were analyzed, and the ideal Cur-Ls formulation was chosen based on the criteria presented in Table 14, ensuring optimal performance. The smaller particle size of liposomes, which is typically associated with enhanced stability and improved cellular uptake and distribution, thus sets the goal for minimizing particle size. Additionally, the PDI values obtained from all experiments were found to be acceptable, constantly below 0.4, thus the experimentally observed range was used as the criteria for optimization. As a zeta potential within the range of ±35 mV is considered sufficient for particle stability, the range between -35 and -15 mV was determined as criteria for optimized formulation (106) . Lastly, the loading capacity of Cur was set to be maximized using the software. By using the numerical point prediction optimization method within Design Expert®11

software, the formulation comprising Tween® 20 (2.7%), Oleic acid (0.04%), and Cur (8.1%) was identified as the optimized formulation for Cur-Ls. This formulation achieved a desirability value of 1, indicating its alignment with the specified criteria and optimal performance.

Table 14. The criteria for the optimization of Cur-Ls and the optimized formulation

Factors & responses	**Goal**	**Lower limit**	**Upper limit**	**Solution**	**Desirability**
X_1: Tween® 20 (%)	is in range	0	3	2.7	1.000
X_2: Oleic acid (%)	is in range	0	1.5	0.04	
X_3: Curcumin (%)	is in range	1	10	8.116	
Size (nm)	minimize	58	114		
PDI	none	0.01	0.39		
Zeta (mV)	is in range	-35	-15		
LC (µg/mg)	maximize	1.9	21.8		

To confirm the optimal Cur-Ls formulation, the confirmation experiments (n=3) were conducted. Then, the predicted responses values acquired from the software were compared with the actual values obtained from the experiments. This comparison served to validate the accuracy and reliability of the optimized formulation in achieving the desired outcomes. According to the data presented in Table 15, it was observed that all the responses obtained from the confirmation experiments were closely aligned with the predicted values, with no significant difference ($p>0.05$). The optimized formulation yielded a desirable nanosized, homogeneity, and a negative charge liposome with a maximized loading efficiency of Cur, as evidenced by the comparable results between predicted and actual values. With these favorable results of confirmation, the optimized Cur-Ls were prepared for further experiments and analysis.

Table 15. The comparison of the predicted values of the optimized Cur-Ls formulation vs the actual value

Responses	Predicted mean	Actual mean	P-value
Size (nm)	55.80 ± 6.34	64.02±3.37	0.1187
PDI	0.08 ± 0.03	0.11±0.026	0.2262
Zeta (mV)	-15.03 ± 1.55	–17.26±3.56	0.1979
LC (µg/mg)	22.08 ± 2.22	19.92±0.54	0.1758

4.1.2.2. Characterization and evaluation of the optimized Cur-Ls

4.1.2.2.1. Transmission electron microscopy (TEM)

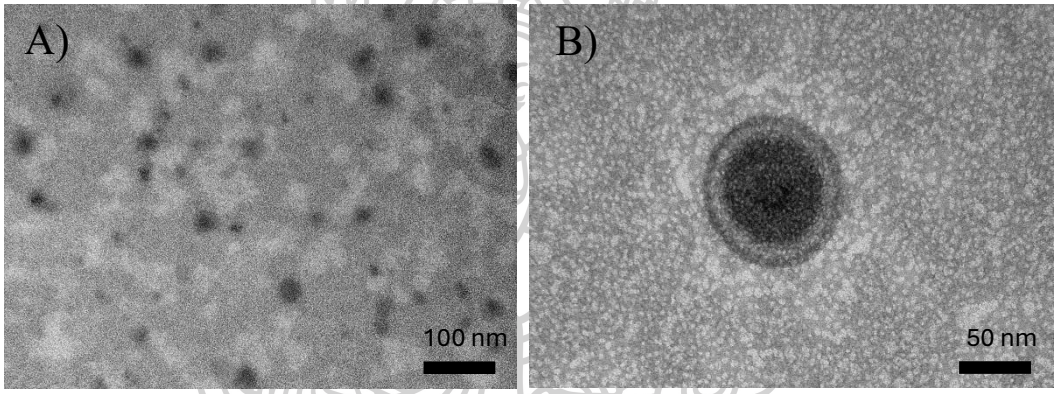

Figure 14. TEM images of Cur-Ls in the magnification **A)** 100 nm and **B)** 50 nm

The TEM images of Cur-Ls in the magnification A) 100 nm and B) 50 nm depicted in Fig. 14 provide crucial insights into their structural characteristics. They highlighted not only the characteristic spherical shape of liposomes but also the importance of size distribution and uniformity, which is essential for evaluating their stability and suitability for drug delivery purposes (107). Moreover, these images may reveal information regarding the efficiency of Cur encapsulation and prove that stable liposomes were formed.

4.1.2.2.2. DPPH assay

The antioxidant capacity of Cur and Cur-Ls was assessed by their ability to inhibit DPPH radicals, as shown in Fig. 15. The analysis revealed that the percentage of DPPH inhibition increased with increasing concentration for both formulations. The antioxidant activity of the Cur suspension started at a concentration of 16 µg/mL,

while the Cur-Ls formulation showed activity starting at 1 µg/mL and reached nearly 90% inhibition at the highest concentration of 256 µg/mL. In contrast, the Cur suspension exhibited significantly lower inhibition, peaking below 30%. The IC50 value of Cur-Ls was 16.42 ± 0.0724 µg/mL. These findings were attributed to the greater stability and solubility of Cur in the liposomal formulation in aqueous media (108, 109). Therefore, the enhanced solubility of Cur in Cur-Ls significantly affects its ability to act as an antioxidant. The antioxidant properties of Cur are crucial for wound healing, mainly through the reduction of inflammation. Cur's impact on oxidative stress markers is due to its unique properties that target the neutralization of reactive oxygen and nitrogen species, its ability to bind metals, and its influence on the activity of different enzymes (110, 111). Moreover, Cur contributes to various stages of the healing process, where its antioxidant effects can specifically enhance wound healing (112). While Cur's poor water solubility limits its effectiveness (113), the enhanced solubility of Cur in liposomes improves its potential for aiding wound healing (114).

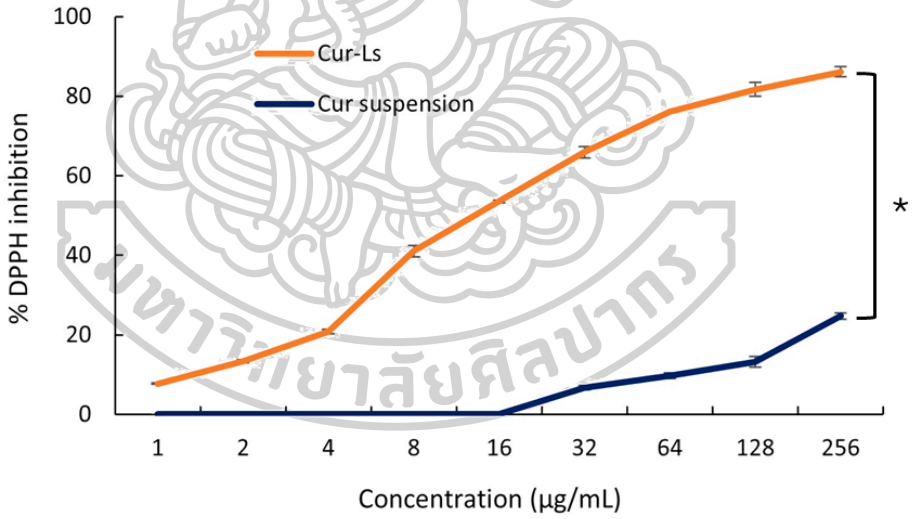

Figure 15. The antioxidant activity of Cur-Ls and Cur suspension through DPPH radical inhibition (*Significant difference, $p<0.05$)

4.1.2.2.3. Cytotoxicity

The cell cytotoxicity of Cur-Ls and Cur solution was determined in NHF cells using the MTT assay. NHF cells were treated with increasing concentrations of free Cur and Cur-Ls ranging from 0.78 to 6.25µg/mL for 24 h. Percentage cell viability for each treatment relative to the control (untreated cells) was shown in Fig. 16. The safety of Cur-Ls was observed at all tested concentrations, maintaining over 80% cell viability. These results indicated that the components included in the liposome formulation, such as Tween® 20, oleic acid, PC, and CHO, were nontoxic to the normal fibroblast cells, in agreement with the previous research (115). The beneficial effects of incorporating Cur into phospholipid-based nano-systems on cell viability and proliferation have been established. (66).

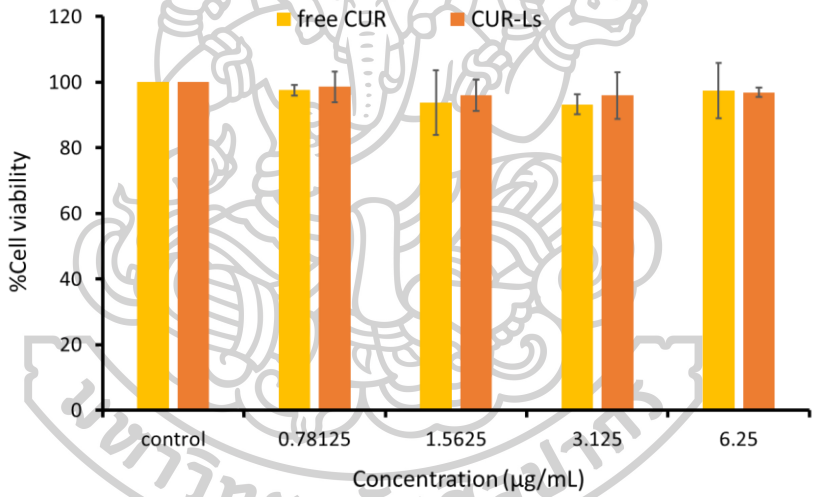

Figure 16. Percent cell viability of free Cur and Cur-Ls toward NHF cells

4.2. Hydrogel patches

4.2.1. Genipin-crosslinked CS/PVP hydrogel patch

4.2.1.1. Experimental design and optimization

The genipin crosslinked CS-based hydrogels were obtained after a 24-h crosslinking process. Initially, the polymer mixtures exhibited a pale-yellow color, gradually transitioning from a light to a deep blue upon crosslinking. The color of the hydrogels was correlated with the CS content, displaying a darker blue hue with higher CS concentrations. During this process, genipin served as a crosslinking bridge between the glucosamine units of CS chains through two main reactions. The primary reaction

involved a nucleophilic attack by a CS amino group on genipin, opening the dihydropyran ring and forming a tertiary amine. The secondary reaction was a nucleophilic substitution of the ester group of genipin, resulting in the formation of an amide bond (116). The formation of blue pigments can be attributed to crosslinking reactions and possibly oxygen radical-induced polymerization (117, 118). A simplex centroid mixture design was chosen to determine the optimal mixture proportion of polymers for the hydrogel matrix that maximized the percentage of swelling (%SW), degree of crosslinking (DC), and mechanical strength (MS). This design approach is an effective method for evaluating the impact of composition changes on hydrogel properties (22). The design was implemented as an optimization technique by adjusting the quantities of three components while maintaining their total concentration constant. The design comprised 2^3-1 distinct design points, encompassing single-component blends (1, 0, 0), binary mixtures (1/2, 1/2, 0), and a ternary mixture (1/3, 1/3, 1/3) [30]. The responses for each design point are presented in Table 3. It was observed that %SW ranged from 242 to 587%. Hydrogels rich in PVP exhibited higher swelling due to their hydrophilicity and functionality, allowing for greater interaction with water molecules than PVA (119). When PVP and PVA were combined, the hydrogel showed lower swelling, possibly due to additional crosslinking interactions among the polymers. The formation of bonds between the amine group of CS and the hydroxyl groups of genipin, PVP, and PVA could reduce the presence of hydrophilic functional groups, thereby decreasing the swelling capacity of the hydrogels (120). However, the interaction of CS with PVA and PVP positively affected the degree of crosslinking of all hydrogels, which exceeded 78%. This also translated to the MS, which ranged from 224 to 245 g/cm^2, demonstrating desirable mechanical properties.

$$\%SW = 341.54A+425.83B+378.01C+723.07AB+195.57AC-533.68BC-5773.52ABC \quad \text{Eq. 22}$$

$$DC = 81.23A+87.91B+80.48C-22.35AB+5.30AC+4.35BC \quad \text{Eq. 23}$$

$$MS = 231.70A+238.50B+230.50C-25.19AB+55.41AC-41.98BC-429.60A^2BC+338.86AB^2C-704.26ABC^2 \quad \text{Eq. 24}$$

The response data in Table 3 was transformed into polynomial equations with three independent variables. These equations (Eq. 22-24) can be utilized to assess the relative impact of variable factors by comparing the positive and negative coefficients within the mathematical models. The mixture contour plots of the responses are illustrated in Fig. 17 to present the effect of each factor on the responses. The highest and lowest values of the response are represented in red and blue areas, respectively. Figure 14(A) shows that the %SW was strongly affected by the PVP ratio regardless of CS content. As mentioned, an increased CS content results in stronger covalent bonds, leading to a tighter structure. Consequently, the polymeric chains within the hydrogel exhibit reduced mobility and limited swelling. The degree of swelling can also be tuned by the number of hydrophilic moieties in the hydrogel network (121). Thus, a higher proportion of PVP resulted in a higher swelling capability of the hydrogel. A positive relationship with the DC was found when the proportion of PVP was increased and the CS amount decreased, as shown in Fig. 14(B). Considering the MS of the hydrogel, the strength was significantly increased in the presence of PVA or PVP, as depicted in Fig. 14(C). Therefore, the proportion of PVA or PVP largely influences the DC and MS of the hydrogels.

A mathematical approach was employed to determine the optimal conditions to obtain a desirable hydrogel under the criteria set for each parameter, as shown in Table 16. The hydrogel should possess high swelling capability, DC, and MS to absorb exudates while maintaining its solidity, robustness, and durability. Thus, the maximum response values were set as the desired criteria, and an overall desirability score was calculated by taking the geometric average of individual desirability. The optimal hydrogel formulation, composed of a binary mixture containing 70% CS and 30% PVP, was identified. Under these conditions, the model predicted the optimized hydrogel's %SW, DC, and MS, as shown in Table 17. Additionally, the confirmation of the optimized condition was analyzed, and the results were compared with the predicted values. It was found that the attributes of the optimized hydrogel were comparable to the predictions and that the attained condition possesses the desired properties.

Table 16. Selected criteria of the responses with the formulations of the desired hydrogels

Factors & responses	Goal	Lower limit	Upper limit	Solution	Desirability
A: 3%CS	is in range	70	100	70	0.704
B: 5%PVP	is in range	0	30	30	
C: 5%PVA	is in range	0	30	0	
Y_1: %SW	maximize	242.36	587.40		
Y_2: DC	maximize	78.74	88.26		
Y_3: MS	maximize	224	245.27		

Table 17. Confirmation data of the optimized hydrogel compared to the predicted values

Responses	Predicted	Confirmation	P-value
%SW	425.83±38.16	486.18±11.60	0.059
DC (%)	87.91±2.05	85.89±0.58	0.176
MS (g/cm^2)	238.50±0.49	238.27±2.14	0.863

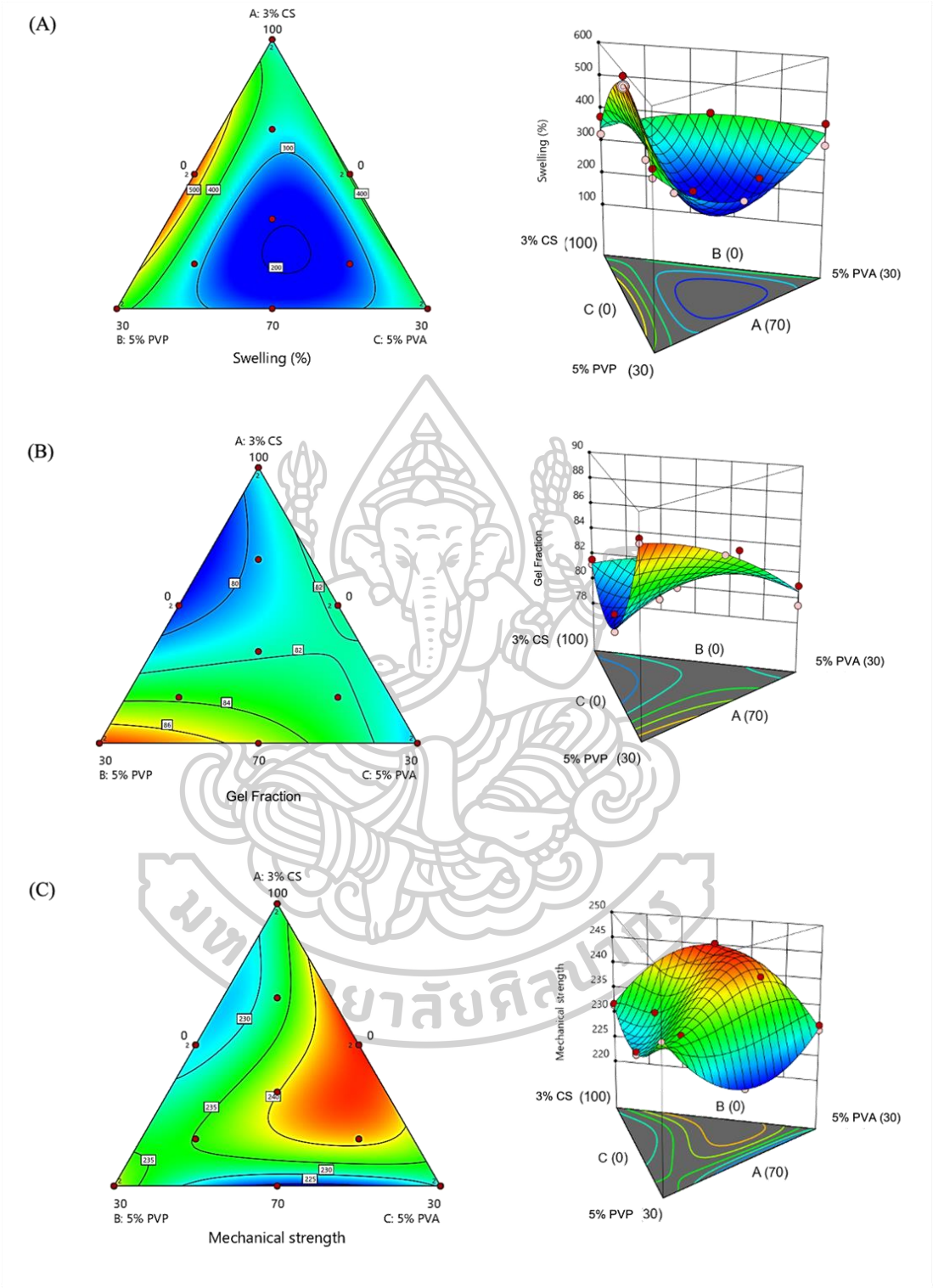

Figure 17. Contour plots and 3D surface response curve of the effect of different combinations on **A)** % SW, **B)** DC, and **C)** MS of the hydrogels

4.2.2. HA/PVA hydrogel patch

4.2.2.1. Experimental design and optimization

The hydrogels were prepared using the polymer casting method, with the composition of each hydrogel adjusted based on experimental runs. By varying the input factors (HA (A_1) and PVA (A_2)), the corresponding responses were obtained (Table 2). The % swelling (R_1) ranged from 121% to 213%, Young's modulus (R_2) was between 97 and 146 Pa/%, and % erosion (R_3) was between 16% and 37%. An appropriate model was selected to explain these responses and predictions regarding the input factors were made based on the assessment of various parameters from the regression analysis. ANOVA and multiple regression analyses were conducted to determine the model's significance. The cubic model showed p-values <0.05 for all responses, highlighting its significance in describing the relationships between the input factors and output responses (Table 5). Additionally, the lack-of-fit test ($p > 0.05$) confirmed the adequacy of the multiple regression model. The R^2 values for R_1, R_2, and R_3 were 0.8424, 0.9957, and 0.9788, respectively, indicating that the predicted models were highly appropriate, as these values are close to 1.000 (122).

The two polymers were selected based on their characteristics and physicochemical properties. HA, a naturally occurring polymer found in the extracellular matrix of connective tissues, possesses unique viscoelastic and mucoadhesive qualities, making it highly suitable for producing wound dressings that can adhere to injured tissues. Additionally, HA plays a crucial role in various phases of wound healing by promoting the migration, proliferation, and stimulation of fibroblast and keratinocyte tissues (123). Moreover, PVA offers several benefits, such as being non-toxic, highly biocompatible, biodegradable, and possessing exceptional hydrophilic properties. It is frequently used in transdermal applications (124). However, PVA is constrained by its inadequate swelling capacity, essential for effective wound healing (125). PVA is commonly blended with other polymers to enhance its swelling properties. In this study, the proposed hydrogel would be formed through bifunctional cross-linking, involving physical interactions such as hydrogen bonding and hydrophobic forces and a metal coordination complex. The physical interactions were induced using the freeze-thaw technique, where hydrogen bonds formed as the

hydroxyl groups in the polymer chain interacted with water molecules. The polymer solution underwent crystal growth upon freezing, acting as cross-linking points for the polymer chains. Upon thawing, the polymer chains became more flexible. Repeated freeze-thaw cycles resulted in the construction of numerous cross-linking points. (126). On the other hand, the metal coordination complex was formed between aluminum ions, the coordination center, and the surrounding hydroxyls, carbonyls, and amines. This coordinate covalent bond would enhance the mechanical properties of the hydrogel. Additionally, the bifunctional cross-linking process would assist in the delivery of Cur-Ls by enhancing the resilience of the hydrogel patch against water, moisture, and exudates. When wound dressings are applied, water absorption can weaken the hydrogel as the patch swells. The multi-mechanism cross-linking would mitigate the degradation of the hydrogel patch. This dual-cross-linking mechanism was anticipated to enhance the hydrogels' structural integrity, toughness, and longevity.

Table 18. Results summary of the ANOVA and multiple regression analysis

Responses	**Model**	**p-value**	**Lack of fit**	**R^2**	**Predicted R^2**
%Swelling	Cubic	0.0241	0.8901	0.8424	0.7647
Young's modulus	Cubic	< 0.0001	0.8076	0.9957	0.9935
%Erosion	Cubic	0.0083	0.2588	0.9788	0.9515
Multiple regression equation model (coded equation)					
$\%Swelling = 189.03A_1 + 121.86A_2 + 95.18A_1A_2 - 295.83A_1A_2 (A_1–A_2)$					
$Young's\ modulus = 144.29A_1 + 99.16A_2 - 90.84A_1A_2 - 106.25A_1A_2(A_1–A_2)$					
$\%Erosion = 37.95A_1 + 18.36A_2 + 40.52A_1A_2 - 41.18A_1A_2(A_1–A_2)$					

The RSM was used to investigate how parameters interact and relate to one another. Analysis of both the regression equation and the response surface plots showed that increasing the concentrations of HA and PVA positively influenced all measured responses, which included swelling percentage, Young's modulus, and erosion percentage, as seen in Table 18. On the other hand, the combined effect of

these components (A_1A_2) had negative consequences on both swelling and mechanical robustness, implying that reducing the amounts of these polymers might lead to improvements in these areas.

The optimized model suggested an ideal hydrogel formulation of 5% HA and 10% PVA with a desirability score of 0.412 (Table 19). The lower desirability was attributed to the % erosion response, which exhibited an opposite trend compared to the other responses. The combination of HA and PVA at the optimized ratio was predicted to result in maximum % swelling and Young's modulus. However, according to the predicted model, % erosion would increase, which is undesirable. This could be due to the hydrogel being loosely cross-linked after the freeze-thaw cycles, as the hydrogen bonds formed were not as abundant compared to formulas with higher PVA content (126). The optimized hydrogel patch was prepared to ensure optimization and actual responses were compared with predicted values (Table 19). It was observed that all responses were consistent with the computerized solution, confirming that the selected composition was optimized and reproducible with the desired characteristics.

Table 19. The criteria for the optimization of HA/PVA hydrogel

Variables	Goal	Solution	Desirability	Confirmation	P-value
HA	in range	5	0.412		
PVA	in range	10			
%Swelling	maximize	177.94±12.58		176.23±12.02	0.8731
Young's modulus	maximize	133.56±1.38		131.03±18.04	0.8297
%Erosion	minimize	38.28±1.36		38.31±1.84	0.9850

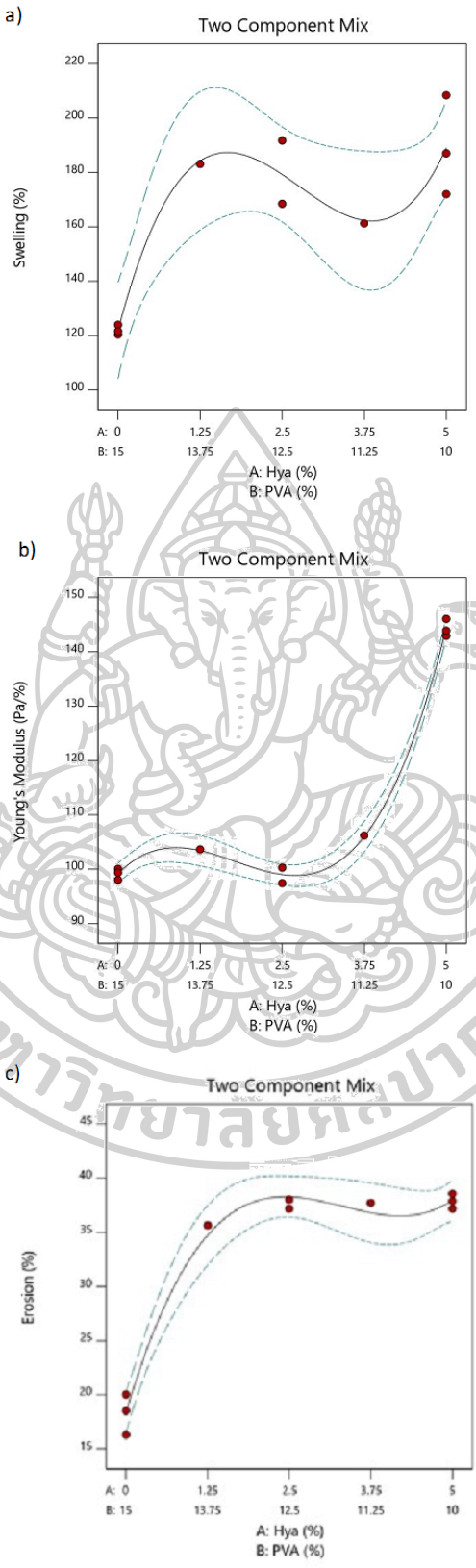

Figure 18. Response surface model graphs showing the area of maximization of the responses **a)** Swelling (%), **b)** Young's modulus (Pa/%), and **c)** Erosion (%)

4.2.2.2. Synthesis and characterization of PNVP-ITA copolymer

The PNVP-ITA copolymer was synthesized using a polymerization reaction, outlined in Fig. 19. The reaction occurred by heating a free-radical initiator (V_{50}), which produced radicals that started the polymer chain construction. These radicals caused an electron transfer between the vinyl groups of ITA and NVP, converting double bonds to single bonds and connecting the monomers together to form the long-chain PNVP-ITA copolymer.

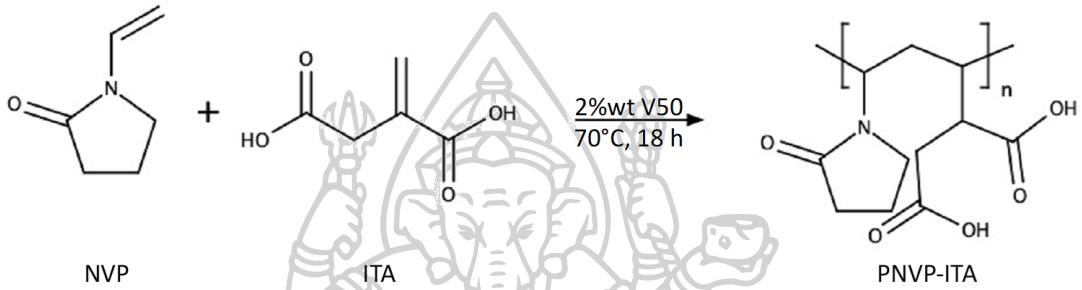

Figure 19. Synthesis scheme of PNVP-ITA

The synthesized polymer was characterized using ^{1}H-NMR and FTIR analyses to confirm the successful synthesis. In the ^{1}H-NMR spectra, the disappearance of peaks at 4.65–4.70 and 6.82 ppm, corresponding to the vinyl groups of NVP, in the PNVP-ITA spectrum indicated the acquisition of functional groups during the polymerization reaction. Subsequently, ITA displayed peaks around 3.4, 5.8, and 6.3 ppm, attributed to its methylene groups. The absence of a methylene peak in the PNVP-ITA spectrum after chain propagation confirmed polymerization, signifying the successful synthesis of the PNVP-ITA. In the FTIR spectra, the C–H asymmetric stretching of the polymer chain was observed at 2,925 cm^{-1}. Strong peaks at 1,555 and 1,397 cm^{-1} corresponded to ITA's symmetric stretching of carboxylate groups. A broad band at 3,357 cm^{-1} indicated O–H stretching from carboxylic acid and hydrogen bonding. Additionally, cyclic amide (O=CN) and CN– of NVP were observed at 1,635 and 1,198 cm^{-1}, respectively. All of these signals found in Fig. 20 and 21 confirm the structure of the PNVP-ITA as expected.

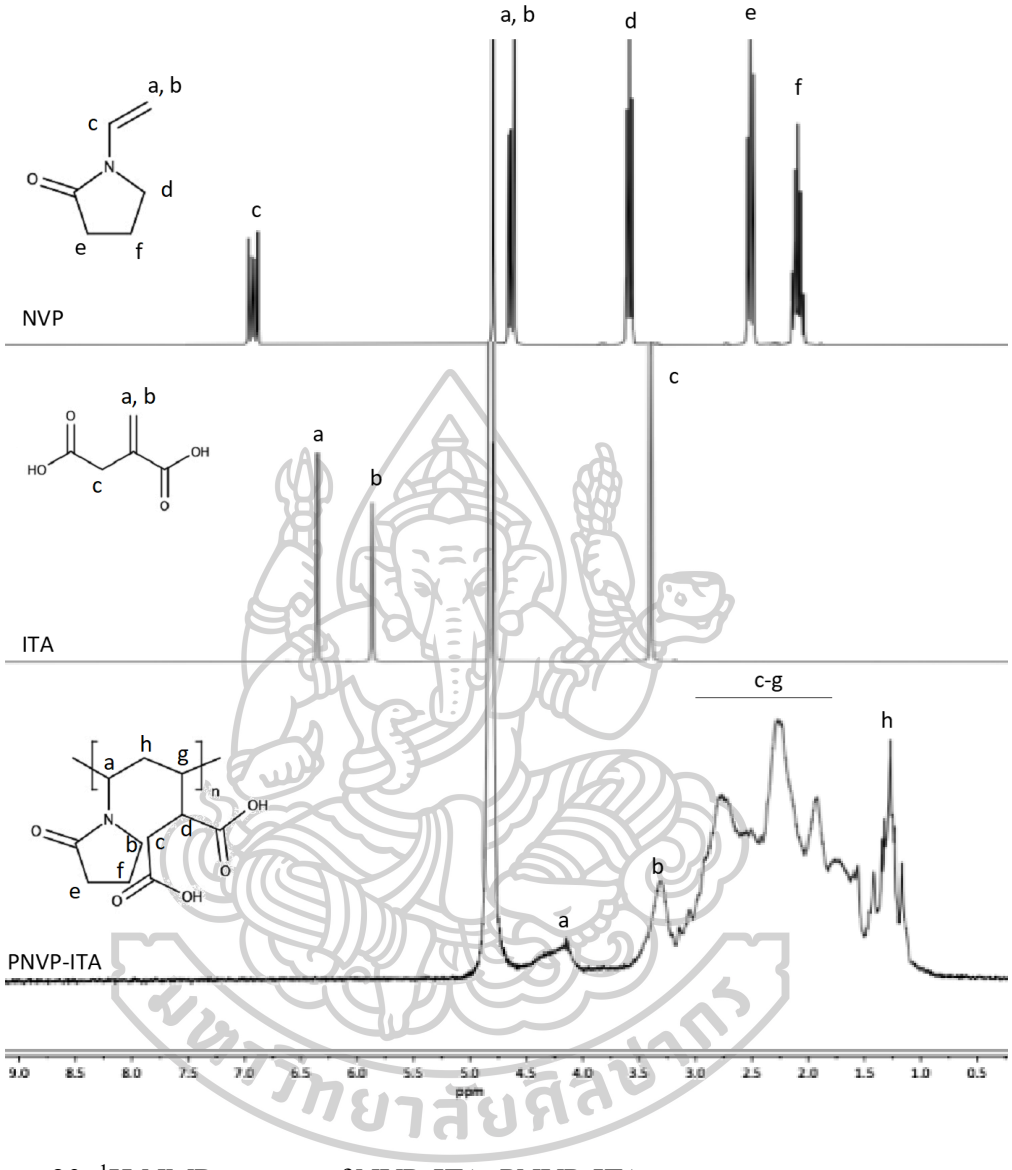

Figure 20. ^{1}H-NMR spectra of NVP, ITA, PNVP-ITA

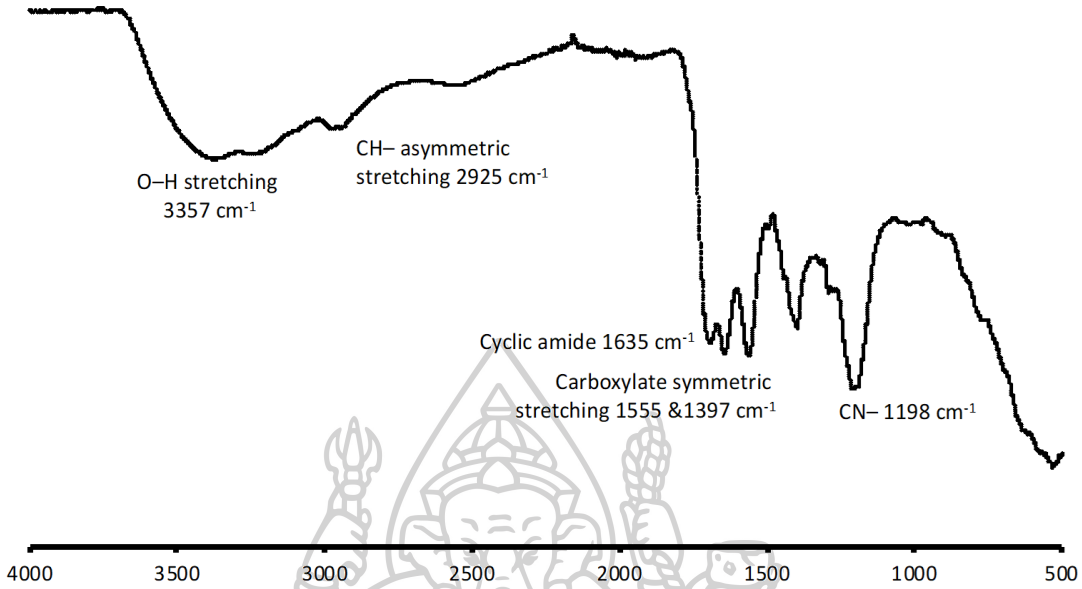

Figure 21. ATR-FTIR spectrum of PNVP-ITA

4.2.2.3. Synthesis and characterization of HA/PVA/PNVP-ITA hydrogel patch

The optimal hydrogel formula generated by the DoE was improved by incorporating 2% by weight of the newly synthesized PNVP-ITA to enhance the patch's properties. This led to significant increases in both % swelling and Young's modulus by 40.4% and 35.0%, respectively, as depicted in Fig. 22, along with a reduction in % erosion by 6.3%.

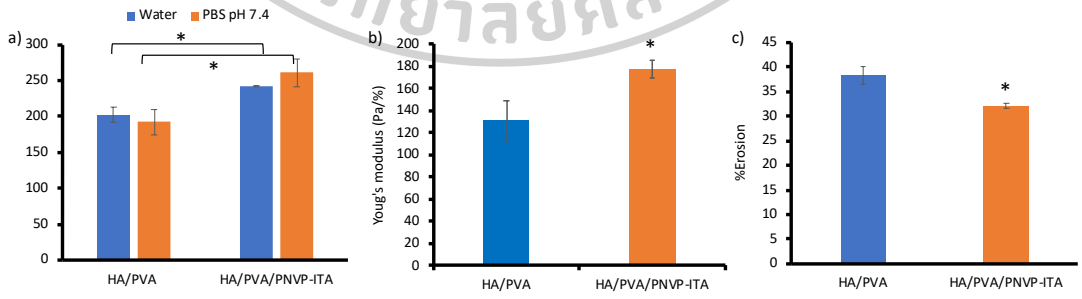

Figure 22. Comparative analysis of **a)** swelling capacity, **b)** Young's modulus, and **c)** erosion between HA-PVA and HA/PVA/PNVP-ITA hydrogels (*Significant difference, $p<0.05$)

These results provided evidence of the dual crosslinking mechanism within the initial polymers. PNVP-ITA was specifically designed to be rich in carbonyl and carboxyl groups, making it highly suitable for coordination crosslinking. Adding PNVP-ITA facilitated stronger metal coordination bonding with aluminum ions (Al^{3+}), acting as the cross-linking agent. Furthermore, the polymer enhanced the cross-linking interaction with the larger HA and PVA chains during the freeze-thaw processes. Consequently, through crosslinking enhancement, erosion was reduced, and Young's modulus increased. The hydrogel, strengthened by bifunctional crosslinking, might experience augmented swelling due to the creation of additional spaces capable of capturing water molecules. The establishment of metal coordinate covalent bonds has been demonstrated to enhance hydrogels' physical and mechanical properties. This intricate cross-linking approach could facilitate the effective delivery of active substances while maintaining the structural integrity of the hydrogel and resisting erosion caused by the absorption of wound exudate. Without sufficient cross-linking, the patch might lose its durability and effectiveness in retaining its form and function as the hydrogel expands. (127, 128). Furthermore, the swelling capacities in both water and PBS at pH 7.4 were similar, highlighting the advantages when applied to wounds. Including the synthesized polymer enhanced the mechanical properties and degradation of the hydrogel patch, as evidenced by the low % erosion. The incorporation of PNVP-ITA further enhanced the hydrogel's properties and confirmed the dual-cross-linking mechanism of the HA/PVA/PNVP-ITA hydrogel.

4.3. Characterization and evaluation of nanocomposite hydrogel patches

4.3.1. Cur-NS loaded CS/PVP hydrogel patches

4.3.1.1. Physiochemical properties of hydrogel patches

Table 20 presents the %SW, %erosion, compressive toughness, and WVTR of blank CS/PVP hydrogels and Cur-NS embedded hydrogels. Both hydrogels exhibited excellent swelling over three times their weight when immersed in a PBS solution (pH 7.4, 37°C), mimicking physiological wound exudate. Notably, the blank hydrogels displayed a higher %SW than the Cur-NS-loaded hydrogel ($p < 0.05$). This difference is presumably due to the interaction of Cur-NS with the hydrophilic functional groups of the hydrogel polymer chains. By occupying space within the hydrogel matrix, Cur-

NS obstructs the uptake and migration of water molecules into the polymer network, thereby reducing water absorption and swelling capacity. Swelling ability is one of the important parameters of hydrogel dressings as it helps absorb excess wound exudate through swelling, maintains a moist environment, and allows the release of incorporated drugs into the wound bed, making an exceptional %SW preferred (9). The increased percent erosion of Cur-NS loaded hydrogel could be due to some factors. As the hydrogel absorbs water and swells, the polymer chains expand, creating spaces within the network, potentially weakened structure. The water molecules then disrupt the interactions holding the polymer chains together, leading to the breakdown and erosion of the hydrogel. This erosion process, in turn, can facilitate the release of Cur-NS from the polymeric matrix. Furthermore, the durability of the hydrogel patch was evaluated through a compression test. The compressive toughness of both hydrogels was found to be 230 g/cm^2. Though a precise benchmark of the strength was not mentioned in the literature, we suggest that the value obtained is sufficient to provide a bearable patch characteristic that is neither too fragile nor rugged. The WVTR is a fundamental property of wound dressing that determines the ability to regulate moisture, facilitate gas exchange, and control water loss during wound healing (129). The observed WVTR for blank and Cur-NS loaded hydrogels was found practical, as they would regulate moisture levels without causing excessive drying or an unwanted accumulation of moisture. The results prove that adding Cur-NS to the hydrogel did not significantly impact the compressive toughness and WVTR of the blank hydrogel.

Table 20. The physicochemical properties of hydrogels

Hydrogel patches	**Swelling (%)**	**Erosion (%)**	**Compressive toughness (g/cm^2)**	**WVTR (g/m^2/24h)**
Blank hydrogel	462.46 ± 15.61	13.57 ± 2.19	238.26 ± 2.13	819.92 ± 150.72
Cur-NS hydrogel	303.38 ± 12.91	27.17 ± 1.33	231.45 ± 7.00	808.27 ± 94.73

4.3.1.2. SEM

SEM analysis was performed to visualize the morphology and network structure of genipin-crosslinked CS/PVP hydrogels before and after Cur-NSs were embedded. Hydrogel samples were swollen for 24 h and lyophilized to preserve the porous structure. The cross-sectional images of the hydrogels were captured at 100× and 10,000× magnifications, as shown in Fig. 23. It can be observed that both hydrogels were interconnected, displaying a uniformly distributed microporous structure arranged as long hollow tubes, as presented in Fig. 23(A) and Fig. 23(C). This structure is conducive to efficiently removing wound exudate, delivering the loaded drug in a controlled manner, and facilitating gas exchange to the wound, thereby promoting cell growth (130). The incorporation of Cur-NS within the hydrogel structure yielded a more compact structure with decreased pore size of the hydrogel network, as shown in Fig. 23(B) and Fig. 23(D) (131). This pore size reduction corresponded with the lower %SW in Cur-NS loaded hydrogel compared to the blank hydrogel aforementioned.

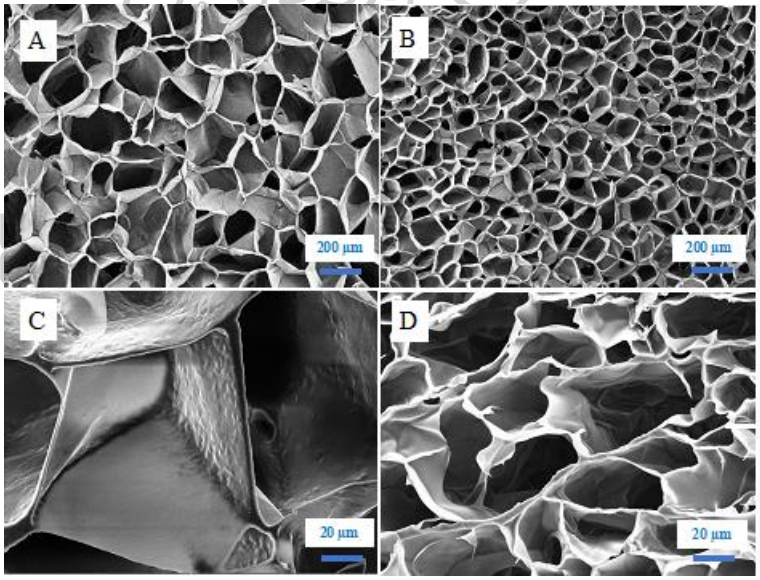

Figure 23. SEM images of **A**) blank hydrogel (100×), **B**) Cur-NS loaded hydrogel (100×), **C**) blank hydrogel (10k×), and **D**) Cur-NS loaded hydrogel (10k×) taken at the swollen state

4.3.1.3. FTIR

Fig. 24 illustrates the FTIR spectra of CS/PVP hydrogel, Cur-NS, and Cur-NS loaded CS/PVP hydrogel, highlighting the interactions between the Cur-NS and the

CS/PVP hydrogel. In the combined spectra of the Cur-NS loaded CS/PVP hydrogel, the typical peaks of Cur-NS were observed. The C-H stretching vibrations around 2870 cm^{-1} indicate the presence of aliphatic methylene groups. The C-O stretching vibration at 1341 cm^{-1} is characteristic of the phenolic structures in Cur, while the C-O-C stretching vibrations at 1102 cm^{-1} are attributed to ether linkages found in both Pluronic® F-127 and Tween® 20, as well as in the Cur molecule (132). The characteristic peaks of the hydrogel matrix were observed at 3445 cm^{-1} for O-H stretching and 1650 cm^{-1} for C=O stretching, suggesting the formation of hydrogen bonds within the hydrogel matrix. There were no shifts found in the key amide regions, and the O-H stretching peak was a slight shift in the combined spectra, indicating the interaction between Cur and the hydrogel matrix and confirming the integration of Cur into the hydrogel.

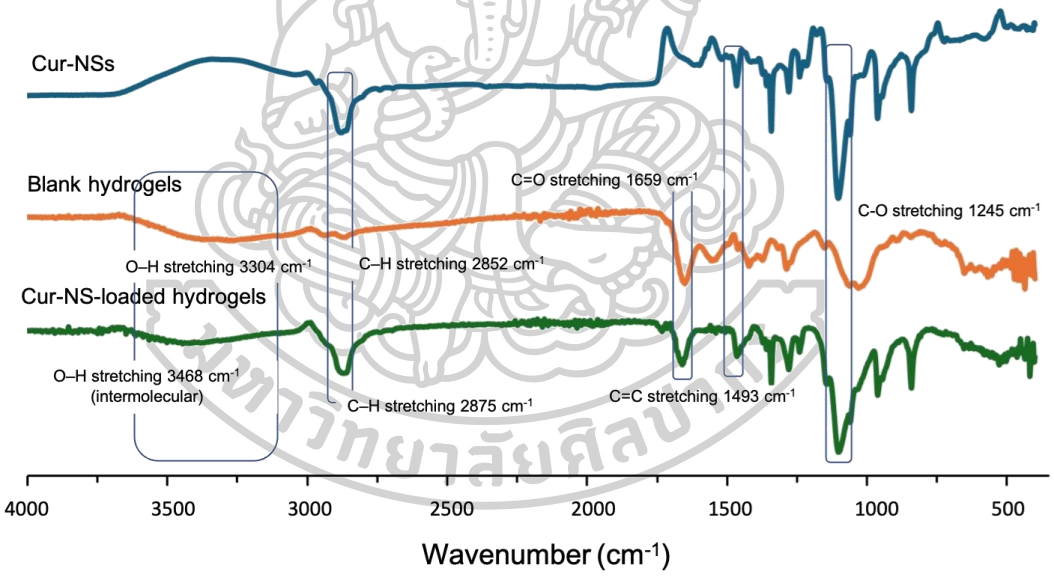

Figure 24. The ATR-FTIR spectra of CurNS, CS/PVP hydrogel, and Cur-NS loaded CS/PVP hydrogel

4.3.1.4. Drug loading

Due to the polymeric hydrogels' numerous porous structures and functional groups, nanomaterials containing hydrogel-based dressings have been extensively reported as the most effective drug delivery cargos for efficient wound healing (133). In this study, different concentrations of Cur-NS were incorporated into the optimized

hydrogel formulation by blending with the polymer mixtures. Notably, the optimization of Cur-NS was conducted using the Box-Behnken design in our previous research (132). The LC and %EE of Cur-NS in the fabricated hydrogels are summarized in Table 21. The highest LC and %EE were achieved when 5% of Cur-NS (Cur-NS 5) of the total polymer weight was added to the hydrogel. An increase in %LE and LC were observed with an increase in the Cur content; thus, further addition of Cur-NS into the hydrogel was not conducted as %EE of 100 was achieved at Cur-NS 5, and this formula was selected for other experiments.

Table 21. Loading capacity and entrapment efficiency of Cur-NS in the optimized hydrogels (* Significant difference from Cur-NS 1, # Significant difference from Cur-NS 1 and Cur-NS 3)

Loaded Cur-NS (%)	LC (mg/g)	%EE
Cur-NS 1 (1%)	0.12±0.01	33.44±3.37
Cur-NS 3 (3%)	0.91±0.01	84.36±1.15*
Cur-NS 5 (5%)	1.75±0.11	97.54±4.54*, #

4.3.1.5. *In vitro* release studies

The *in vitro* release behavior of the Cur-NS-embedded hydrogel was conducted in a mixture of PBS and 0.5% Tween® 80 with a pH of 7.4, simulating the natural wound environment (134). Fig. 25 illustrates the percentage of cumulative Cur release from the hydrogel compared to the release from Cur-NS and Cur solution. The release of Cur solution was limited to 25% after 24 h, attributed to the poor aqueous solubility of the compound. Cur-NS exhibited a biphasic release pattern with an initial burst release of 50% after 2 h, followed by a continuous release, reaching nearly 100% at 24 h. The NSs significantly enhanced the aqueous solubility of Cur, leading to an improved release profile. However, the release rate of Cur-NS after incorporation into the hydrogel was dramatically decreased compared to Cur-NS alone. Only 15% of Cur was released from the hydrogel after 2 h. Subsequently, Cur-NS released at a slower rate, reaching 42% at 12 h and eventually 60% at 24 h. This may be advantageous to the healing process once applied to the wound, prolonging the effect of Cur-NS through the extended-release profile proposed by the findings. Though the release of Cur-NS from the hydrogel was

retarded, the improved dissolution of the active compound was still evident compared to Cur.

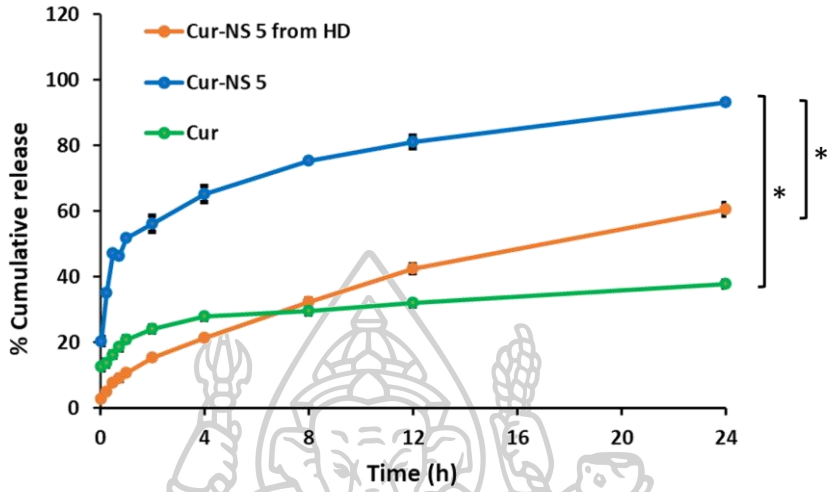

Figure 25. The cumulative release profile of Cur, Cur-NS, and Cur-NS-loaded hydrogel (*Significant difference, $p<0.05$)

Furthermore, we investigated the release kinetics of Cur from the hydrogel by fitting mathematical models to the release data. The obtained correlation coefficients (R^2), release rate constants (K_0, K_1, and K_H), and release exponent (n) values are presented in Table 22. The results indicated that the release of Cur does not conform to zero-order or first-order kinetics models, as evidenced by low R^2 values. Instead, Cur-NS release from the hydrogel was more likely to fit the Higuchi and Korsmeyer-Peppas models, with higher R^2 values. Notably, the Korsmeyer-Peppas model provided the best fit for Cur release from the hydrogel at pH 7.4. The value of *n* in the Korsmeyer-Peppas model is crucial as it provides insights into the release mechanism of the drug. When $n \leq 0.5$, the drug release is controlled by Fickian diffusion through the polymer matrix, while when $0.5 < n < 1$, it follows anomalous (non-Fickian) transport, indicating a combination of diffusion and polymer relaxation (135). According to the model, the value of $n = 0.501$ was remarkably close to the boundary between Fickian diffusion and anomalous transport mechanism, indicating a predominately diffusion-driven process with a minor contribution from relaxation or erosion. The moderate percent erosion of Cur-NS loaded hydrogel observed in section 4.3.1.1 suggests controlled matrix

degradation, facilitating a steady release of Cur. The *n* value close to 0.5 signifies that while diffusion is the primary mechanism, there is a slight anomalous transport influence, likely due to the combined effects of diffusion and swelling or relaxation of polymeric chains (136). The selection of the most appropriate release kinetic model can be influenced by the particular type of polymer used in the hydrogel. For instance, a study reported a plant protein hydrogel that exhibited Korsmeyer-Peppas release behavior indicative of a diffusion and swelling-controlled mechanism (137). This aligns with the diffusion-erosion model observed in our study with the CS/PVP hydrogel, suggesting a similar interplay between drug diffusion and hydrogel matrix relaxation during the release process. This highlights the interplay between Cur diffusion and hydrogel properties in controlling the release profile.

Table 22. Regression coefficients and constants of the model fitted to Cur-NS release from the CS/PVP hydrogel

Sample	Zero Order		First Order		Higuchi		Korsmeyer-Peppas	
	R^2	K_0	R^2	K_1	R^2	K_H	R^2	*n*
Cur-NS-loaded hydrogel	0.5851	9.108	0.6532	0.1000	0.9937	11.920	0.9959	0.501

4.3.1.6. Biocompatibility

As the hydrogels were intended to be applied on open wounds, it is important to assess their possible toxicity, especially on human skin cells. The cytotoxicity of genipin crosslinked CS/PVP hydrogels was studied on NHF cells. The cell viability for all tested hydrogels was found to be above 100% (Fig. 26), which could be considered non-toxic to the epithelial cells. Moreover, the higher viability of cells observed may be due to the genipin-crosslinked CS/PVP hydrogel's potential to induce cell proliferation, as reported in the literature that genipin-crosslinked CS-based hydrogels promote cellular growth in wound healing (138). Additionally, the toxicity of Cur-NS was previously investigated and found to have no significant toxic effect on skin cells (132).

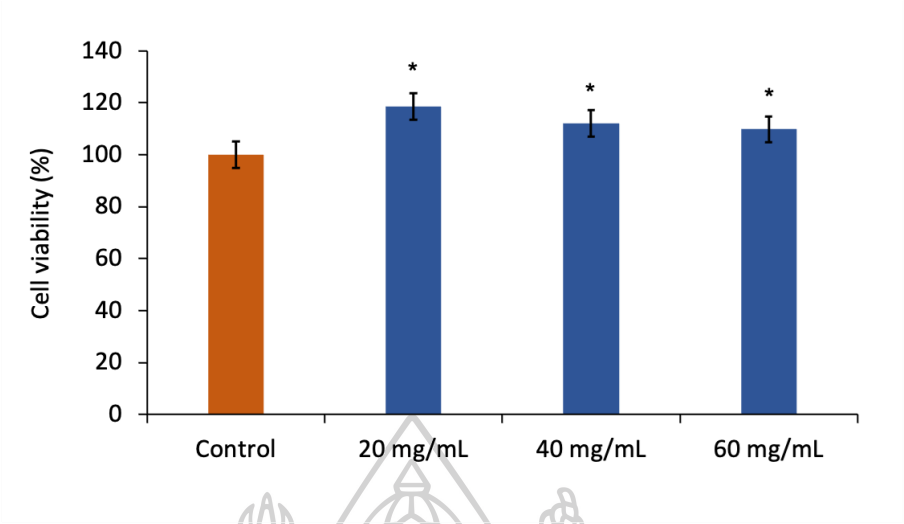

Figure 26. Cell viability of hydrogels after 24 h treatment (*Significant difference, $p<0.05$)

4.3.1.7. Anti-bacterial studies

As the antimicrobial efficacy was assessed using the disc diffusion method, it was observed that the CS/PVP hydrogel had no zones of inhibition against *S. aureus*, suggesting an absence of intrinsic antibacterial characteristics. Similarly, discs impregnated with 100 µg/mL of Cur-NSs, and Cur-NS-loaded hydrogels did not show any inhibition zones, indicating that under the conditions tested, there was no discernible antibacterial activity against *S. aureus*. These results may be attributable to various factors. Firstly, the concentration of Cur-NS might have been below the minimum inhibitory concentration necessary to exert an antibacterial effect on *S. aureus.* It is known that Cur exhibits antimicrobial properties at certain concentrations and under specific conditions (139-142). Secondly, the lack of antibacterial activity could also be attributed to around 50% of Cur release from the hydrogel matrix at 24 h, which may impede the concentration of Cur to exert an antimicrobial effect (143). It is essential to conduct further research to understand the interaction between the hydrogel matrix, nanocurcumin, and bacterial cells.

4.3.1.8. *In vivo* wound healing studies

To investigate the wound healing effect of Cur-NS-loaded hydrogel, the patch was applied to the incised animal dorsal skin, and wound closure was measured through the diameter of the wound. Fig. 27(A) displays the gradual reduction in wound size of

treated animals for the control (gauze), commercial hydrogel product, and Cur-NS-loaded hydrogel. No signs of infection, inflammation, or hemorrhage were observed in any animals during the study. It was noted that there was an acceleration in the re-epithelialization process in all treated wound lesions, resulting in a reduced area of the wounds. However, the wound treated with Cur-NS-loaded hydrogel showed almost complete healing, with the granulation tissue nearly healed, representing a significant improvement compared to the control group. Furthermore, the percentage of wound recovery was calculated and graphically presented in Fig. 27(B). All groups exhibited approximately 50% recovery on day 5; thus, the recovery rate was significantly faster for both the commercial hydrogel and Cur-NS-loaded hydrogel groups. These hydrogels presented over 80% recovery on day 7. The Cur-NS-loaded hydrogel showed a promising wound closure response similar to the commercial hydrogel. It is suggested that the slow and sustained release of nanocurcumin from the hydrogel aided the wound healing, thereby reducing the inflammatory response and stimulating fibroblast proliferation, collagen deposition, and epidermal tissue regeneration (20, 144). Moreover, many studies have reported using CS-based hydrogel matrices for promoting wound healing owing to their inherent biological activity (138, 145, 146). Another contributing factor to the improved healing rate possibly resulted from the wet environment provided by the hydrogel preparations. The hydration of wounds, along with optimal gas transfer, is conducive to accelerating the wound healing process, which these parameters were provided to the incision by the developed formulation. These results indicate the effect of nanocurcumin and CS-based hydrogel in wound repair with a reduced risk of infection and inflammation.

(A)

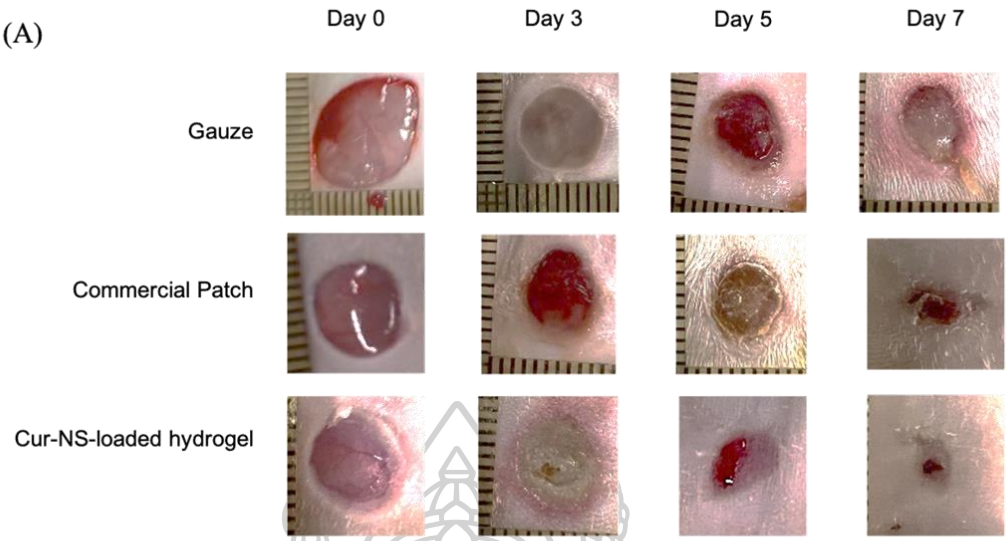

Wound diameter, cm	Day 0	Day 3	Day 5	Day 7
Gauze	1.13±0.10	0.78±0.04	0.61±0.04	0.52±0. 05
Nexcare® Hydrocolloid (positive control)	0.96±0.21	0.70±0.08	0.62±0.04	0.21±0.06*
Cur-NS-loaded hydrogel	0.97±0.21	0.71±0.06	0.51±0.05	0.10±0.06*

(B)

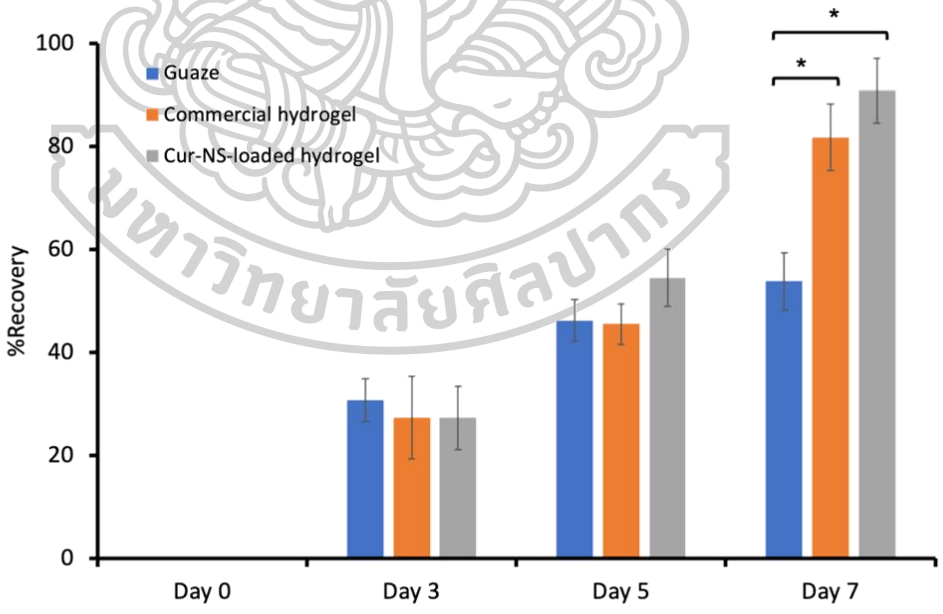

Figure 27. A) The incised wound on rat dorsal skin and recovery and **B**) %recovery of the wound on Days 0, 3, 5, and 7 after treated with each sample (*Significant difference, $p<0.05$)

4.3.2. Cur-L loaded HA/PVA/PNVP-ITA hydrogel patches

4.3.2.1. SEM

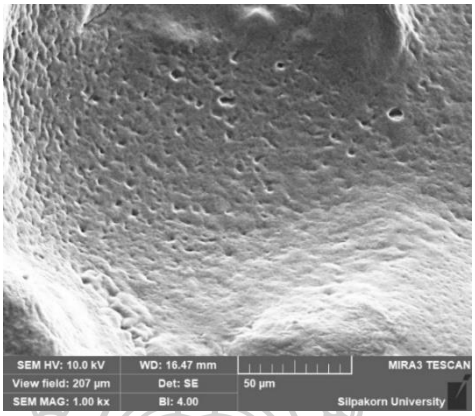

Figure 28. SEM image of Cur-L@HA/PVA/PNVP-ITA hydrogel at the magnification of 1000x

4.3.2.2. FTIR

Figure 29 illustrates the FTIR spectra of HA/PVA/PNVP-ITA hydrogel, Cur-L, and Cur-L loaded HA/PVA/PNVP-ITA hydrogel, highlighting the interactions between the Cur-L and the HA/PVA/PNVP-ITA hydrogel. The combined Cur-L and the HA/PVA/PNVP-ITA hydrogel FTIR spectra indicate significant interactions between the components. The O-H stretching peak shift to 3307 cm^{-1} suggests hydrogen bonding between the liposome and hydrogel. The C-H stretching peak at 2923 cm^{-1} suggests the aliphatic chain interactions are retained, indicating the presence of both lipid and hydrogel components. The C=O stretching peak at 1716 cm^{-1}, consistent with the hydrogel, implies stabilization through hydrogen bonding or coordination. The slight shifts in C-H and C-O stretching peaks and the new C-H bending peak at 1375 cm^{-1} point to van der Waals interactions and structural integration. These observations confirm the successful incorporation and stabilization of Cur-L within the hydrogel matrix.

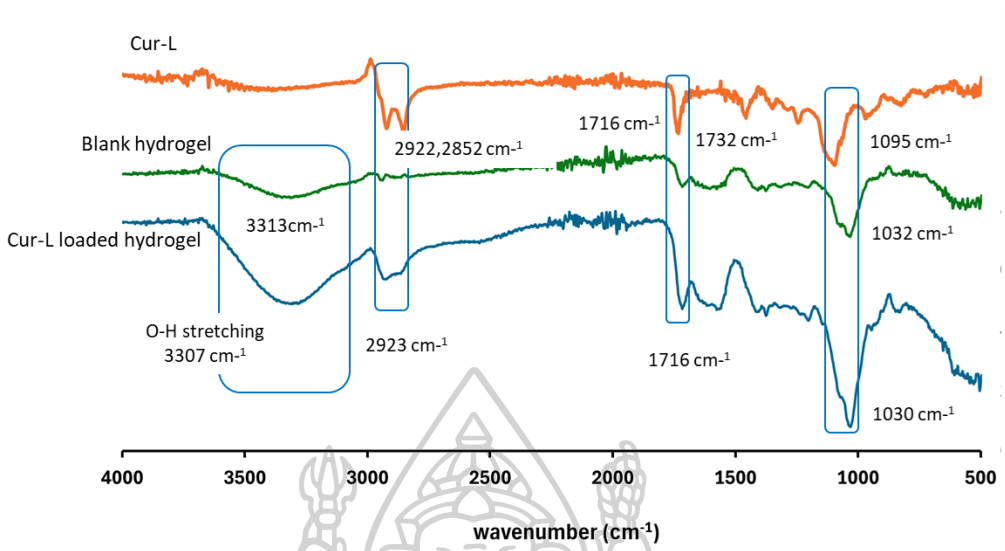

Figure 29. The ATR-FTIR spectra of Cur-Ls, HA/PVA/PNVP-ITA hydrogel, and Cur-L loaded HA/PVA/PNVP-ITA hydrogel

4.3.2.3. Drug loading and *in vitro* drug release profile

The release behaviors of Cur from the Cur-Ls and Cur suspensions were compared using the dialysis method. Fig. 30 presents a distinct release pattern. Cur-Ls exhibited a more rapid release profile than Cur suspensions, which showed a gradual release into the medium due to its poor solubility. The %cumulative Cur release from Cur-Ls exceeded that of Cur suspensions, possibly due to the improved solubility of Cur. Liposomes exhibit superior features over traditional drug delivery systems, including regulated or prolonged release, protection against drug degradation, increased therapeutic effect, and reduced risk of severe side effects (147). Moreover, Cur-L embedded in the hydrogel exhibited a biphasic release pattern, with a rapid release observed within an initial 2 h, followed by a steady, slower release. The fast release is probably caused by hydrogel swelling, which leads to a swift release of the surface-bound Cur. The subsequent slower release phase is due to the Cur-L diffusion through the swollen crosslinked hydrogel matrix.

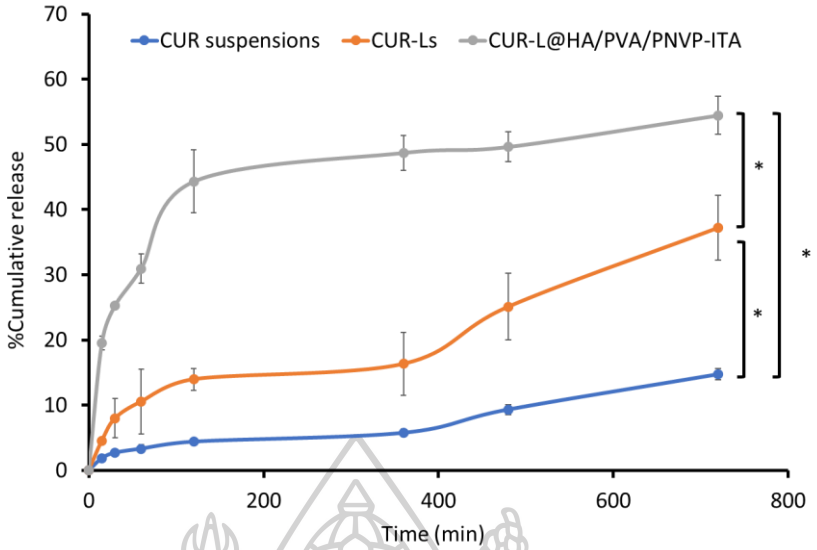

Figure 30. The cumulative release profile of Cur suspensions, Cur-Ls, and Cur-L@HA/PVA/PNVP-ITA (*Significant difference, $p<0.05$)

The release patterns of Cur were fitted to different mathematical models to understand their release kinetics. Table 23 presents the correlation coefficient and equations used to calculate and predict the release according to each model. The results indicate that the Korsmeyer-Peppas model offered the best fit for the release of Cur-L from the HA/PVA/PNVP-ITA hydrogel, as evidenced by the highest correlation coefficient (148, 149). Especially, the Cur-L release from the hydrogel showed the highest model selection criterion (MSC), indicating a strong fit with the Korsmeyer-Peppas model. An *n* value of 0.232 indicates a Fickian diffusion-controlled release of Cur from the hydrogel, which is beneficial for achieving a controlled and sustained drug release in wound healing applications (150). The R^2 and MSC are indicators of goodness-of-fit when comparing multiple models (151). Thus, Cur delivery through Cur-L-embedded hydrogels was effectively described by the Korsmeyer-Peppas model, following a diffusion-controlled release mechanism.

Table 23. Release kinetic models of the Cur suspensions, the Cur-Ls, and CurL-loaded hydrogels

Kinetic model	Parameter	Cur-L @HA/PVA/PNVP-ITA hydrogels
Zero-order	R^2	0.8682
	MSC	1.2668
	Equation	F=0.099t
First-order	R^2	0.9139
	MSC	0.9367
	Equation	$F=100(1-e^{-0.002t})$
Higuchi	R^2	0.9186
	MSC	0.1710
	Equation	$F=2.472\sqrt{t}$
Korsmeyer-Peppas	R^2	0.9850
	MSC	2.3622
	Equation	$12.191t^{n-1}$
	n	0.232

4.3.2.4. Anti-bacterial studies

The disc diffusion method was employed to assess the antimicrobial efficacy of the formulations. The results indicated that the HA/PVA/PNVP-ITA hydrogel exhibited no inhibition zones against S. *aureus*, suggesting an absence of intrinsic antibacterial properties. Similarly, 50 µg/mL of Cur-L and Cur-L loaded hydrogels also showed no inhibition zones against S. aureus. As for the above formulations, it could be explained by the concentration of Cur and the release rate of Cur from the liposome under tested conditions. Future studies could focus on increasing the concentration of Cur and modifying the hydrogel matrix and the tested method used.

4.3.2.5. *In vivo* wound healing study

The evaluation of wound healing progress, facilitated by the Cur-L@HA/PVA/PNVP-ITA hydrogel patch compared to the controls in an incisional wound model, is presented in Fig. 31 A). On visual evaluation of the macroscopic images taken over time, it was observed that all groups demonstrated progressive wound healing without any signs of redness, inflammation, or infection. The wound area was monitored over time, and the degree of wound closure was determined by comparing the wound size to its initial dimensions, expressed as a percentage of skin recovery. Fig. 31 B) plots the percentage of relative wound recovery over 10 days. The Cur-L@HA/PVA/PNVP-ITA hydrogel showed significantly greater skin healing than control samples at all time points. The wound with sterile gauze (negative control) had the slowest recovery rate. Cur-L@HA/PVA/PNVP-ITA healed wounds faster than a commercial hydrogel patch (positive control), with significantly higher recovery on day 5. By day 10, Cur-L@HA/PVA/PNVP-ITA achieved almost complete wound closure (95.23±2.10%), unlike the commercial patch, which showed no improvement since day 7. It was suggested that Cur could shorten the inflammatory phase by inducing inflammatory cell apoptosis, thereby accelerating TGF-β1 formation, stimulating fibroblast growth, improving integrin receptor expression, and facilitating cell migration (55, 152). Moreover, its antioxidant properties are essential for wound care (153). The enhanced antioxidant activity of Cur-Ls may contribute to better wound healing, resulting in quicker skin recovery. The deformable nature of the liposomes enables efficient penetration and retention of Cur within the skin layers (154), bolstered by the characteristic sustained release profile that ensures a constant supply of the therapeutic agent to the wound site. Concurrently, the hydrogel not only serves as a supportive matrix facilitating cellular activities imperative to healing such as migration and proliferation but also maintains an optimal moist wound environment (155-157). Additionally, the hydrogels absorbed wound exudates, creating a more favorable healing environment, and protecting the wound from external damage (158). Therefore, the bifunctional cross-linking mechanism ensured that the hydrogel patch remained rigid throughout the study despite fluid absorption. These findings highlight the potential of Cur-L@HA/PVA/PNVP-ITA as a wound dressing, whereas the impact of the blank hydrogel or Cur-L alone was not assessed.

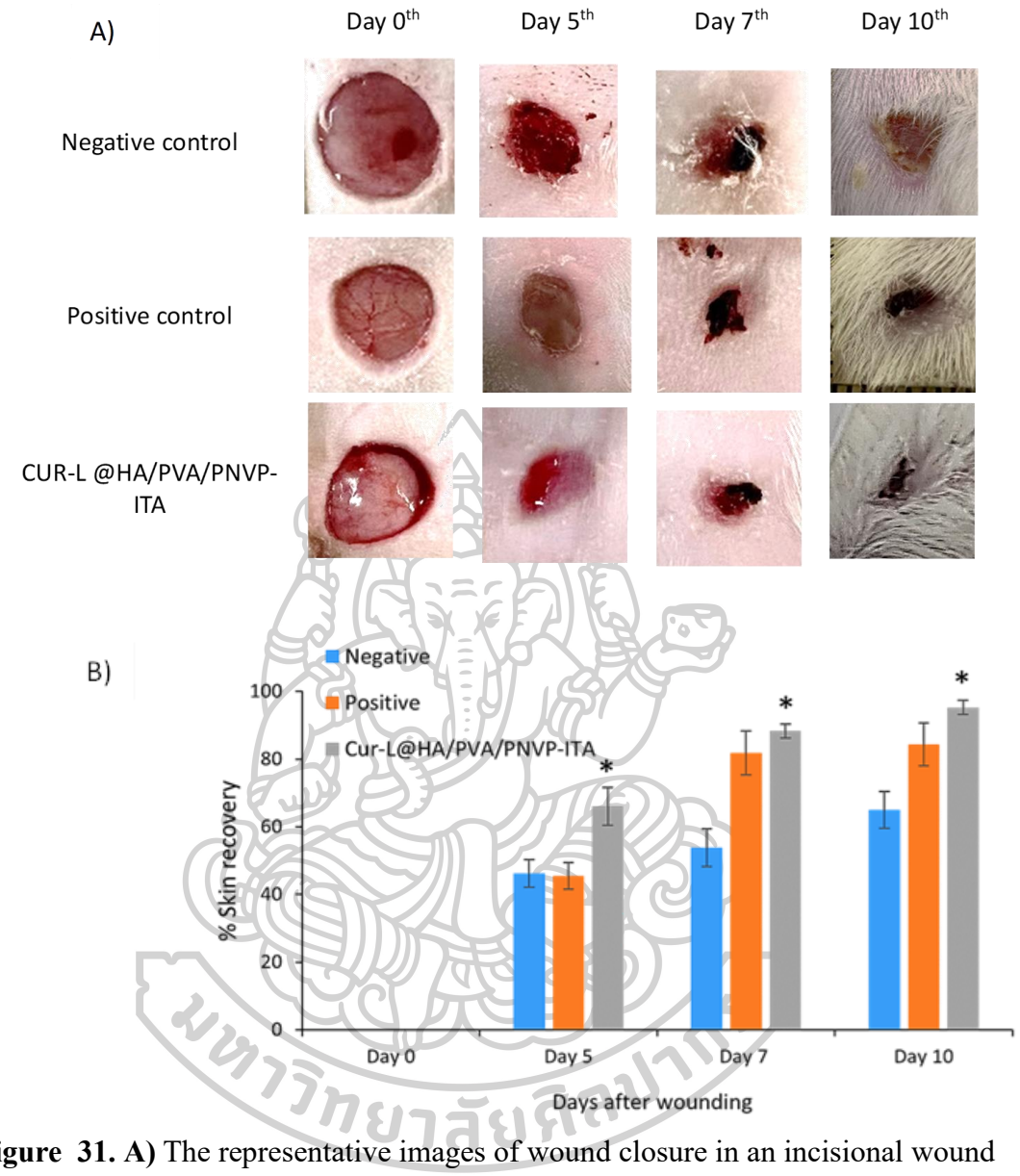

Figure 31. A) The representative images of wound closure in an incisional wound model and **B)** The percentage of skin recovery observed on days 0, 5, 7, and 10 post-application of each treatments (* Significant difference compared to positive control, $p<0.05$).

CHAPTER 5
CONCLUSIONS

5.1. Development of Cur-NS loaded genipin-crosslinked CS/PVP hydrogel for wound healing

This study showed the effectiveness of a Cur-NS loaded genipin-crosslinked CS/PVP hydrogel in enhancing wound healing. The DoE methods enabled the formulations of Cur-NSs and hydrogels to exhibit the desired characteristics. An optimized Cur-NS formulation with uniform nanosized particles and a slightly negative surface charge remained stable for up to 15 days at both 5˚C and 25˚C. As indicated by thermal and crystallinity analysis, improved Cur-NS solubility resulted from amorphization. Its antioxidant capacity was superior in aqueous medium compared to Cur suspension, and it proved non-toxic to NHF cells, enhancing cell migration. Furthermore, an optimized genipin-crosslinked CS/PVP hydrogel was developed, exhibiting high porosity, excellent swelling performance, efficient toughness, and desirable WVTR. The incorporation of Cur-NSs into the hydrogel did not negatively impact its performance. Cur-NSs were released more quickly than Cur solution, reaching nearly full release in 24 hours because it dissolves better in water. Still, this release was regulated by the diffusion-erosion process of the hydrogel, which is in line with the Korsmeyer-Peppas model. *In vivo* experiments demonstrated faster wound repair than commercial hydrogels by day 5 post-wounding. Hence, the developed Cur-NS loaded genipin-crosslinked CS/PVP hydrogel proved to be a promising platform for efficient wound healing.

5.2. Development of Cur-L@ HA/PVA/PNVP-ITA hydrogels for wound healing

This research revealed the efficacy of a Cur-L@HA/PVA/PNVP-ITA hydrogel in promoting wound healing. Using DoE techniques, the liposomes and hydrogel formulations were effectively tailored to possess specific characteristics ideal for wound healing applications. Optimized liposomes achieved small particle size, suitable zeta potential, and maximized Cur content, showing better antioxidant activity in aqueous medium and comparable safety to Cur suspensions. The HA/PVA/PNVP-ITA hydrogels were formulated with promising physical and mechanical properties. Incorporating Cur into the liposomes improved its release, likely due to increased

solubility. The release of Cur from the nanocomposite hydrogel followed Korsmeyer-Peppas model, suggesting a Fickian diffusion through the swollen matrix. Moreover, *in vivo* experiments demonstrated that the Cur-L@HA/PVA/PNVP-ITA hydrogel accelerated skin healing compared to the controls. The developed Cur-L@HA/PVA/PNVP-ITA hydrogel effectively delivers Cur for wound healing, featuring improved solubility and durable, swellable characteristics. Thus, the Cur-L@HA/PVA/PNVP-ITA hydrogel could be a promising candidate for addressing healing challenges in wound care.

REFERENCES

1. Wilkinson HN, Hardman MJ. Wound healing: cellular mechanisms and pathological outcomes. Open Biol. 2020;10(9):200223.
2. Sen CK. Human Wound and Its Burden: Updated 2020 Compendium of Estimates. Adv Wound Care (New Rochelle). 2021;10(5):281-92.
3. Sood A, Granick MS, Tomaselli NL. Wound Dressings and Comparative Effectiveness Data. Adv Wound Care (New Rochelle). 2014;3(8):511-29.
4. Koehler J, Brandl FP, Goepferich AM. Hydrogel wound dressings for bioactive treatment of acute and chronic wounds. European Polymer Journal. 2018;100:1-11.
5. Fan F, Saha S, Hanjaya-Putra D. Biomimetic Hydrogels to Promote Wound Healing. Front Bioeng Biotechnol. 2021;9:718377.
6. Feng P, Luo Y, Ke C, Qiu H, Wang W, Zhu Y, et al. Chitosan-Based Functional Materials for Skin Wound Repair: Mechanisms and Applications. Front Bioeng Biotechnol. 2021;9:650598.
7. Yang X, Wang B, Peng D, Nie X, Wang J, Yu C-Y, et al. Hyaluronic Acid-Based Injectable Hydrogels for Wound Dressing and Localized Tumor Therapy: A Review. Advanced NanoBiomed Research. 2022;2(12).
8. Luo Y, Hong Y, Shen L, Wu F, Lin X. Multifunctional Role of Polyvinylpyrrolidone in Pharmaceutical Formulations. AAPS PharmSciTech. 2021;22(1):34.
9. Kamoun EA, Kenawy ES, Chen X. A review on polymeric hydrogel membranes for wound dressing applications: PVA-based hydrogel dressings. J Adv Res. 2017;8(3):217-33.
10. Vo NTN, Huang L, Lemos H, Mellor AL, Novakovic K. Genipin-crosslinked chitosan hydrogels: Preliminary evaluation of the in vitro biocompatibility and biodegradation. Journal of Applied Polymer Science. 2021;138(34).
11. Waresindo WX, Luthfianti HR, Priyanto A, Hapidin DA, Edikresnha D, Aimon AH, et al. Freeze–thaw hydrogel fabrication method: basic principles, synthesis parameters, properties, and biomedical applications. Materials Research Express. 2023;10(2).
12. Parhi R. Cross-Linked Hydrogel for Pharmaceutical Applications: A Review. Adv Pharm Bull. 2017;7(4):515-30.
13. Tabasi H, Babaei M, Abnous K, Taghdisi SM, Saljooghi AS, Ramezani M, et al. Metal–polymer-coordinated complexes as potential nanovehicles for drug delivery. Journal of Nanostructure in Chemistry. 2021;11(4):501-26.
14. Maheshwari RK, Singh AK, Gaddipati J, Srimal RC. Multiple biological activities of curcumin: a short review. Life Sci. 2006;78(18):2081-7.
15. Farhat F, Sohail SS, Siddiqui F, Irshad RR, Madsen DO. Curcumin in Wound Healing-A Bibliometric Analysis. Life (Basel). 2023;13(1).
16. Dreifke MB, Jayasuriya AA, Jayasuriya AC. Current wound healing procedures and potential care. Mater Sci Eng C Mater Biol Appl. 2015;48:651-62.
17. Emiroglu G, Ozergin Coskun Z, Kalkan Y, Celebi Erdivanli O, Tumkaya L, Terzi S, et al. The Effects of Curcumin on Wound Healing in a Rat Model of Nasal Mucosal Trauma. Evid Based Complement Alternat Med. 2017;2017:9452392.
18. Kulac M, Aktas C, Tulubas F, Uygur R, Kanter M, Erboga M, et al. The effects of topical treatment with curcumin on burn wound healing in rats. J Mol Histol. 2013;44(1):83-90.

19. Cao M, Duan Z, Wang X, Gong P, Zhang L, Ruan B. Curcumin Promotes Diabetic Foot Ulcer Wound Healing by Inhibiting miR-152-3p and Activating the FBN1/TGF-beta Pathway. Mol Biotechnol. 2024.
20. Alibolandi M, Mohammadi M, Taghdisi SM, Abnous K, Ramezani M. Synthesis and preparation of biodegradable hybrid dextran hydrogel incorporated with biodegradable curcumin nanomicelles for full thickness wound healing. Int J Pharm. 2017;532(1):466-77.
21. Cardoso-Daodu IM, Ilomuanya MO, Azubuike CP. Development of curcumin-loaded liposomes in lysine–collagen hydrogel for surgical wound healing. Beni-Suef University Journal of Basic and Applied Sciences. 2022;11(1).
22. Williamson EM, Sun Z, Mora-Tamez L, Brutchey RL. Design of Experiments for Nanocrystal Syntheses: A How-To Guide for Proper Implementation. Chemistry of Materials. 2022;34(22):9823-35.
23. Almadani YH, Vorstenbosch J, Davison PG, Murphy AM. Wound Healing: A Comprehensive Review. Semin Plast Surg. 2021;35(3):141-4.
24. stages of soft tissue healing [Internet]. december 22, 2019 [cited December 22, 2019]. Available from: https://mdanderson.libanswers.com/faq/26219.
25. Larouche J, Sheoran S, Maruyama K, Martino MM. Immune Regulation of Skin Wound Healing: Mechanisms and Novel Therapeutic Targets. Adv Wound Care (New Rochelle). 2018;7(7):209-31.
26. Basu S, Shukla V. Complications of Wound Healing. Measurements in Wound Healing2012. p. 109-44.
27. Lima TPL, Passos MF. Skin wounds, the healing process, and hydrogel-based wound dressings: a short review. J Biomater Sci Polym Ed. 2021;32(14):1910-25.
28. Burgess JL, Wyant WA, Abdo Abujamra B, Kirsner RS, Jozic I. Diabetic Wound-Healing Science. Medicina (Kaunas). 2021;57(10).
29. Kus KJB, Ruiz ES. Wound Dressings – A Practical Review. Current Dermatology Reports. 2020;9(4):298-308.
30. Winter GD. Formation of the Scab and the Rate of Epithelization of Superficial Wounds in the Skin of the Young Domestic Pig. Nature. 1962;193(4812):293-4.
31. Rezvani Ghomi E, Khalili S, Nouri Khorasani S, Esmaeely Neisiany R, Ramakrishna S. Wound dressings: Current advances and future directions. Journal of Applied Polymer Science. 2019;136(27).
32. Dhivya S, Padma VV, Santhini E. Wound dressings - a review. Biomedicine (Taipei). 2015;5(4):22.
33. Brumberg V, Astrelina T, Malivanova T, Samoilov A. Modern Wound Dressings: Hydrogel Dressings. Biomedicines. 2021;9(9).
34. Mirhaj M, Labbaf S, Tavakoli M, Seifalian AM. Emerging treatment strategies in wound care. Int Wound J. 2022;19(7):1934-54.
35. Peppas NA, Hoffman AS. Hydrogels. Biomaterials Science2020. p. 153-66.
36. Minsart M, Van Vlierberghe S, Dubruel P, Mignon A. Commercial wound dressings for the treatment of exuding wounds: an in-depth physico-chemical comparative study. Burns Trauma. 2022;10:tkac024.
37. Op 't Veld RC, Walboomers XF, Jansen JA, Wagener F. Design Considerations for Hydrogel Wound Dressings: Strategic and Molecular Advances. Tissue Eng Part B Rev. 2020;26(3):230-48.

38. Madduma-Bandarage USK, Madihally SV. Synthetic hydrogels: Synthesis, novel trends, and applications. Journal of Applied Polymer Science. 2020;138(19).
39. Sheokand B, Vats M, Kumar A, Srivastava CM, Bahadur I, Pathak SR. Natural polymers used in the dressing materials for wound healing: Past, present and future. Journal of Polymer Science. 2023;61(14):1389-414.
40. Liu H, Wang C, Li C, Qin Y, Wang Z, Yang F, et al. A functional chitosan-based hydrogel as a wound dressing and drug delivery system in the treatment of wound healing. RSC Adv. 2018;8(14):7533-49.
41. Gupta A, Kowalczuk M, Heaselgrave W, Britland ST, Martin C, Radecka I. The production and application of hydrogels for wound management: A review. European Polymer Journal. 2019;111:134-51.
42. Graca MFP, Miguel SP, Cabral CSD, Correia IJ. Hyaluronic acid-Based wound dressings: A review. Carbohydr Polym. 2020;241:116364.
43. Wu S, Deng L, Hsia H, Xu K, He Y, Huang Q, et al. Evaluation of gelatin-hyaluronic acid composite hydrogels for accelerating wound healing. J Biomater Appl. 2017;31(10):1380-90.
44. Fahmy A, Kamoun EA, El-Eisawy R, El-Fakharany EM, Taha TH, El-Damhougy BK, et al. Poly(vinyl alcohol)-hyaluronic Acid Membranes for Wound Dressing Applications: Synthesis andin vitroBio-Evaluations. Journal of the Brazilian Chemical Society. 2015.
45. Wang M, Bai J, Shao K, Tang W, Zhao X, Lin D, et al. Poly(vinyl alcohol) Hydrogels: The Old and New Functional Materials. International Journal of Polymer Science. 2021;2021:1-16.
46. Choudhary V, Shivakumar HG. A Review on Curcumin: Wound Healing Properties and Biomarkers of Wound Healing. International Research Journal Of Pharmacy. 2018;9(9):1-5.
47. Wikipedia. 2024. "Curcumin." Wikimedia Foundation. Last modified May 2 hewowC.
48. Akbik D, Ghadiri M, Chrzanowski W, Rohanizadeh R. Curcumin as a wound healing agent. Life Sci. 2014;116(1):1-7.
49. Kumari A, Raina N, Wahi A, Goh KW, Sharma P, Nagpal R, et al. Wound-Healing Effects of Curcumin and Its Nanoformulations: A Comprehensive Review. Pharmaceutics. 2022;14(11).
50. Zheng D, Huang C, Huang H, Zhao Y, Khan MRU, Zhao H, et al. Antibacterial Mechanism of Curcumin: A Review. Chem Biodivers. 2020;17(8):e2000171.
51. Zheng B, McClements DJ. Formulation of More Efficacious Curcumin Delivery Systems Using Colloid Science: Enhanced Solubility, Stability, and Bioavailability. Molecules. 2020;25(12).
52. Dai M, Zheng X, Xu X, Kong X, Li X, Guo G, et al. Chitosan-alginate sponge: preparation and application in curcumin delivery for dermal wound healing in rat. J Biomed Biotechnol. 2009;2009:595126.
53. Mohanty C, Das M, Sahoo SK. Sustained wound healing activity of curcumin loaded oleic acid based polymeric bandage in a rat model. Mol Pharm. 2012;9(10):2801-11.
54. Hegge AB, Andersen T, Melvik JE, Bruzell E, Kristensen S, Tonnesen HH. Formulation and bacterial phototoxicity of curcumin loaded alginate foams for wound

treatment applications: studies on curcumin and curcuminoides XLII. J Pharm Sci. 2011;100(1):174-85.
55. Gopinath D, Ahmed MR, Gomathi K, Chitra K, Sehgal PK, Jayakumar R. Dermal wound healing processes with curcumin incorporated collagen films. Biomaterials. 2004;25(10):1911-7.
56. Krausz AE, Adler BL, Cabral V, Navati M, Doerner J, Charafeddine RA, et al. Curcumin-encapsulated nanoparticles as innovative antimicrobial and wound healing agent. Nanomedicine. 2015;11(1):195-206.
57. Huang F, Gao Y, Zhang Y, Cheng T, Ou H, Yang L, et al. Silver-Decorated Polymeric Micelles Combined with Curcumin for Enhanced Antibacterial Activity. ACS Appl Mater Interfaces. 2017;9(20):16880-9.
58. Ternullo S, Schulte Werning LV, Holsaeter AM, Skalko-Basnet N. Curcumin-In-Deformable Liposomes-In-Chitosan-Hydrogel as a Novel Wound Dressing. Pharmaceutics. 2019;12(1).
59. Shi T, Lv Y, Huang W, Fang Z, Qi J, Chen Z, et al. Enhanced transdermal delivery of curcumin nanosuspensions: A mechanistic study based on co-localization of particle and drug signals. Int J Pharm. 2020;588:119737.
60. Jacob S, Nair AB, Shah J. Emerging role of nanosuspensions in drug delivery systems. Biomater Res. 2020;24:3.
61. Campani V, Scotti L, Silvestri T, Biondi M, De Rosa G. Skin permeation and thermodynamic features of curcumin-loaded liposomes. J Mater Sci Mater Med. 2020;31(2):18.
62. Elbaz NM, Tatham LM, Owen A, Rannard S, McDonald TO. Redispersible nanosuspensions as a plausible oral delivery system for curcumin. Food Hydrocolloids. 2021;121.
63. Sideek SA, El-Nassan HB, Fares AR, ElMeshad AN, Elkasabgy NA. Different Curcumin-Loaded Delivery Systems for Wound Healing Applications: A Comprehensive Review. Pharmaceutics. 2022;15(1).
64. N K, R G. Optimization and Evaluation of Oleic Acid Based Unsaturated Fatty Acid Liposomes Gel. Journal of Bioequivalence & Bioavailability. 2017;09(03).
65. Xu HL, Chen PP, ZhuGe DL, Zhu QY, Jin BH, Shen BX, et al. Liposomes with Silk Fibroin Hydrogel Core to Stabilize bFGF and Promote the Wound Healing of Mice with Deep Second-Degree Scald. Adv Healthc Mater. 2017;6(19).
66. Ternullo S, Gagnat E, Julin K, Johannessen M, Basnet P, Vanic Z, et al. Liposomes augment biological benefits of curcumin for multitargeted skin therapy. Eur J Pharm Biopharm. 2019;144:154-64.
67. Thoniyot P, Tan MJ, Karim AA, Young DJ, Loh XJ. Nanoparticle-Hydrogel Composites: Concept, Design, and Applications of These Promising, Multi-Functional Materials. Adv Sci (Weinh). 2015;2(1-2):1400010.
68. Campea MA, Majcher MJ, Lofts A, Hoare T. A Review of Design and Fabrication Methods for Nanoparticle Network Hydrogels for Biomedical, Environmental, and Industrial Applications. Advanced Functional Materials. 2021;31(33).
69. Fonseca-Santos B, Gremião MPD, Chorilli M. A simple reversed phase high-performance liquid chromatography (HPLC) method for determination of in situ gelling curcumin-loaded liquid crystals in in vitro performance tests. Arabian Journal of Chemistry. 2017;10(7):1029-37.

70. Hirlekar SDS, Bhairy S, Bhairy S, Hirlekar R, Hirlekar R. Preparation and Characterization of Oral Nanosuspension Loaded with Curcumin. International Journal of Pharmacy and Pharmaceutical Sciences. 2018;10(6).
71. Abdul Razak Hussein AM, Narciso Ramos, Sinnathamby Rajaratnam, Thanat Khoman. ASEAN GUIDELINE ON STABILITY STUDY OF DRUG PRODUCT (R1). 2018.
72. Dokovic JB, Savic SM, Mitrovic JR, Nikolic I, Markovic BD, Randjelovic DV, et al. Curcumin Loaded PEGylated Nanoemulsions Designed for Maintained Antioxidant Effects and Improved Bioavailability: A Pilot Study on Rats. Int J Mol Sci. 2021;22(15).
73. Martinotti S, Ranzato E. Scratch Wound Healing Assay. Methods Mol Biol. 2020;2109:225-9.
74. Eakwaropas P, Myat YY, Ngawhirunpat T, Rojanarata T, Patrojanasophon P, Akkaramongkolporn P, et al. Optimization of boesenbergia rotunda extract-loaded polyvinyl alcohol hydrogel wound dressing by box-behnken design. Key Engineering Materials. 2019;819:38-44.
75. Pornpitchanarong C, Rojanarata T, Opanasopit P, Ngawhirunpat T, Patrojanasophon P. Clotrimazole nanosuspensions-loaded hyaluronic acid-catechol/polyvinyl alcohol mucoadhesive films for oral candidiasis treatment. Journal of Drug Delivery Science and Technology. 2020;60:101927.
76. Rao S, Song Y, Peddie F, Evans AM. Particle size reduction to the nanometer range: a promising approach to improve buccal absorption of poorly water-soluble drugs. Int J Nanomedicine. 2011;6:1245-51.
77. Niksirat M, Sadeghi R, Esmaili J. Removal of Mn from aqueous solutions, by activated carbon obtained from tire residuals. SN Applied Sciences. 2019;1(7).
78. Oh H-S, Oh J-G, Hong Y-G, Kim H. Investigation of carbon-supported Pt nanocatalyst preparation by the polyol process for fuel cell applications. Electrochimica Acta. 2007;52(25):7278-85.
79. Pengnam S, Patrojanasophon P, Rojanarata T, Ngawhirunpat T, Yingyongnarongkul B-e, Radchatawedchakoon W, et al. A novel plier-like gemini cationic niosome for nucleic acid delivery. Journal of Drug Delivery Science and Technology. 2019;52:325-33.
80. Mohtar LG, Ledesma AE, Disalvo EA, Frias MA. Influence of carbonyl groups on the interaction of PLA2 with lipid interphases. Colloid and Interface Science Communications. 2020;39.
81. Suriyaamporn P, Opanasopit P, Rangsimawong W, Ngawhirunpat T. Optimal Design of Novel Microemulsions-Based Two-Layered Dissolving Microneedles for Delivering Fluconazole in Treatment of Fungal Eye Infection. Pharmaceutics. 2022;14(3).
82. Lindfors L, Skantze P, Skantze U, Westergren J, Olsson U. Amorphous Drug Nanosuspensions. 3. Particle Dissolution and Crystal Growth. Langmuir. 2007;23(19):9866-74.
83. Capek I. Nanosuspensions. In: Tadros T, editor. Encyclopedia of Colloid and Interface Science. Berlin, Heidelberg: Springer Berlin Heidelberg; 2013. p. 748-82.
84. Borchard G. Drug Nanocrystals. Non-Biological Complex Drugs. AAPS Advances in the Pharmaceutical Sciences Series2015. p. 171-89.

85. Rahman M, Arevalo F, Coelho A, Bilgili E. Hybrid nanocrystal-amorphous solid dispersions (HyNASDs) as alternative to ASDs for enhanced release of BCS Class II drugs. Eur J Pharm Biopharm. 2019;145:12-26.
86. Pornpitchanarong C, Rojanarata T, Opanasopit P, Ngawhirunpat T, Patrojanasophon P. Clotrimazole nanosuspensions-loaded hyaluronic acid-catechol/polyvinyl alcohol mucoadhesive films for oral candidiasis treatment. Journal of Drug Delivery Science and Technology. 2020;60.
87. Aghrbi I, Fülöp V, Jakab G, Kállai-Szabó N, Balogh E, Antal I. Nanosuspension with improved saturated solubility and dissolution rate of cilostazol and effect of solidification on stability. Journal of Drug Delivery Science and Technology. 2021;61.
88. Managa M, Pitchou Ngoy B, Mafukidze D, Nyokong T. Incorporation of metal free and Ga 5,10,15,20-tetrakis(4-bromophenyl) porphyrin into Pluronic F127-folic acid micelles. Journal of Luminescence. 2018;194:739-46.
89. Verma S, Huey BD, Burgess DJ. Scanning probe microscopy method for nanosuspension stabilizer selection. Langmuir. 2009;25(21):12481-7.
90. Patel VR, Agrawal YK. Nanosuspension: An approach to enhance solubility of drugs. J Adv Pharm Technol Res. 2011;2(2):81-7.
91. Kansom T, Sajomsang W, Saeeng R, Rojanarata T, Ngawhirunpat T, Patrojanasophon P, et al. Fabrication and characterization of andrographolide analogue (3A.1) nanosuspensions stabilized by amphiphilic chitosan derivatives for colorectal cancer therapy. Journal of Drug Delivery Science and Technology. 2019;54.
92. Salehi N, Kuminek G, Al-Gousous J, Sperry DC, Greenwood DE, Waltz NM, et al. Improving Dissolution Behavior and Oral Absorption of Drugs with pH-Dependent Solubility Using pH Modifiers: A Physiologically Realistic Mass Transport Analysis. Mol Pharm. 2021;18(9):3326-41.
93. Borra SK, Mahendra J, Gurumurthy P, Jayamathi, Iqbal SS, Mahendra L. Effect of curcumin against oxidation of biomolecules by hydroxyl radicals. J Clin Diagn Res. 2014;8(10):CC01-5.
94. Sokmen M, Akram Khan M. The antioxidant activity of some curcuminoids and chalcones. Inflammopharmacology. 2016;24(2-3):81-6.
95. Vollono L, Falconi M, Gaziano R, Iacovelli F, Dika E, Terracciano C, et al. Potential of Curcumin in Skin Disorders. Nutrients. 2019;11(9).
96. Tansathien K, Suriyaaumporn P, Charoenputtakhun P, Ngawhirunpat T, Opanasopit P, Rangsimawong W. Development of Sponge Microspicule Cream as a Transdermal Delivery System for Protein and Growth Factors from Deer Antler Velvet Extract. Biological & pharmaceutical bulletin. 2019;42(7):1207-15.
97. Sahoo SK, Labhasetwar V. Nanotech approaches to drug delivery and imaging. Drug Discov Today. 2003;8(24):1112-20.
98. Subongkot T, Ngawhirunpat T, Opanasopit P. Development of Ultradeformable Liposomes with Fatty Acids for Enhanced Dermal Rosmarinic Acid Delivery. Pharmaceutics. 2021;13(3).
99. Verma DD, Verma S, Blume G, Fahr A. Particle size of liposomes influences dermal delivery of substances into skin. Int J Pharm. 2003;258(1-2):141-51.
100. Danaei M, Dehghankhold M, Ataei S, Hasanzadeh Davarani F, Javanmard R, Dokhani A, et al. Impact of Particle Size and Polydispersity Index on the Clinical Applications of Lipidic Nanocarrier Systems. Pharmaceutics. 2018;10(2).

101. Malhotra A, Coupland JN. The effect of surfactants on the solubility, zeta potential, and viscosity of soy protein isolates. Food Hydrocolloids. 2004;18(1):101-8.
102. Oh YK, Kim MY, Shin JY, Kim TW, Yun MO, Yang SJ, et al. Skin permeation of retinol in Tween 20-based deformable liposomes: in-vitro evaluation in human skin and keratinocyte models. J Pharm Pharmacol. 2006;58(2):161-6.
103. Shaker S, Gardouh AR, Ghorab MM. Factors affecting liposomes particle size prepared by ethanol injection method. Res Pharm Sci. 2017;12(5):346-52.
104. Marwah M, Badhan RKS, Lowry D. Development of a novel polymer-based carrier for deformable liposomes for the controlled dermal delivery of naringenin. Journal of Liposome Research. 2022;32(2):181-94.
105. Ameri M, Al-Mudhaffer MF, Almyahi F, Fardell GC, Marks M, Al-Ahmad A, et al. Role of stabilizing surfactants on capacitance, charge, and ion transport in organic nanoparticle-based electronic devices. ACS Applied Materials & Interfaces. 2019;11(10):10074-88.
106. Muneer R, Hashmet MR, Pourafshary P, Shakeel M. Unlocking the power of artificial intelligence: Accurate zeta potential prediction using machine learning. Nanomaterials (Basel). 2023;13(7).
107. Maja L, Željko K, Mateja P. Sustainable technologies for liposome preparation. The Journal of Supercritical Fluids. 2020;165.
108. Battista S, Maggi MA, Bellio P, Galantini L, D'Archivio AA, Celenza G, et al. Curcuminoids-loaded liposomes: influence of lipid composition on their physicochemical properties and efficacy as delivery systems. Colloids and Surfaces A: Physicochemical and Engineering Aspects. 2020;597.
109. Pylypenko D, Gorbach T, Krasnopolsky Y. Study of antioxidant activity of liposomal forms of quercetin and curcumin in ischemic heart disease. BioTechnologia. 2020;101(4):273-82.
110. Jakubczyk K, Druzga A, Katarzyna J, Skonieczna-Zydecka K. Antioxidant Potential of Curcumin-A Meta-Analysis of Randomized Clinical Trials. Antioxidants (Basel). 2020;9(11).
111. Menon VP, Sudheer AR. Antioxidant and anti-inflammatory properties of curcumin. Adv Exp Med Biol. 2007;595:105-25.
112. Alven S, Nqoro X, Aderibigbe BA. Polymer-Based Materials Loaded with Curcumin for Wound Healing Applications. Polymers (Basel). 2020;12(10).
113. Comino-Sanz IM, Lopez-Franco MD, Castro B, Pancorbo-Hidalgo PL. The Role of Antioxidants on Wound Healing: A Review of the Current Evidence. J Clin Med. 2021;10(16).
114. Aye KC, Rojanarata T, Ngawhirunpat T, Opanasopit P, Pornpitchanarong C, Patrojanasophon P. Development and optimization of curcumin-nanosuspensions with improved wound healing effect. Journal of Drug Delivery Science and Technology. 2023;89:104997.
115. Sureewan Duangjit, Praneet Opanasopit, Theerasak Rojanarata, Ngawhirunpat T. Physicochemical stability of meloxicam loaded liposome formulation: Effect of cationic and anionic surfactant. Thai J Pharm Sci. 2013;38.
116. Butler MF, Ng Y-F, Pudney PDAJJoPSPA. Mechanism and kinetics of the crosslinking reaction between biopolymers containing primary amine groups and genipin. 2003;41:3941-53.

117. Muzzarelli RAA. Genipin-crosslinked chitosan hydrogels as biomedical and pharmaceutical aids. Carbohydrate Polymers. 2009;77(1):1-9.
118. Pizzolitto C, Cok M, Asaro F, Scognamiglio F, Marsich E, Lopez F, et al. On the Mechanism of Genipin Binding to Primary Amines in Lactose-Modified Chitosan at Neutral pH. Int J Mol Sci. 2020;21(18).
119. Khurma JR, Rohindra DR, Nand AV. Swelling and Thermal Characteristics of Genipin Crosslinked Chitosan and Poly(vinyl pyrrolidone) Hydrogels. Polymer Bulletin. 2005;54(3):195-204.
120. Khan S, Ranjha NM. Effect of degree of cross-linking on swelling and on drug release of low viscous chitosan/poly(vinyl alcohol) hydrogels. Polymer Bulletin. 2014;71(8):2133-58.
121. Shi Y, Xiong D, Liu Y, Wang N, Zhao X. Swelling, mechanical and friction properties of PVA/PVP hydrogels after swelling in osmotic pressure solution. Mater Sci Eng C Mater Biol Appl. 2016;65:172-80.
122. Schober P, Boer C, Schwarte LA. Correlation Coefficients: Appropriate Use and Interpretation. Anesthesia & Analgesia. 2018;126(5).
123. Hussein Y, El-Fakharany EM, Kamoun EA, Loutfy SA, Amin R, Taha TH, et al. Electrospun PVA/hyaluronic acid/L-arginine nanofibers for wound healing applications: Nanofibers optimization and in vitro bioevaluation. International Journal of Biological Macromolecules. 2020;164:667-76.
124. Stauffer SR, Peppast NA. Poly(vinyl alcohol) hydrogels prepared by freezing-thawing cyclic processing. Polymer. 1992;33(18):3932-6.
125. Quintero SMM, Ponce F RV, Cremona M, Triques ALC, d'Almeida AR, Braga AMB. Swelling and morphological properties of poly(vinyl alcohol) (PVA) and poly(acrylic acid) (PAA) hydrogels in solution with high salt concentration. Polymer. 2010;51(4):953-8.
126. Waresindo WX, Luthfianti HR, Priyanto A, Hapidin DA, Edikresnha D, Aimon AH, et al. Freeze–thaw hydrogel fabrication method: basic principles, synthesis parameters, properties, and biomedical applications. Materials Research Express. 2023;10(2):024003.
127. Dou X, Wang H, Yang F, Shen H, Wang X, Wu D. One-Step Soaking Strategy toward Anti-Swelling Hydrogels with a Stiff "Armor". Adv Sci (Weinh). 2023;10(9):e2206242.
128. Wu F, Pang Y, Liu J. Swelling-strengthening hydrogels by embedding with deformable nanobarriers. Nature Communications. 2020;11(1):4502.
129. Boateng JS, Matthews KH, Stevens HN, Eccleston GM. Wound healing dressings and drug delivery systems: a review. J Pharm Sci. 2008;97(8):2892-923.
130. Foudazi R, Zowada R, Manas-Zloczower I, Feke DL. Porous Hydrogels: Present Challenges and Future Opportunities. Langmuir. 2023;39(6):2092-111.
131. Li J, Mooney DJ. Designing hydrogels for controlled drug delivery. Nature Reviews Materials. 2016;1(12):16071.
132. Aye KC, Rojanarata T, Ngawhirunpat T, Opanasopit P, Pornpitchanarong C, Patrojanasophon P. Development and optimization of curcumin-nanosuspensions with improved wound healing effect. Journal of Drug Delivery Science and Technology. 2023;89.
133. Raghuwanshi VS, Garnier G. Characterisation of hydrogels: Linking the nano to the microscale. Adv Colloid Interface Sci. 2019;274:102044.

134. Schneider LA, Korber A, Grabbe S, Dissemond J. Influence of pH on wound-healing: a new perspective for wound-therapy? Arch Dermatol Res. 2007;298(9):413-20.
135. 5 - Mathematical models of drug release. In: Bruschi ML, editor. Strategies to Modify the Drug Release from Pharmaceutical Systems: Woodhead Publishing; 2015. p. 63-86.
136. Kim SW, Bae YH, Okano T. Hydrogels: swelling, drug loading, and release. Pharmaceutical research. 1992;9(3):283-90.
137. Gupta S, Ghoshal G. Plant protein hydrogel as a delivery system of curcumin: Characterization and in vitro release Kinetics. Food and Bioproducts Processing. 2024;143:66-79.
138. Heimbuck AM, Priddy-Arrington TR, Padgett ML, Llamas CB, Barnett HH, Bunnell BA, et al. Development of Responsive Chitosan-Genipin Hydrogels for the Treatment of Wounds. ACS Appl Bio Mater. 2019;2(7):2879-88.
139. Adamczak A, Ożarowski M, Karpiński TM. Curcumin, a Natural Antimicrobial Agent with Strain-Specific Activity. Pharmaceuticals. 2020;13(7).
140. Kour P, Afzal S, Gani A, Zargar MI, Nabi Tak U, Rashid S, et al. Effect of nanoemulsion-loaded hybrid biopolymeric hydrogel beads on the release kinetics, antioxidant potential and antibacterial activity of encapsulated curcumin. Food Chem. 2021;376:131925.
141. Dai C, Lin J, Li H, Shen Z, Wang Y, Velkov T, et al. The Natural Product Curcumin as an Antibacterial Agent: Current Achievements and Problems. Antioxidants (Basel). 2022;11(3).
142. Snetkov P, Rogacheva E, Kremleva A, Morozkina S, Uspenskaya M, Kraeva L. In-Vitro Antibacterial Activity of Curcumin-Loaded Nanofibers Based on Hyaluronic Acid against Multidrug-Resistant ESKAPE Pathogens. Pharmaceutics. 2022;14(6).
143. Trigo-Gutierrez JK, Vega-Chacon Y, Soares AB, Mima EGO. Antimicrobial Activity of Curcumin in Nanoformulations: A Comprehensive Review. Int J Mol Sci. 2021;22(13).
144. El-Refaie WM, Elnaggar YS, El-Massik MA, Abdallah OY. Novel curcumin-loaded gel-core hyaluosomes with promising burn-wound healing potential: Development, in-vitro appraisal and in-vivo studies. Int J Pharm. 2015;486(1-2):88-98.
145. Huang L, Zhu Z, Wu D, Gan W, Zhu S, Li W, et al. Antibacterial poly (ethylene glycol) diacrylate/chitosan hydrogels enhance mechanical adhesiveness and promote skin regeneration. Carbohydr Polym. 2019;225:115110.
146. Song R, Zheng J, Liu Y, Tan Y, Yang Z, Song X, et al. A natural cordycepin/chitosan complex hydrogel with outstanding self-healable and wound healing properties. Int J Biol Macromol. 2019;134:91-9.
147. Liu P, Chen G, Zhang J. A review of liposomes as a drug delivery system: Current status of approved products, regulatory environments, and future perspectives. Molecules. 2022;27(4).
148. Pornpitchanarong C, Rojanarata T, Opanasopit P, Ngawhirunpat T, Bradley M, Patrojanasophon P. Maleimide-functionalized carboxymethyl cellulose: A novel mucoadhesive polymer for transmucosal drug delivery. Carbohydr Polym. 2022;288:119368.

149. Zhang Y, Huo M, Zhou J, Zou A, Li W, Yao C, et al. DDSolver: an add-in program for modeling and comparison of drug dissolution profiles. AAPS J. 2010;12(3):263-71.
150. Jayachandran P, Ilango S, Suseela V, Nirmaladevi R, Shaik MR, Khan M, et al. Green synthesized silver nanoparticle-loaded liposome-based nanoarchitectonics for cancer management: In vitro drug release analysis. Biomedicines. 2023;11(1).
151. Zhu W, Long J, Shi M. Release Kinetics Model Fitting of Drugs with Different Structures from Viscose Fabric. Materials [Internet]. 2023; 16(8).
152. Barchitta M, Maugeri A, Favara G, Magnano San Lio R, Evola G, Agodi A, et al. Nutrition and Wound Healing: An Overview Focusing on the Beneficial Effects of Curcumin. Int J Mol Sci. 2019;20(5).
153. Gopinath D, Ahmed MR, Gomathi K, Chitra K, Sehgal PK, Jayakumar R. Dermal wound healing processes with curcumin incorporated collagen films. Biomaterials. 2004;25(10):1911-7.
154. Nayak D, Tippavajhala VK. A Comprehensive Review on Preparation, Evaluation and Applications of Deformable Liposomes. Iran J Pharm Res. 2021;20(1):186-205.
155. Medeiros Soares Celani L, Soares Lopes I, Cunha Medeiros A. The effect of hyaluronic acid on the skin healing in rats. Journal of Surgical and Clinical Research. 2019;10(2):65-75.
156. Cho JR, Lee MH, Oh HK, Kim H, Kweon DK, Kang SM, et al. Efficacy of hyaluronic acid film on perianal wound healing in a rat model. Ann Surg Treat Res. 2021;101(4):206-13.
157. Lee JH, Lee KE, Nam OH, Chae YK, Lee MH, Kweon DK, et al. Orodispersible hyaluronic acid film delivery for oral wound healing in rats. J Dent Sci. 2022;17(4):1595-603.
158. Gounden V, Singh M. Hydrogels and Wound Healing: Current and Future Prospects. Gels. 2024;10(1).

VITA

NAME	Khin Cho Aye
INSTITUTIONS ATTENDED	University of Pharmacy, Mandalay
PUBLICATION	1. Aye KC, Rojanarata T, Ngawhirunpat T, Opanasopit P, Pornpitchanarong C, Patrojanasophon P. Development and optimization of curcumin-nanosuspensions with improved wound healing effect. Journal of Drug Delivery Science and Technology. 2023;89. 2. Aye KC, Rojanarata T, Ngawhirunpat T, Opanasopit P, Pornpitchanarong C, Patrojanasophon P. Development and characterization of curcumin nanosuspension-embedded genipin-crosslinked chitosan/polyvinylpyrrolidone hydrogel patch for effective wound healing. Int J Biol Macromol. 2024:133519.